SCUOLA DI DOTTORATO
UNIVERSITÀ DEGLI STUDI DI MILANO-BICOCCA

Department of Environmental and Earth Sciences

Ph.D. program: **Chemical, Geological and Environmental Sciences** Cycle: **XXXI**

Curriculum in: **Environmental Sciences**

LINKING VEGETATION OPTICAL PROPERTIES FROM MULTI-SOURCE REMOTE SENSING TO PLANT TRAITS AND ECOSYSTEM FUNCTIONAL PROPERTIES

Surname: **Tagliabue**

Name: **Giulia**

Registration number: **726870**

Tutor: **Dr. Micol Rossini**

Co-tutor: **Dr. Cinzia Panigada**

Coordinator: **Prof. Maria Luce Frezzotti**

ACADEMIC YEAR: 2017/2018

CONTENTS

LIST OF FIGURES

LIST OF TABLES

ACRONYMS

ALA	Average leaf inclination
APAR	Absorbed Photosynthetically Active Radiation
APEX	Airborne Prism EXperiment
ARTMO	Automated Radiative Transfer Models Operator
BESS	Breathing Earth System Simulator
CAL/VAL	Calibration-Validation
CEST	Central European Summer Time
cd	Crown diameter
CF	Cost Function
DLR	Deutsches Zentrum für Luft- und Raumfahrt
DTM	Digital Terrain Model
DUAL	Dual Channel Imager
EC	Eddy Covariance
EFP	Ecosystem Functional Property
ENVI	ENvironment for Visualizing Images
ESA	European Space Agency
ESU	Elementary Sampling Unit
F	Sun-induced chlorophyll fluorescence
$\mathbf{F_{687}}$	F measured at 687 nm
$\mathbf{F_{760}}$	F measured at 760 nm
Fy	Fluorescence yield
$\mathbf{Fy_{687}}$	Fy measured at 687 nm

Fy_{760}	Fy measured at 760 nm
fAPAR	fraction of Absorbed Photosynthetically Active Radiation
FLEX	FLuorescence EXplorer
FLIM	Forest-LIght interaction Model
FLUO	Fluorescence Imager
FWHM	Full Width at Half Maximum
GOME-2	Global Ozone Monitoring Experiment 2
GPP	Gross Primary Production
GPS	Global Positioning System
GSA	Global Sensitivity Analysis
H	Shannon's Index
h	Tree height
IDL	Interactive Data Language
IMU	Inertial Measurement Unit
INFORM	INvertible FOrest Reflectance Model
λ	Wavelength
LAI	Leaf Area Index
LAIu	Leaf Area Index of understory
LCC	Leaf Chlorophyll Content
LDMC	Leaf dry matter content
LiDAR	Light Detection And Ranging
LST	Local Solar Time
LUE	Light Use Efficiency
LUT	Look-Up-Table
LWC	Leaf water content

ML	Maximum Likelihood
MODIS	Moderate-Resolution Imaging Spetroradiometer
N	Leaf structural parameter
NDSI	Normalised Difference Spectral Index
NDVI	Normalised Difference Vegetation Index
NDVIre	NDVI Red Edge
NIR	Near InfraRed
NOAA	National Oceanic and Atmospheric Administration
NPQ	Non-Photochemical Quenching
Φ	Relative Azimuth angle
OA	Overall Accuracy
OCO-2	Orbiting Carbon Observatory 2
O_2-A	Oxygen A band
O_2-B	Oxygen B band
PA	Producer's Accuracy
PAR	Photosynthetically Active Radiation
PC	Principal Component
PCA	Principal Component Analysis
PQ	Photochemical Quenching
PROSPECT	Model of leaf optical PROperties SPECTra
PT	Plant Trait
Q	Rao's Q diversity
ρ	Reflectance
RMSE	Root Mean Squared Error
rRMSE	Relative Root Mean Squared Error

RS	Remote Sensing
RT	Radiative Transfer
RTM	Radiative Transfer Model
SAIL	Scattering from Arbitrary Inclined Leaves
SAILH	SAIL model accounting for the hot spot
SAR	Synthetic Aperture Radar
SCOPE	Soil-Canopy-Observation of Photosynthesis and the Energy balance
sd	Stem density
SFM	Spectral Fitting Methods
skyl	Fraction of diffuse radiation
SRTM	Shuttle Radar Topography Mission
SVM	Support Vector Machine
SWIR	Short Wave InfraRed
Θ_o	Observer zenith angle
Θ_s	Sun zenith angle
TANSO	Thermal And Near infrared Sensor for carbon Observation
TOC	Top Of Canopy
UA	User's Accuracy
UAV	Unmanned Aerial Vehicle
UTM	Universal Transverse of Mercator
UV	Ultraviolet
Vcmax	Maximum carboxylation rate
$\mathbf{Vcmax}_{25}$	Maximum carboxylation rate normalised to 25°C
VI	Vegetation Index
VIS	Visible
VITO	Vlaamse Instelling voor Technologisch Onderzoek

ABSTRACT

Remote Sensing (RS) data have been successfully exploited in the last decades to monitor vegetation due to their inherent capacity of providing repeated and spatially-distributed quantitative information about vegetation properties in a cost-effective way. However, until recently, most of the studies focused on describing the structural and biochemical properties of vegetation rather than on understanding of its functioning. Nowadays, the challenges imposed by global change on the ecosystem functioning are fostering research towards a deeper understanding of the vegetation dynamics and of the imprint of plants on the Earth system.

In the last decade, RS of sun-induced chlorophyll fluorescence (F) emerged as a novel and promising tool for assessing plant functional status. F is a weak electromagnetic signal emitted by the core of the photosynthetic machinery in the red and far-red spectral regions (~650-800 nm) as a side product of light absorption. The potential of F relies on the relationship between photochemistry and the energy dissipation pathways: since photochemistry competes with F emission and heat dissipation for the same excitation energy, F can provide information on the actual functional status of vegetation.

The main aim of this Ph.D. research was to exploit optical data (*i.e.*, reflectance and fluorescence) to advance the understanding of vegetation functioning and of its variability across space. In particular, the work aimed at better understanding the link between vegetation optical properties, plant traits (PTs) and ecosystem functional properties (EFPs) in a case study represented by a mid-latitude forest ecosystem. For this purpose, innovative RS techniques as well as process-based models were exploited to infer information about the vegetation functioning from fine and ultra-fine spectral resolution optical measurements acquired with the *HyPlant* airborne imaging spectrometer. The analyses were carried out following two main work streams: i) the investigation of the spatial relationship between F and EFPs (*e.g.*, light use efficiency) in order to better understand the variability of the ecosystem functioning at regional scale; ii) the analysis of the potential of F as a synthetic descriptor of the functional diversity of the ecosystem.

Results provided evidence of the effectiveness of F as a tool for assessing vegetation functioning, but also pointed out the complexity of the link existing between F, PTs and EFPs and the need to integrate different RS derived products to obtain an unambiguous interpretation of the F signal. In particular, results showed that: i) F can be related to the spatial variability of the EFPs, thus demonstrating that

this link usually observed in the temporal domain holds in the spatial domain; ii) F is a more powerful tool compared to traditional reflectance-based indices for explaining the functional diversity.

Overall, the results obtained in this thesis advance the understanding of the complex relationship between F and vegetation functioning by adding new insights into the critical role of the spatial heterogeneity in controlling the carbon uptake. Further research in this direction constitutes a high priority for improving the understanding of the imprint of plants on the global carbon balance and the prediction of their response to the global change.

1 INTRODUCTION

Remote Sensing (RS) of sun-induced chlorophyll fluorescence (F) emitted by terrestrial vegetation emerged in the last decade as a novel and promising tool for measuring plants functioning (*e.g.*, Porcar-Castell et al. 2014). Traditional RS based on the analysis of the radiation reflected by vegetation has been providing valuable quantitative information about vegetation for decades (Thenkabail, Lyon, and Huete, 2011; Verrelst et al., 2015a, 2018). In this respect, the strength of RS relies in its intrinsic capacity of providing repeated and spatially-distributed information about vegetation properties in a costly-effective way. However, due to the inherent characteristics of reflectance-based RS, most of the studies focused in the past on characterising the structural and biochemical properties of vegetation rather than on understanding its functioning.

Nowadays, the global change is determining unprecedented pressures on the functionality of the ecosystems, to a degree that threatens their capacity to provide services (Ciais et al., 2013; Zhu et al., 2016). Because of the major role played by the terrestrial ecosystems in the global carbon dynamics (Beer et al., 2010; Heimann and Reichstein, 2008), the quantification of their imprint on the biosphere dynamics is critical to assess vegetation-climate feedbacks. Unlike traditional reflectance-based RS, RS of F has the potential of accomplishing this goal.

F is a faint electromagnetic signal that originates from the core of the photosynthetic machinery as a side product of light absorption (Papageorgiou and Govindjee, 2004). During photosynthesis, chlorophyll molecules absorb the incoming sunlight in the photosynthetically active radiation (PAR) region (400-700 nm). The fate of this energy is threefold. In optimal conditions, the majority of the absorbed energy is stored as chemical energy in energy-rich organic compounds, a process known as Photochemical Quenching (PQ). The fraction of energy that is not used for PQ is rapidly dissipated in order to avoid the generation of radicals that can

damage the photosynthetic apparatus. Over time, plants evolved two alternative pathways to release the excess of absorbed PAR: the Non-Photochemical Quenching (NPQ), which refers to a non-radiative dissipation as heat, and F, which refers to light emission in the red and far-red spectral regions (*i.e.*, 650-800 nm), with two emission peaks located at ~685 nm and ~740 nm. Since PQ, NPQ and F emission are in direct competition for the same excitation energy, the variation in the efficiency of each process affects the others (Baker, 2008). This link constitutes the rationale underlying the use of F to infer information about plant functional status and overwhelmingly motivates the interest posed by the RS scientific community in exploring the F signal over the last years.

Passively detecting F is challenging because it requires disentangling the weak F signal from the upwelling reflected radiation, but it can be achieved exploiting narrow dark regions of the solar and atmospheric spectrum where the irradiance is strongly attenuated (Moya et al., 1998; Plascyk, 1975; Sioris, Bazalgette Courrèges-Lacoste, and Stoll, 2003). The retrieval of F at the far-red emission peak has been proved to be feasible exploiting high spectral resolution radiance measurements collected with spectrometers mounted on multiple platforms: from the top-of-canopy (*e.g.*, Damm et al. 2010; Guanter et al. 2013; Rossini et al. 2016, 2010), to the Unmanned Aerial Vehicle (UAV) (*e.g.*, Garzonio et al. 2017; Zarco-Tejada et al. 2013), to the airborne (*e.g.*, Colombo et al. 2018; Damm et al. 2014; Rascher et al. 2015; Rossini et al. 2015; Zarco-Tejada et al. 2013) to the satellite scale (*e.g.*, Frankenberg et al. 2011; Guanter et al. 2012, 2014; Joiner et al. 2011; Sun et al. 2018, 2017). Conversely, the detection of red F has been restricted to a more limited number of studies primarily because of the technical constraints related to the retrieval, but recent literature demonstrated its feasibility at different scales (*e.g.*, Fournier et al. 2012; Joiner et al. 2016; Liu et al. 2017; Rossini et al. 2016, 2015).

While considerable advances have been achieved in the quantification of F due to the refinement of the retrieval algorithms as well as to the technical improvement of the sensors in terms of spectral resolution and signal-to-noise ratio, the unambiguous interpretation of the signal still constitutes a major challenge. Several recent studies showed that remotely sensed F can be effectively used for tracking physiological dynamics of vegetation (*e.g.*, Guanter et al. 2014; Li, Xiao, and He 2018; Rossini et al. 2015; Sun et al. 2017; Wieneke et al. 2016; Yang et al. 2015). These studies provided empirical evidence of the relationship between measured F and photochemistry in determined conditions. However, while decades of research based on active fluorescence measurements led to a mechanistic understanding of this link at the sub-cellular and leaf level (Baker, 2008; Genty, Briantais, and Baker, 1989; Porcar-Castell et al., 2014), the relationship is not well established at the canopy scale yet. This ambiguity is caused by multiple reasons. Firstly, the amount of energy re-emitted as F also depends on a number of non-physiology

related factors (Porcar-Castell et al., 2014; Verrelst et al., 2015b). Among these, the spatio-temporal variation of plant traits (PTs) - *i.e.* the morphological, structural, biochemical and phenological attributes characterising vegetation (Violle et al., 2007) - *e.g.* leaf chlorophyll content (LCC), leaf area index (LAI) and maximum carboxylation capacity (Vcmax) as well as the illumination conditions affect the F signal emitted by vegetation. Secondly, the reabsorption and scattering of F within the leaf and the canopy influence the amount of F that is detected remotely. Thirdly, the spatial and temporal scales at which the relationship is investigated influence its behaviour. These factors confound the link between F and photosynthesis, either masking or misleadingly emphasizing the variation of F and thus leading to potentially erroneous conclusions. For these reasons, it appears critical to take all of them into account to effectively relate F to meaningful descriptors of the ecosystem processes (*i.e.*, the ecosystem functional properties (EFPs) (Reichstein et al., 2014). The EFPs are directly related to the ecosystem functioning. For this reason, it is critical to characterise their spatial and temporal variability in order to explain and monitor the ecosystem capacity of providing services.

Since the variability of the ecosystem functioning is strongly determined by the spatial and temporal variation of PTs, a robust, accurate and operational mapping of PTs is critical for investigating the the ecosystem dynamics and their response to a changing climate (Chapin et al., 2000; Reichstein et al., 2014). In this regard, considerable efforts have been posed over the last decades in the development and testing of retrieval approaches to translate optical RS observations into PTs, including parametric and non-parametric regressions, physically-based models and hybrid methods (Verrelst et al. (2015a, 2018) for a review). Among these, the retrieval based on radiative transfer models is generally considered one of the most reliable and generic methods being founded on a physical relationship between the measured radiometric signal and the characteristics of the vegetation medium (Houborg et al., 2015; Verrelst et al., 2015c). However, the operational mapping of PTs remains a challenge since the quantitative estimation of PTs from optical data is ill-posed and hampered by several confounding factors, *e.g.*, the canopy structure, the influence of the atmosphere, the illumination conditions and the sun-sensor geometries (Houborg et al., 2015; Malenovský et al., 2013; Wang et al., 2018; Zarco-Tejada et al., 2004). For these reasons, it is critical to investigate strategies to regularise the inversion in order to mitigate the drawbacks of ill-posedness and reduce the uncertainties in the PTs quantification (Baret and Buis, 2008; Combal et al., 2002; Houborg et al., 2015; Verrelst et al., 2014, 2015c).

Due to the recognised influence of the PTs variability on the ecosystem dynamics, the concept of ecosystem functioning has been recently associated to the concept of functional diversity. As a matter of fact, multiple experimental studies found a positive relationship between ecosystem productivity and plant diversity

(Balvanera et al., 2006; Cardinale et al., 2011; Hooper et al., 2005), that can be explained by a higher efficiency in the resources utilization and by an increased ecosystem stability. Based on this link, the relationship between biodiversity and ecosystem functioning has emerged as a critical issue in ecological and environmental studies during the last decade (Loreau et al., 2001). Conversely to the traditional concept of biodiversity which refers to the taxonomic diversity (*i.e.*, the diversity in terms of species composition and abundance), the functional diversity considers the variability of the PT mean and variance due to differences among organs, individuals, or species (Musavi et al., 2015). The exploitation of the link between functional diversity and ecosystem functioning depends on the efficiency of mapping the functional diversity across space. Due to the close relationship between PTs and EFPs, several approaches based on mapping the variability of PTs have been proposed recently to quantify the functional diversity (Mouchet et al., 2010; Petchey and Gaston, 2006; Schneider et al., 2017). These kind of approaches, besides providing information on the variability of PTs, do not provide a direct link to the EFPs. Conversely, the relation of F to both the variability of PTs and the physiology suggests its potential as a novel synthetic metric for mapping the functional diversity.

1.1 OBJECTIVES

The main objective of this Ph.D. was the exploitation of hyperspectral remotely sensed data in the optical domain to advance the understanding of vegetation functioning. In particular, this research explored the relationship between vegetation optical properties of vegetation, PTs and EFPs describing the ecosystem functioning measurable from RS. The link between PTs, EFPs and vegetation optical properties was analysed and fully explained using a high spectral and spatial resolution dataset of RS data collected in the same focus area (*i.e.*, a temperate forest ecosystem) with multiple sensors. In particular, the research focused on the use of innovative RS techniques applied to reflectance and fluorescence airborne-derived images as well as of state-of-the-art process-based models.

The specific objectives of this research can be summarised as follows:

i. To map the distribution of the dominant tree species in a mixed forest ecosystem using multi-temporal hyperspectral images acquired with the APEX airborne sensor (Chapter 2);

ii. To explore the spatial relationship between red and far-red F derived from high spatial and spectral resolution data collected with the *HyPlant* airborne

sensor over a forest ecosystem and process-based EFP estimates obtained driving an ecophysiological model with airborne-derived spatially resolved PTs (Chapter 3);

iii. To test the potential of a novel indicator of the functional diversity in a forest ecosystem based on the use of entropy metrics applied to *HyPlant*-derived far-red F images (Chapter 4).

1.2 THESIS OUTLINE

This Ph.D. thesis is organised as a collection of three scientific papers, each one presented in a dedicated chapter with its own introduction, material and methods, results, discussion, conclusions and references.

Although with different research questions and objectives, all the analyses presented in this thesis are based on a dataset acquired during a field campaign supporting the selection of the FLuorescence EXplorer (FLEX) satellite mission as the 8th Earth Explorer mission of the European Space Agency (ESA). The campaign was organised in 2013 in the Hardt forest, a mid-latitude mixed forest located in Alsace, France. A comprehensive dataset including airborne hyperspectral acquisitions using the APEX and *HyPlant* imaging sensors, UAV acquisitions and ground measurements for calibration and validation activities was collected during the campaign and constitutes the source of all the analyses presented in this thesis.

Chapter 1 is a general introduction, in which the framework of the Ph.D. project and the overall and specific objectives are presented.

In Chapter 2, the activities addressing the first objective of this Ph.D. research, aiming at mapping the distribution of the dominant tree species within the Hardt forest based on APEX data are presented. The classification of remotely sensed images is a widespread topic in remote sensing. In this study, the potential of using airborne images acquired in correspondence of different phenological stages was evaluated.

In Chapter 3, the second objective of this Ph.D. research is presented. The study focused on four main activities: firstly, the retrieval of ground-validated maps of F at the red and far-red emission peaks from *HyPlant* ultra-fine resolution images using spectral fitting methods; secondly, the retrieval of ground-validated maps of key PTs from *HyPlant* hyperspectral reflectance using an optimised inversion of radiative transfer models; thirdly, the modelling of gross primary productivity (GPP), absorbed photosynthetically active radiation (APAR) and light use efficiency (LUE) using a process-based model driven with the obtained airborne-derived PTs; fourthly, the analysis of the variability of the ecosystem functioning

at detailed scale by exploring the spatial relationship between measured F and modelled GPP, APAR and LUE.

In Chapter 4, the outcomes of the activities addressing the third objective of this thesis are presented. This study explored the possibility of defining a novel indicator of the ecosystem functional diversity based on F. To this end, traditional and innovative entropy metrics were applied to F, to a traditional vegetation index calculated on reflectance (*i.e.*, NDVI) and to a map of functional traits obtained as a combination of key PTs retrieved using radiative transfer model inversion. The results were compared to investigate if F can be a better descriptor of the functional diversity compared to traditional indices.

Chapter 5 concludes this thesis by summarising the main findings of this research and proposing suggestions for future work.

2 FOREST SPECIES MAPPING USING AIRBORNE HYPERSPECTRAL APEX DATA

ABSTRACT

[1] Accurate mapping of forest species is a very important task in relation to the increasing need to better understand forest ecosystem role within environmental dynamics. Objective of this work is the investigation of the potential of a multi-temporal hyperspectral dataset for the production of a thematic map of the dominant species in the Forêt de Hardt (France). Hyperspectral data were collected in June and September 2013 using the Airborne Prism EXperiment (APEX) sensor covering the visible, near-infrared and shortwave infrared spectral regions with a spatial resolution of 3×3 m. The map was realized by means of a maximum likelihood supervised classification. The classification was first performed on June and September images separately and then on the two images together. Class discrimination was performed using as input three spectral indices computed as ratios between red edge bands and a blue band for each image. The map was validated using a testing set selected on the basis of a random stratified sampling scheme. Results showed that the algorithm performances improved from an overall accuracy of 59.5% and 48%, for the June and September images respectively, to an overall accuracy of 74.4%, with producer's accuracy ranging from 60% to 86% and a user's accuracy ranging from 61% to 90% when both images (June and September) were combined. This study demonstrates that the use of multi-temporal high-resolution images acquired in two different vegetation development stages (*i.e.*, 17th June 2013 and 4th September 2013) allows to obtain

1 The content of this chapter is published on Miscellanea Geographica - Regional Studies on Development as: Tagliabue, G., Panigada, C., Colombo, R., Fava, F., Cilia, C., Baret, F., Vreys, K., Meuleman, K., Rossini, M. 2016, "Forest species mapping using airborne hyperspectral APEX data", *Miscellanea Geographica, Regional Studies on Development*, vol. 20, no. 1, pp. 1-6

accurate (overall accuracy 74.4%) local-scale thematic products in an operational way.

2.1 INTRODUCTION

Forests play a key role in local and global scale environmental dynamics, therefore, the temporal and spatial monitoring of their functioning is critical for the purpose of efficient and sustainable management (Linke et al., 2006). In this context, remote sensing (RS) is a very useful tool compared with traditional surveying techniques, as it allows the production of large scale digital thematic maps in a fast and accurate way (Franklin, 2001; Panigada et al., 2010). In particular, the composition and distribution of forest ecosystems is a fundamental factor within carbon, nitrogen and water biogeochemical cycles. For this reason, the accurate mapping of forest species is a very important task. In the last few years, several studies have been carried out using different RS sensors, evaluating the potentialities of both passive sensors (*i.e.*, multispectral and hyperspectral sensors) and active systems (*i.e.*, Light Detection and Ranging (LiDAR) and Synthetic Aperture Radar (SAR) systems).

In case of sparse canopy, such as urban vegetation (Alonzo, Bookhagen, and Roberts, 2014) and Savannah (Cho et al., 2012; Colgan et al., 2012), or dense canopy characterized by species with different heights or dominated by definable growth stages (Dalponte, Bruzzone, and Gianelle, 2008, 2012; Jones, Coops, and Sharma, 2010; Kempeneers et al., 2014), best results in species classification were obtained by integrating hyperspectral data with the information about tree height and canopy structure supplied by LiDAR data. Conversely, in mixed forests with closed canopy and a single dominant layer Ghosh et al. (2014) evidenced that the canopy height provided by LiDAR data did not affect significantly the mapping accuracy. In these conditions, the use of hyperspectral data alone showed good results using either a traditional algorithm such as Maximum Likelihood (ML) applied on selected indices in order to reduce spectral dimensionality (Boschetti et al., 2007; Pandey, Tate, and Balzter, 2014), or more sophisticated approaches such as the vector machines (Marcinkowska et al., 2014), with higher accuracy level for higher spatial resolution (Baldeck et al., 2015; Clark, Roberts, and Clark, 2005; Dalponte et al., 2013).

The objective of this study was to investigate the operational use of Airborne Prism EXperiment (APEX) images for tree species mapping in a complex mixed forest ecosystem. APEX images were acquired on the Forêt de Hardt (Mulhouse, France) with a spatial resolution of 3 m in June and September 2013. Given the fact that an image segmentation to detect single tree crowns was not feasible in a closed

canopy forest at this spatial resolution, pixel based classification algorithms were investigated. The possibility to improve species spectral discrimination through the combination of the spectral information derived from images acquired during two different phenological development stages (*i.e.*, growing season and incipient senescence) was evaluated and results were discussed.

2.2 MATERIAL AND METHODS

2.2.1 Remotely sensed data collection and processing

Remotely sensed data were acquired with the hyperspectral airborne push broom imaging spectrometer Airborne Prism EXperiment (APEX), developed by a Swiss-Belgian consortium on behalf of the European Space Agency (ESA). APEX covers a wide spectral range from the visible to the shortwave infrared region of the spectrum (380-2500 nm) with 288 narrow bands, which allows a detailed characterization of the spectral response of different surfaces.

Data were acquired over the Forêt de Hardt on 17th June 2013 and 4th September 2013 at 12:30±30 local solar time (LST), with APEX flying at about 6000 m height, which results in a 3 m ground spatial resolution. To cover the entire study area, 7 flight lines with 30% lateral overlap were planned with a track in the principal solar plane (195.3°), in order to minimize shadow effects.

Radiometric calibration of the APEX data was performed through a dedicated software developed and maintained by the APEX consortium, using as input the calibration cubes generated from data collected before the flight season on the APEX Calibration Home Base (Deutsches Zentrum für Luft- und Raumfahrt (DLR), Oberpfaffenhofen, Germany) and the dark current data collected in-flight. Following the regular radiometric calibration, a vicarious calibration was applied to the spectral regions suffering from slightly higher calibration uncertainties, *i.e.*, the region around 1030 nm and the end of the SWIR (1300-2500 nm). This was based on four artificial targets (two black, one grey and one white) made of PVC coated canvas material ('Odyssey' trademark material, from Kayospruce Ltd., UK) and some 'pseudo-invariant' features: concrete, asphalt with different brightness and pit material. Their radiance and reflectance were measured with an ASD spectrometer simultaneously with the APEX overflights.

Spectral misregistrations were detected for every across track pixel, following a spectrum-matching technique (Gao, Montes, and Davis, 2004) that was applied on the continuum removed at sensor radiance across selected atmospheric absorption features.

Geometric processing of the APEX data was performed by means of direct georeferencing, using a dedicated software developed by VITO (Vlaamse Instelling voor Technologisch Onderzoek). Direct georeferencing requires the knowledge of the position and look direction of the sensor, and the elevation data to adjust for the topographic relief.

The position and orientation of each image scan line was obtained from the post-processed GPS (Global Positioning System) and IMU (Inertial Measurement Unit) data. Angular offsets in X, Y and Z directions between the APEX and IMU frame were determined through a boresight calibration and accounted for in the boresight misalignment angles. The elevation data were originated from a DTM (Digital Terrain Model) of the Mulhouse region at 25 m horizontal resolution. From this data, the geographic location and the sun-viewing geometry was calculated for every image pixel. The resulting absolute geolocation accuracy was found to be at sub-pixel level.

The data were projected to UTM zone 32N, WGS84, with a spatial resolution of 3 $\times$ 3 m. The USGS (United States Geological Survey) GCTP (General Cartographic Transformation Package) was used for the coordinate projection, while the nearest neighbour method was applied for the spatial resampling.

2.2.2 Species classification method

The forest species map was realized on the North portion of the Forêt de Hardt, where the ground surveys were conducted. A spectral endmember set was selected in order to train the algorithm to identify and assign all the pixels of the image to the proper class, as required by a supervised classification approach. The tree species present in the study area were identified by forest experts through a ground survey conducted over an extensive area. The forest experts visually evaluated the species composition in 42 elementary sampling units (ESU) of 20 $\times$ 20 m, considering all the species representing more than 5% of the leaf area of the ESU. The centre of the ESU was geo-located by means of a high precision global positioning system Trimble Geo-XT (Trimble, California, USA). Out of the dominant species found, five - hornbeam (*Carpinus betulus* L.), oak (*Quercus petraea* (Matt.) Liebl., *Quercus robur* L.), linden (*Tilia* L.) and pine (*Pinus* L.) – were identified as the most present. These forest species together represent on average the 93% of each ESU. Therefore, they were accounted in the production of the forest species map. Other species were not taken into account due to the fact that they were identified only in few ESU (*e.g.*, maple - *Acer campestre* L., *Acer platanoides* L.) or they were mainly found as single trees (*e.g.*, larch - *Larix decidua* Mill.). The endmember set was selected on the APEX images by integrating visual interpretation

of high resolution orthophotos and ground surveys. It included a total of ~400 pixels distributed among the four forest species. For each species, homogeneous polygons composed of ten to twelve pure vegetation pixels – selected on two to three crowns, based on the crown dimension – were defined within several ESU (Table 1). An example of crown pixel selection is depicted in Figure 1. Each polygon was considered as a separate spectral class in the classification process in order to take into account the intrinsic spectral variability of the species over the study area. The spectral classes belonging to the same species were then merged in the post-classification process. *Quercus petraea* (Matt.) Liebl. and *Quercus robur* L. were considered as the same classification unit (Table 1), due to their spectral similarity. An additional class "shadow", that accounts for the plant inter-crown shadows, was included in the spectral endmember set. Hence, the spectral endmember set was used to train a ML algorithm to distinguish the different forest species. Solely spectral indices (*i.e.*, APEX band ratios) based on the red edge portion of the spectrum (*i.e.*, 680-750 nm) were used as input of the ML algorithm, in order to avoid information redundancy that may decrease the classification accuracy (Hughes, 1968). The spectral indices selected in this study were proposed by Boschetti et al. (2007) in a previous work on the classification of deciduous tree species in the Ticino Park (Italy) using airborne hyperspectral data (Boschetti et al., 2007). Three indices expressed as band ratios between APEX bands 45 (659.2 nm), 58 (701.6 nm) and 68 (740.2 nm) and band 7 (480.8 nm) were calculated on June and September APEX radiance images. The indices selected were located in the red edge because spectral differences in this region mirror differences in photosynthetic pigments and canopy greenness that vary between species and within their phenological cycle (Filella and Penuelas, 1994; Horler, Dockray, and Barber, 1983; Hu et al., 2008; Zarco-Tejada and Miller, 1999). The ratio with the blue band is useful to correct for atmospheric effects.

The multi-temporal endmember set used to train the ML algorithm is shown in Figure 2). Since APEX images were acquired in two different vegetation phenological development stages, the classification was first performed on June and September images separately and then on the jointed images in order to assess the improvement on the classification accuracy of the multitemporal information. The maps obtained were slightly filtered in order to improve the clarity of the thematic product; isolated pixels were identified by the sieve class function (ENVI 5.0, ITT Visual Information Solution, Boulder, USA). Then, a majority analysis was used to assign these spurious pixels to the major class considering a 3×3 kernel.

Finally, the maps were validated using a testing set composed of 250 pixels selected on the basis of a random stratified sampling scheme, taking into account the unequal distribution of the classes. The number of testing pixels for each class reflected the size of that class: 90 testing pixel were randomly selected for

Table 1: Characteristics of the endmember set: for each class, the number of ESUs in which pixels to assembly the spectral endmember set were selected and the number of pixels per ESU collected are reported.

Forest species	Classification unit	N of ESU	N of pixels per ESU
Carpinus betulus L.	Hornbeam	12	10
Quercus robur L., *Quercus petraea* (Matt.) Liebl.	Oak	4	10
Tilia L.	Linden	2	12
Pinus L.	Pine	6	10
-	Shadow	3	50

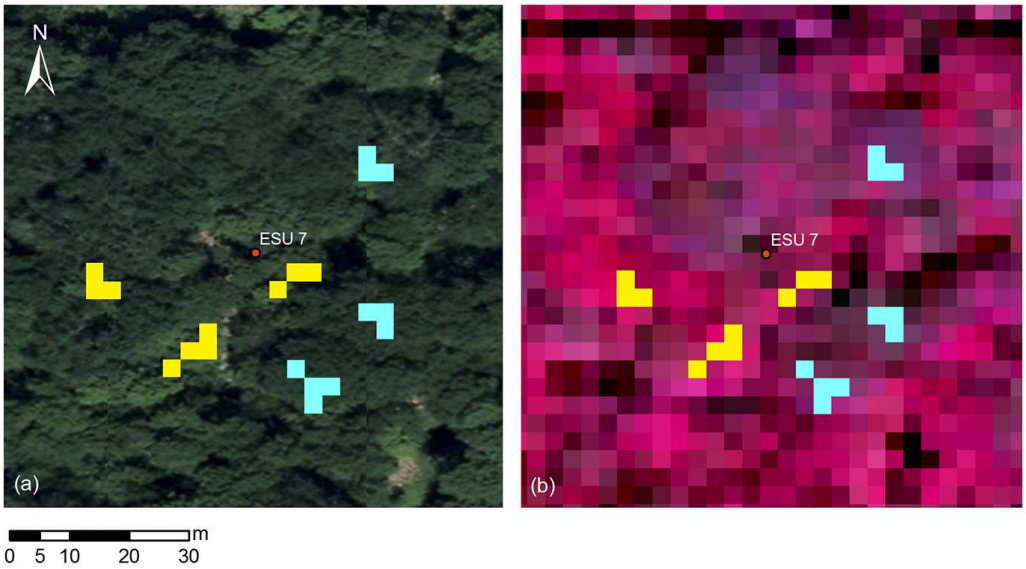

Figure 1: Example of the spectral endmember collection for the training of the Maximum Likelihood (ML) algorithm: pure crown pixel of hornbeam (yellow) and oak (cyan) identified on a) high resolution orthophoto and b) APEX false colour image (APEX bands 92, 42, 16).

hornbeam, 100 for oak, 20 for linden, 20 for pine and 20 for shadow. The testing pixels were labelled by visual interpretation of high resolution orthophotos and used as ground truth in the validation process. The classification performances were then evaluated by computing the Overall Accuracy (OA), the Producer's Accuracy (PA) and the User's Accuracy (UA) of the map. OA was calculated as the ratio between the sum of pixels that are classified in the correct class and the total number of testing pixels. PA refers to the probability that the classifier has labelled a pixel into a class given that the ground truth is that class. It was computed for each class as the ratio between the number of correctly classified pixels and the total number of testing pixels for that class. UA refers to the probability that a pixel belong to a class given that the classifier has labelled it into that class. It was calculated for each class as the ratio between the number of correctly classified pixels and the total number of pixels that were assigned to that class.

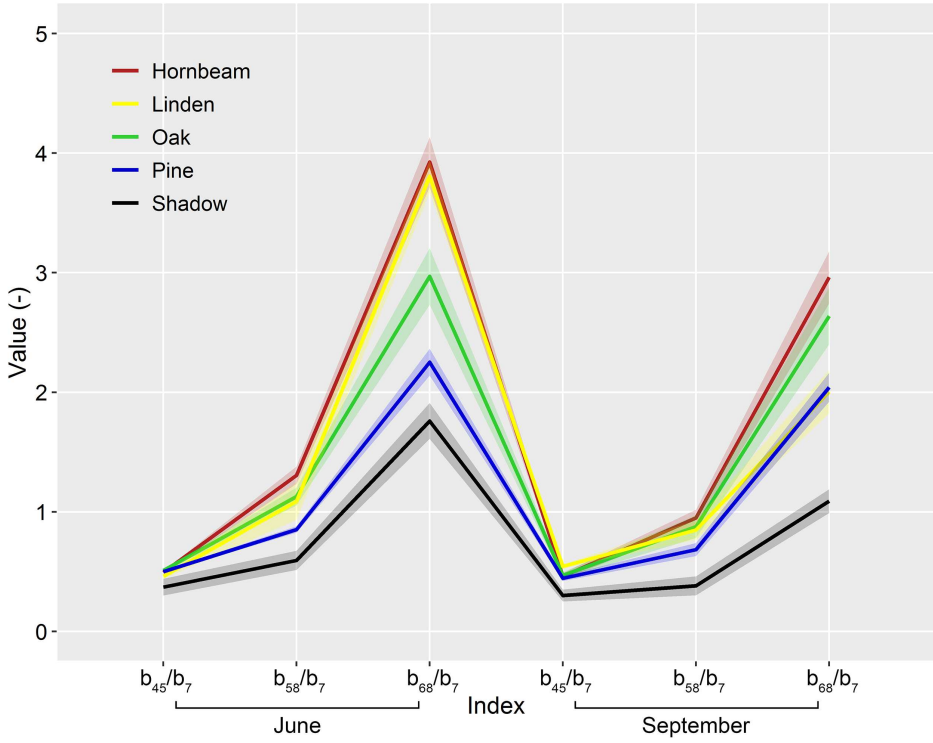

Figure 2: Spectral endmember set used to train the Maximum Likelihood (ML) algorithm in order to classify the different forest species.

2.3 RESULTS

The classification process enabled the production of thematic maps of the most present forest species in the Forêt de Hardt. The classification accuracy was assessed on the maps obtained using as input: i) only the image acquired in June, ii) only the image acquired in September, and iii) June and September images together. Results of the classification performed with only one image as input, showed better results with the June image (OA = 59.5%), than with the September one (OA = 48%). This may be explained by the fact that the vegetation in June is in its maximum seasonal development stage and the illumination conditions are better (*i.e.*, maximum solar elevation that minimizes shadows effects). June image, though, did not allow an accurate classification of linden, that showed high commission errors with hornbeam (UA = 36%), while in September the incoming senescence allowed a better discrimination of linden from hornbeam (UA = 53%). The use of both images improved significantly the classification result (OA = 74.4%), confirming that the use of multitemporal images supplies additional information, leading to a better spectral class discrimination. PA and UA also showed an improvement for all the classes, with PA ranging from 60% to 86% and UA ranging from 61% to 90%, except for pine PA that decreased from 85% to 80%. This may be again explained by the lighting conditions that were not optimal in September, with shadow effects affecting the conifer canopies more than deciduous ones.

The confusion matrix obtained crossing the ground truth data with the results of the multi-temporal classification is shown in Table 2. An example of the best classification result obtained using the multi-temporal information is depicted in Figure 3. The map shows a sharp predominance of hornbeam-oak association, climax of the area, while the distribution of pine and linden is more restricted.
In previous studies, higher accuracy levels were achieved in case of higher spatial resolution (1 m or less), with OA close to 90% for pixel-based classifications, and up to 95% when individual tree classification was conducted (Baldeck et al., 2015; Clark, Roberts, and Clark, 2005; Dalponte et al., 2013). OA consistent with our results are shown in previous studies with lower spatial resolution ($\geqslant$ 3 m). Boschetti et al. (2007) in a similar mixed forest ecosystem evidenced that classes with lower accuracy are those whose fragmentation is higher, such as the typical association *Quercus robur* L.-*Carpinus betulus* L.. This is confirmed by our results: the commission error between oak and hornbeam classes is in fact higher compared to the one with other classes (*i.e.*, pine and linden). Marcinkowska et al. (2014) used APEX images with spatial resolution up to about 2 m to map vegetation communities more than single tree species, confirming that, at this spatial resolution, it is worth to scale up at community level more than at tree species level

Table 2: Confusion matrix obtained crossing the reference data with the classification result. In each cell the value is expressed as number of pixels (top) and percentage (bottom). The last line and column represent Producer's Accuracy (PA) and User's Accuracy (UA) respectively.

		Testing set						
		Hornbeam	Oak	Linden	Pine	Shadow	Tot	UA
APEX classification	Hornbeam	78 70.91%	9 12.68%	3 15.79%	0 0%	0 0%	90 36%	78/90 86.67%
	Oak	30 27.27%	61 85.92%	3 15.79%	1 5%	5 16.67%	100 40%	61/100 61%
	Linden	2 1.82%	1 1.41%	13 68.42%	1 5%	3 10%	20 8% 65%	13/20
	Pine	0 0%	0 0%	0 0%	16 80%	4 13.33%	20 8%	16/20 80%
	Shadow	0 0%	0 0%	0 0%	2 10%	18 60%	20 8%	18/20 90%
	Tot	110 100%	71 100%	19 100%	20 100%	30 100%	250 100%	
	PA	78/110 70.91%	61/71 85.92%	13/19 68.42%	16/20 80%	18/30 60%		OA = 74.4% k = 0.6374

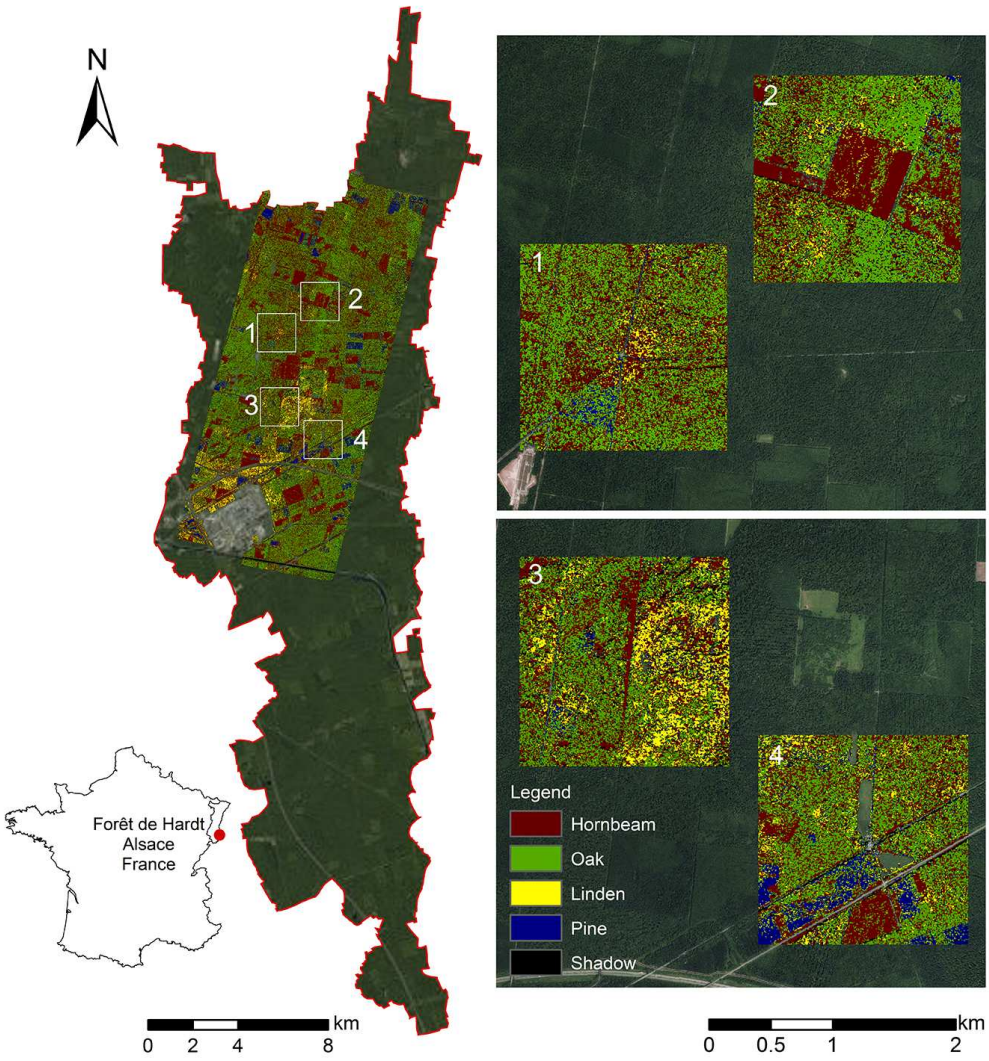

Figure 3: Example of the thematic map that represents the four most common dominant tree species in the Forêt de Hardt.

in order to improve vegetation mapping accuracy. Despite this, the use of multi-temporal images allowed to obtain a reliable thematic product, which quality can also be visually appreciated (Figure 4).

2.4 CONCLUSIONS

In this paper, APEX images at 3 m resolution were used to map forest species in the Forêt de Hardt (Mulhouse, France), a mixed forest ecosystem. The use of an operational algorithm, the ML, was improved by the selection of spectral bands combined in ratio indices sensitive to plant pigment content. We demonstrated that the combination of multi-temporal images in the classification process led to a good accuracy level (OA = 74% in forest species mapping. Conversely, with only one APEX overpass and a spatial resolution of 3 m the accuracy level of species classification was significantly lower (OA < 60%). As a matter of fact, the availability of two images: the first one acquired when vegetation was in its maximum development stage and the second one when senescence was incoming, allowed the detection of variations in the spectral response linked to species-specific phenological development that improved significantly the map accuracy. However, we underline that a flight later in the season would be suggested in order to emphasise the spectral differences between oak and hornbeam. The use of the multi-temporal information was made possible by the high APEX absolute geo-location accuracy (*i.e.*, sub-pixel level), that ensured a good overlapping of the images acquired at different moments. This confirmed the good quality of APEX data and its valuable use in forest applications. In order to improve the classification accuracy through the mapping of individual trees a higher spatial resolution (about 1 m) is suggested.

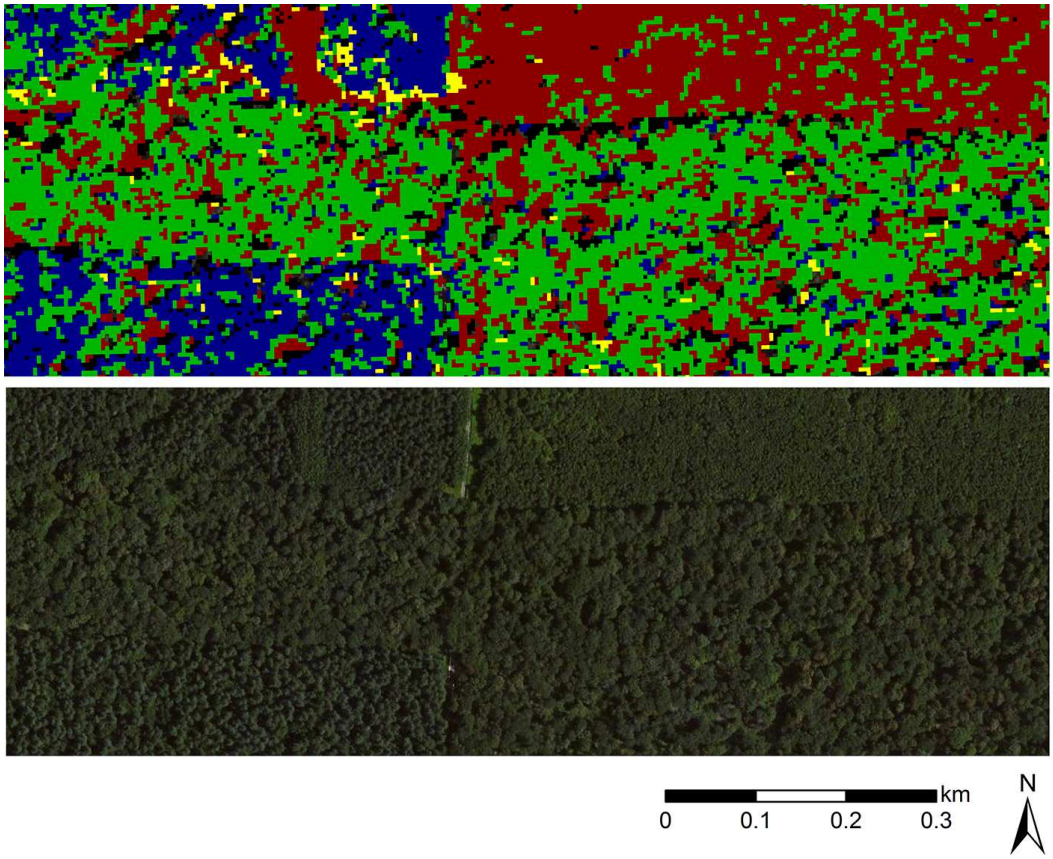

Figure 4: Detail of the thematic product obtained: a) Forest species map; b) High resolution orthophoto of the same area.

3 EXPLORING THE SPATIAL RELATIONSHIP BETWEEN AIRBORNE-DERIVED RED AND FAR-RED SUN-INDUCED FLUORESCENCE AND PROCESS-BASED GPP ESTIMATES IN A FOREST ECOSYSTEM

ABSTRACT

[1] Terrestrial gross primary productivity plays an essential role in the global carbon cycle, but the quantification of the spatial and temporal variations in photosynthesis is still largely uncertain. Our work aimed at investigating the potential of remote sensing to provide new insights into the plant actual photosynthesis at fine spatial resolution. This was achieved exploiting high-resolution images acquired with the FLEX airborne demonstrator *HyPlant*. The sensor was flown over a mixed forest and the images collected were elaborated to obtain two independent estimates of plant photosynthesis. Firstly, maps of sun-induced chlorophyll fluorescence (F), a novel indicator of plant photosynthetic activity, were successfully obtained at both the red and far-red peak ($r^2 = 0.74$, $p < 0.001$ and $r^2 = 0.73$, $p < 0.001$, respectively, compared to top-of-canopy ground-based measurements acquired synchronously with the overflight) over the forested study area. Secondly, maps of gross primary productivity (GPP) and absorbed photosynthetically active radiation (APAR) were derived using a customised version of the coupled biophysical model Breathing Earth System Simulator (BESS). The model driven with airborne-derived maps of key forest traits (*i.e.*, leaf chlorophyll content (LCC) and leaf area index (LAI)) and meteorological data provided a high-resolution snapshot of the variables of interest across the study site. LCC and LAI were accurately estimated (RMSE = 5.66 $\mu g\, cm^{-2}$ and RMSE = 0.51 $m^2\, m^{-2}$, respectively) through

1 The content of this Chapter has been submitted to Remote Sensing of Environment as: Tagliabue, G., Panigada, G., Dechant, B., Baret, F., Cogliati, S., Colombo, R., Migliavacca, M., Rademske, P., Schickling, A., Schüttemeyer, D., Verrelst, J., Rascher, U., Ryu, Y., Rossini, M. "Exploring the spatial relationship between airborne-derived red and far-red sun-induced fluorescence and process-based GPP estimates in a forest ecosystem" and is currently under review.

an optimised Look-Up-Table based inversion of the PROSPECT-4-INFORM radiative transfer model, ensuring the accurate representation of the spatial variation of these determinants of the ecosystem's functionality. The spatial relationships between measured F and modelled BESS outputs were then analysed to interpret the variability of ecosystem functioning at regional scale. Results showed that far-red F is significantly correlated with GPP ($r^2 = 0.46$, $p < 0.001$) and APAR ($r^2 = 0.43$, $p < 0.001$) in the spatial domain, and that this relationship is nonlinear. Conversely, no statistically significant relationships were found between red F and GPP or red F and APAR ($p > 0.05$). The spatial relationships found at high resolution constitute a valuable insight into the critical role of the spatial heterogeneity in controlling the carbon uptake, entailing the need to take it into account at coarser resolution.

3.1 INTRODUCTION

Photosynthesis is the primary process supporting life on Earth. Terrestrial plants exchange CO_2 with the atmosphere through this process, thereby playing a major role within the global carbon cycle (Beer et al., 2010; Heimann and Reichstein, 2008). The carbon sequestration capacity is the result of complex and interconnected dynamics that counterpose in a delicate balance (Cao and Woodward, 1998; Schimel, 1995). Global change is altering this balance, with consequences on the functioning of the Earth system (Ciais et al., 2013; Zhu et al., 2016). This is fostering the quantification of the exact magnitude of these processes, which is still largely unknown (Heimann and Reichstein, 2008; Schimel et al., 2015).

Recent advances in remote sensing of sun-induced chlorophyll fluorescence (F) disclosed unprecedented opportunities in the large-scale monitoring of terrestrial vegetation. F is a faint electromagnetic signal emitted in the red and far-red spectral regions (*i.e.*, 650-800 nm) by the core of the photosynthetic machinery to dissipate the excess of absorbed solar radiation (Papageorgiou and Govindjee, 2004). Photochemistry competes with heat dissipation and F emission for the absorbed radiation. Therefore, measurements of energy de-excitation pathways (*i.e.*, fluorescence and heat dissipation) are expected to provide an indirect assessment of photochemical efficiency (Baker, 2008). This link constitutes the rationale behind the use of F to infer the actual functional status of the photosynthetic machinery.

Although there is a solid evidence of this relationship at sub-cellular to leaf scale due to considerable efforts undertaken using active fluorescence techniques (Baker, 2008; Genty, Briantais, and Baker, 1989; Porcar-Castell et al., 2014), the relationship between passive fluorescence and photosynthesis at the canopy scale is still hazy and the underlying mechanisms need to be fully understood. Lately, various studies showed strong empirical linear relationships (even though in some cases

biome dependent) between F and gross primary production (GPP), which represents the carbon fixation by terrestrial plants via photosynthesis (*e.g.*, Frankenberg et al. 2011; Guanter et al. 2012; Li, Xiao, and He 2018; Sun et al. 2017; Yang et al. 2015), but several knowledge gaps still exist. The majority of these studies was based on the exploitation of space-based retrievals of F from high spectral resolution spectrometers onboard satellites deployed for atmospheric studies, *e.g.*, the Global Ozone Monitoring Experiment 2 (GOME-2) (Munro et al., 2016), the TANSO Fourier Transform Spectrometer (Hamazaki, Kaneko, and Kuze, 2004) and the Orbiting Carbon Observatory-2 (Frankenberg et al., 2015). These sensors opened the possibility to observe F from space but their coarse spatial resolution - from 2 to 80 km - and in some cases sparse spatial sampling is unsuitable to capture the heterogeneity of terrestrial ecosystems. This aspect strongly limited the investigation of the spatial variability of F and GPP.

GPP is the most direct available proxy of photosynthesis, but the uncertainties related to its modelling at the global scale hamper an accurate quantification of the imprint of plants on the carbon cycle. Current models for the quantification of terrestrial GPP (*e.g.*, Beer et al. 2010; Jung et al. 2011; Knorr 2000; Ryu et al. 2011; Tol et al. 2009; Tramontana et al. 2016) are characterised by an advanced process understanding. However, uncertainties in the carbon flux modelling come from the structure of the model employed, the quality of the meteorological forcings and most importantly, from the adequacy of the model parameterisation. Regardless of the typology (*i.e.*, data-driven or process-based model), the effectiveness of these models is in fact severely conditioned by the accuracy of the input parameters (Friedlingstein et al., 2014; Houborg et al., 2015; Jung et al., 2007), that vary across space and over time (Rogers et al., 2017).

Incorporating into the models accurate spatially and temporally resolved plant trait-related information might bridge this gap. As a matter of fact, the variability of plant traits (*e.g.*, leaf chlorophyll content (LCC), leaf area index (LAI)) constitutes a determinant of the ecosystem functionality, that must be taken into account to better constrain the flux estimation (Bodegom et al., 2012; Butler et al., 2017). Regardless of its importance, this aspect was mostly neglected in previous studies due to the lack of adequate spatio-temporal data. The increasing availability of remote sensing (RS) observations might overcome this limitation, as RS is capable of providing plant trait-related information at suitable temporal and spatial scales (Homolová et al., 2013; Schimel et al., 2015).

The retrieval of plant traits from RS observations advanced significantly over the last decades due to a considerable effort posed in the development and testing of multiple retrieval methods (for a review, see Verrelst et al. 2015a, 2018). Among the retrieval algorithms, the inversion of physically-based radiative transfer models (RTMs) is generally considered the most reliable approach (Atzberger et al.,

2015; Dorigo et al., 2007). RTMs exploit physical laws to describe the interactions between the incident solar radiation and the vegetation medium. Being based on a physical relationship between measured radiometric signal and plant traits, the inversion of these models constitutes an accurate, robust and generic approach for plant trait retrievals (Atzberger et al., 2015; Dorigo et al., 2007; Houborg et al., 2015; Verrelst et al., 2015c).

Regardless of the progresses achieved, the retrieval of plant traits remains challenging. Their quantitative estimation is hampered by the influence of various confounding factors (Wang et al., 2018; Zarco-Tejada et al., 2004). In physically-based frameworks, the main challenge is represented by the regularisation of the undetermined and ill-posed nature of the inverse problem (Houborg et al., 2015). Multiple combinations of plant traits might yield analogous simulated spectra, resulting in non-unique solutions. Furthermore, the uncertainties affecting both the model and the data may be source of large inaccuracies in the modelled reflectance (Baret and Buis, 2008; Combal et al., 2002; Houborg et al., 2015). Hence, adequate model parameterisation and regularisation strategies are critical to mitigate the drawbacks of ill-posedness and to obtain trustworthy results (Combal et al., 2002; Houborg, Fisher, and Skidmore, 2015; Verrelst et al., 2014, 2015c). Several studies recognised the importance i) of using prior information to reduce the variability of the input parameters (*e.g.*, Baret and Buis 2008; Darvishzadeh et al. 2008; Malenovský et al. 2006; Meroni, Colombo, and Panigada 2004), ii) of adding noise to the simulated spectra to account for uncertainties in both the model and the data (*e.g.*, Kötz et al. 2005; Richter et al. 2009) and iii) of using multiple solutions of the inversion to regularise the inversion (*e.g.*, Atzberger and Richter 2012; Combal et al. 2002; Kötz et al. 2005). Conversely, the impact of using alternative cost functions to match simulated and measured reflectance has been poorly investigated (Rivera et al., 2013; Verrelst et al., 2014). In this framework, this work aimed at investigating the potential of RS to provide new insights into the actual plant photosynthesis. High-resolution airborne hyperspectral images acquired with the *HyPlant* sensor (Rascher et al., 2015) over a mixed forest were used to provide two independent estimates of plant photosynthesis: red and far-red F on the one hand, GPP on the other. This comprehensive high-resolution analysis was made possible by the characteristics of the *HyPlant* sensor, deployed as airborne demonstrator of the forthcoming FLuorescence EXplorer (FLEX) satellite (Drusch et al., 2017): the sensor was in fact specifically designed to acquire simultaneously sub-nanometric spectral information in the 650-800 nm spectral region and hyperspectral information between 400 and 2500 nm, providing the means to retrieve F as well as to obtain hyperspectral reflectance.

We explored the possibility to:

i. Obtain high resolution ground-validated maps of both red and far-red F from airborne ultra-fine spectral resolution imagery using the spectral fitting method (SFM) (Cogliati et al., 2015);

ii. Obtain high resolution ground-validated maps of key forest traits (*i.e.*, LCC and LAI) from airborne hyperspectral imagery through an optimised RTM inversion;

iii. Obtain high resolution maps of GPP, absorbed photosynthetically active radiation (APAR) and light use efficiency (LUE) through a modelling approach based on the use of the aforementioned airborne-derived spatially resolved traits to drive a process-based ecophysiological model - the Breathing Earth System Simulator (BESS) (Jiang and Ryu, 2016; Ryu et al., 2011) - with the ultimate goal of:

iv. Exploring the spatial relationship between measured F and modelled BESS outputs at high resolution, in order to interpret the variability of ecosystem functioning at regional scale.

3.2 DATA AND METHODS

3.2.1 Study Site

The study was conducted on a mid-latitude plain mixed forest (Hardt Forest) located in France (47°48'29" N, 7°26'53" E; Mulhouse; Alsace). The analysis focused on an area of ~90 ha located in the northern part of the forest, corresponding to a subset of the total area covered by the airborne overpasses (Figure 5). The climate of the region is temperate, with an average temperature of 22°C in summer and of 4 °C in winter. The mean annual rainfall is 680 mm distributed throughout the year, with a prevalence between May and August.

The forest covers ~13000 ha and is relatively managed, with stands of at least 500 m size characterised by a relatively large variability in terms of forest age. Overall, the fraction of deciduous and coniferous tree species is about 90% and 10%, respectively. The dominant canopy layer is characterised by the presence of European hornbeam (*Carpinus betulus* L.), pedunculate and sessile oak (*Quercus robur* L., *Quercus petraea* (Matt.) Liebl.), field maple (*Acer campestre* L.), small-leaved linden (*Tilia cordata* Mill.), Scots pine (*Pinus sylvestris* L.) and European larch (*Larix decidua* Mill.).

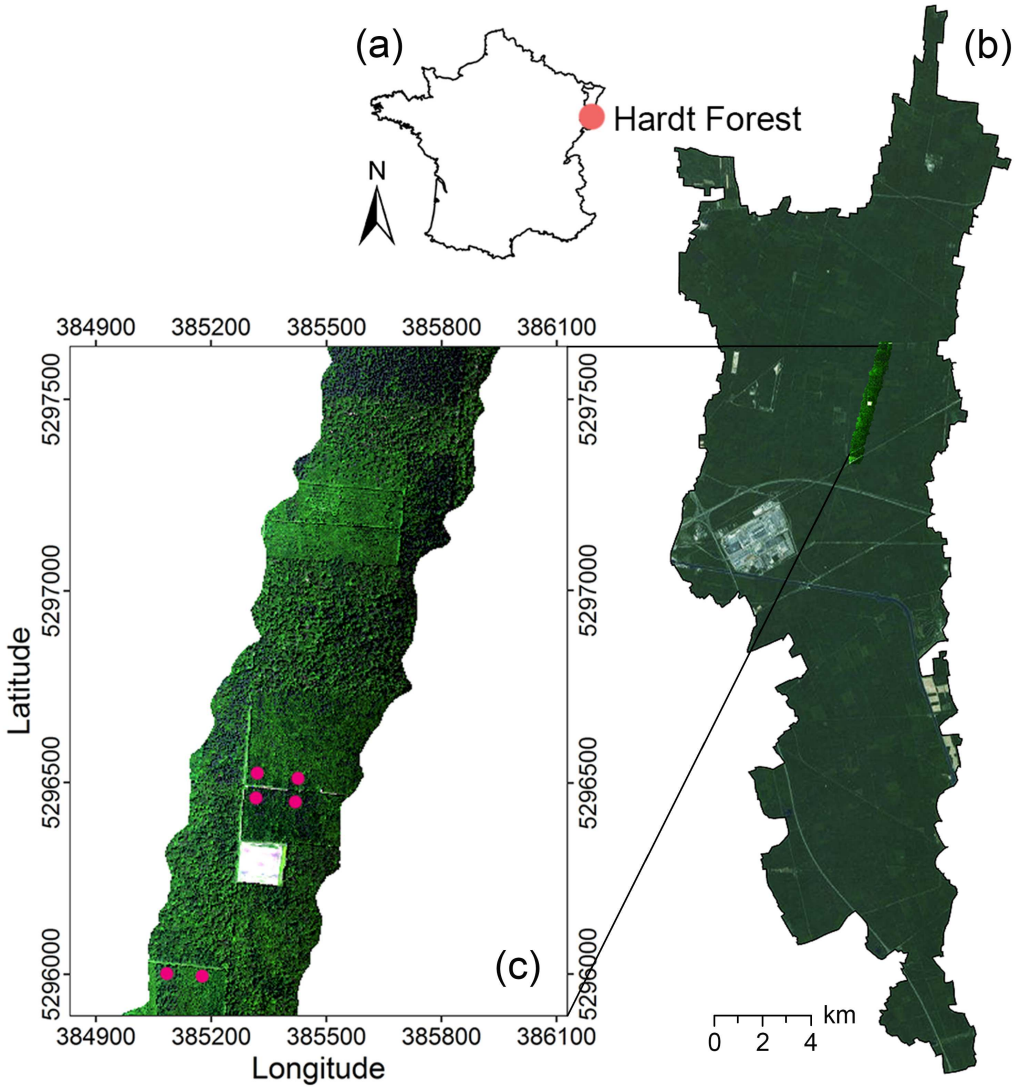

Figure 5: a) Location of the Hardt Forest in Alsace, France; b) Hardt Forest and location of the *HyPlant* flightline used in this study (RGB true colour composite); c) Zoom of the *HyPlant* image and location of the sites where top-of-canopy spectral measurements were collected (purple dots).

3.2.2 Field spectral measurements and plant traits data collection

A field campaign aiming at near-simultaneously collecting spectral measurements, plant traits and ancillary meteorological data was conducted in the summer of 2013.

Top-of-canopy high resolution radiance measurements were acquired on 16th June 2013-17th June 2013 and 2nd July 2013 around midday (10:00-15:00 solar time) under clear-sky conditions using portable spectroradiometers operating in the visible and near-infrared regions. The system included three different instruments (HR4000, HR4000, QE65000; Ocean Optics, Dunedin, USA) characterised by different spectral ranges and resolutions: the first one covering the spectral range 350-1050 nm with a full width at half maximum (FWHM) of 1 nm for reflectance and vegetation indices computation; the second (spectral range 700-800 nm, FWHM = 0.1 nm) and third (spectral range 657-740 nm, FWHM = 0.25 nm) ones specifically designed for the retrieval of sun-induced chlorophyll fluorescence at the O_2-A and O_2-B absorption bands, respectively.

The system was housed in a thermally regulated Peltier box (model NT-16; Magapor, Zaragoza, Spain) and manually operated from the top of a mobile hydraulic platform to measure top-of-canopy reflectance and fluorescence of the representative tree species of the Hardt forest in six sampling sites. The measurements were acquired from nadir using bare optical fibers with an angular field of view of 25° mounted at the end of a 2.5 m long arm held at a height of 3.7-5 m above the canopy, corresponding to a sampling area of 1.7-2.3 m diameter. The arm was manually rotated horizontally to allow the alternative observation of the vegetated target to measure the upwelling radiance and of a levelled calibrated white reference panel (Spectralon; Labsphere, North Sutton, USA) to measure the incident solar radiation.

The spectral data were acquired through the 3S software (Meroni and Colombo, 2009), sandwiching each measurement of the vegetated target between two measurements of the white reference panel, and collecting the dark current of the instruments at the beginning of each set of measurements. The collected data were processed with a dedicated IDL (ITT Visual Information Solutions, Boulder, USA) application described in Meroni et al. (2011). F_{687} and F_{760} were estimated by exploiting the spectral fitting method described in Meroni et al. (2010) and Cogliati et al. (2015).

Field measurements were acquired in correspondence of Elementary Sampling Units (ESUs) of 20 $\times$ 20 distributed all over the study area in order to sample a wide range of different forest species and conditions. The ESUs were selected by forest experts along the forest tracks, at about 50 m distance from the path. The centre of each ESU was tracked with a high precision Trimble Geo-XT GPS

(Trimble, Sunnyvale, USA). Species composition and crown condition were visually evaluated by the forest experts in correspondence of 42 ESUs. All the species representing more than 5% of the dominant layer of the ESU were considered in the estimation of the species composition. LCC was estimated by destructive sampling of leaves collected from different forest species located in 12 ESUs, followed by pigment quantification by UV-VIS spectroscopy. At least 10 leaves were sampled for each species of the ESUs (n ≈ 250). The leaf samples were collected from sunlit leaves sampled by shooting with guns at the top branches and were immediately placed into sealed plastic bags and stored under -80°C until the laboratory biochemical analysis. The pigments were extracted using hydroxide carbonate magnesium buffered with acetone and absorbance was measured at 645 nm, 662 nm and 710 nm using a UVIKON XL spectrophotometer (BioTek Instruments, Winooski, USA) to determine LCC (Lichtenthaler and Buschmann, 2001). LAI was estimated by means of digital hemispherical photos acquired within 14 ESUs using a Sigma camera (Sigma Corporation, Ronkonkoma, USA) equipped with a fisheye lens. The images - 7 looking upward per each plot - were processed with the CAN-EYE (`https://www4.paca.inra.fr/can-eye/CAN-EYE-Home/Welcome`) software to estimate LAI. The clumping effect was taken into account by multiplying the effective LAI by the clumping index (Chen and Black, 1992) computed using the logarithm gap fraction averaging method (Lang and Yueqin, 1986).

3.2.3 Airborne hyperspectral images acquisition and pre-processing

The airborne data were acquired using the hyperspectral imaging sensor *HyPlant* (Rascher et al., 2015). *HyPlant* is made up of two modules: i) the Dual Channel Imager (DUAL) is a hyperspectral imaging spectrometer with 624 spectral channels covering the visible, near-infrared and shortwave infrared (VIS-NIR-SWIR) spectral regions (370-2500 nm) at a full-width at half maximum (FWHM) of 4.0 nm (VIS-NIR) - 13.3 nm (SWIR); ii) the Fluorescence Imager (FLUO) is a high-performance hyperspectral imaging spectrometer with 1024 spectral channels providing contiguous spectral information in the wavelength range 670-780 nm with a FWHM of ≈ 0.25 nm. Both the DUAL and the FLUO sensors are line-imaging push-broom scanners with an angular field of view of 32.3°.

HyPlant was flown over the study site on board a Cessna Grand Caravan C208B on 16th June 2013 around solar noon (12:30±1 CEST (Central European Summer Time)) under clear sky conditions. The flight was conducted heading 195° at an average altitude of 600 m above the ground level, resulting in a pixel size of 1 m.

The pre-processing of the airborne data was performed using the CaliGeo software (Specim Ltd, Oulu, Finland). *HyPlant* raw data were corrected for dark cur-

rent, radiometrically calibrated and georectified using as input the information recorded by *HyPlant* position and attitude sensor. The DUAL data were then atmospherically corrected using the ATCOR-4 atmospheric radiative transfer code to obtain top-of-canopy radiance and reflectance.

3.2.4 HyPlant data product generation

3.2.4.1 *Sun-induced chlorophyll fluorescence retrieval*

The images collected by the FLUO module were processed with a dedicated processing-chain specifically developed to retrieve F from *HyPlant* observations. The SFM retrieval approach, originally developed for FLEX (Cogliati et al., 2015), was adapted to *HyPlant* ultra-fine resolution data at both the O_2-B and O_2-A absorption bands to derive red and far-red F maps (Cogliati et al., 2018). This approach allowed decoupling F and surface reflected radiance spectra from upward radiance spectra detected by the *HyPlant* FLUO module. The rationale behind the SFM relies on mathematical functions to model canopy reflectance and fluorescence spectra at the different wavelengths. The exploitation of the full set of spectral bands provided by *HyPlant* sensor reduces the overall impact of instrumental noise and allows estimating a higher number of model parameters describing the fluorescence/reflectance spectra. The SFM method was implemented and tested for processing *HyPlant* images collected during the campaign, following the surface-atmosphere coupled RT scheme proposed in Verhoef, Tol, and Middleton (2018) and adapted to airborne observations. In fact, the reflectance and fluorescence spectral function parameters were directly estimated comparing forward RT model simulations with *HyPlant* radiance spectra at-sensor level. The forward RT model used for processing *HyPlant* images was limited to estimating surface parameters (*i.e.*, reflectance and fluorescence), while the atmospheric variables were kept constant to pre-defined values. The atmospheric transfer functions (*i.e.*, path radiance, spherical albedo and upward/downward transmittance) used in the forward RT model were computed by MODTRAN5. The atmospheric model input parameters were derived from sunphotometer measurements collected simultaneously to *HyPlant* observations. The retrieval algorithm included a preliminary characterisation of instrumental signal distortions such as spectral-shift and bandwidth on image column base (*i.e.*, sensor across-track). The red and far-red F at the O_2-A and O_2-B bands, respectively, were estimated by analysing each O_2 absorption band independently. The output of the SFM consists of two distinct images, in which the red (684-697 nm) and far-red (750-777 nm) spectra (with a spectral sampling interval resampled to 1 nm in order to reduce the output data volume)

are provided in physical units ($mW\,m^{-2}\,sr^{-1}\,nm^{-1}$). For further analysis, the F values at 687 nm (F_{687}) and 760 nm (F_{760}) were used in this study.

The maps were finally validated comparing the airborne with the ground-based retrievals obtained from top-of-canopy spectral measurements collected over six selected forest targets. The ground targets were precisely identified on the image with the help of RGB images acquired with a drone and statistics were extracted from regions of interest of 3×3 pixels for comparison against the ground-based measurements.

The fluorescence yields (Fy_{687} and Fy_{760}) were calculated as the ratio between F_{687} and F_{760} and APAR ($\mu mol\,photon\,m^{-2}\,s^{-1}$) for each pixel of the image. Before the calculation, F_{687} and F_{760} radiances were converted to $\mu mol\,m^{-2}\,s^{-1}$ using a specific wavelength-dependent coefficient. The resulting Fy_{687} and Fy_{760} maps refer to the emission at 687 nm and 760 nm, respectively, and are thus expressed as $sr^{-1}\,nm^{-1}$.

3.2.4.2 *Plant traits retrieval*

In order to obtain accurate high-resolution maps of key plant traits from *HyPlant* DUAL imagery, a physically based approach was chosen. A systematic evaluation of the RTM parameterisation and of the Look-Up-Table (LUT) based inversion strategy was conducted, in order to propose a reproducible approach that could provide accurate and reliable plant trait retrievals in forest ecosystems, to be used for different purposes. In this case, the inversion strategy was optimised for the retrieval of LCC and LAI, two key traits for the following modelling step using BESS.

Among the variety of existing RTMs, the canopy level INvertible FOrest Reflectance Model (INFORM) (Atzberger, 2000; Schlerf and Atzberger, 2006) coupled with the leaf level PROSPECT-4 model (Feret et al., 2008; Jacquemoud and Baret, 1990) was chosen in this study because of its suitability in simulating forest canopy reflectance while preserving a relative simplicity. INFORM is a hybrid model combining the strengths of the turbid-medium and geometric-optical radiative transfer models. It couples the SAILH model (Kuusk, 1991; Verhoef, 1984) that simulates the radiative transfer within the turbid-medium canopy layer with the FLIM model (Rosema et al., 1992) to account for geometric aspects such as the leaf clumping inside the tree crowns and the crown geometry. The model simulates the forest reflectance in the spectral range 400-2500 nm as a function of several leaf-level (*i.e.*, leaf chlorophyll content (LCC), leaf dry matter content (LDMC), leaf water content (LWC), leaf structural parameter (N)) as well as canopy-level (*i.e.*, LAI of the single trees, LAI of the understory (LAIu), average leaf angle (ALA), tree height (h), crown diameter (cd), stem density (sd)) input parameters, besides

other parameters describing the sun-sensor geometries and irradiance conditions (*i.e.*, sun zenith angle (Θ_s), observer zenith angle (Θ_o), relative azimuth angle (Φ), fraction of diffuse radiation (skyl)).

A global sensitivity analysis (GSA) (Saltelli et al., 2010; Verrelst, Rivera, and Moreno, 2015) was carried out in order to examine the response of the model to the variation of each of its input parameters. This allows to identify the parameters that are less-influential on the modelled reflectance, that can be thereafter set to fixed values in order to reduce the number of unknown variables maximising the predictive power of the model. A total of 2000 simulations were run, varying each parameter according to all the possible variability in the study site. The GSA results were used to improve the parameterisation of the RTM: the less influential parameters on the modelled reflectance were set to constant values, while the other input parameters were varied within ranges defined according to prior knowledge of the study site. The range and distribution of the RTM input parameters used for the generation of the LUT are shown in Table 3. The model was then run in forward mode to generate a LUT of 30000 simulated reflectance spectra obtained by all the possible combinations between the input parameters.

The inversion strategy was optimised by testing the effect of three regularisation options on the retrieval performances: i) the use of different cost functions, ii) the addition of Gaussian noise to the simulated spectra and iii) the use of multiple solutions of the inversion.

Multiple cost functions introduced in Leonenko, Los, and North (2013) and exploited in Rivera et al. (2013) were tested, in order to identify the ones that minimise the mismatch between measured and simulated spectra. The cost functions belong to different fields of mathematics and statistics and can be grouped into three broad families: information measures, M-estimates and minimum contrast estimates.

All these metrics are used to minimise the distance $D[M, S]$ between two functions $M = (m(\lambda_1), m(\lambda_2), \ldots, m(\lambda_n))$ and $S = (s(\lambda_1), s(\lambda_2), \ldots, s(\lambda_n))$, representing the shape of the measured (M) and simulated (S) reflectance spectra at the wavelength λ_n, but different metrics describe D in distinctive ways.

With the information measures (*e.g.*, Kullback Leibler divergence, Pearson chi-square, harmonique Toussaint measure), M and S are considered as probability distributions and their divergence is measured. M-estimates (*e.g.*, least square estimator) are maximum likelihood-based distances based on the search of the minima of sums of M and S functions. They are the most widely used and are generally considered robust estimators, but they can give suboptimal results when their assumptions are violated (*e.g.*, errors not-normally distributed). With minimum contrast estimates (*e.g.*, contrast function), M and S are described as spectral density functions to be minimised. The list and mathematical formulation of the

Table 3: Range and distribution of the input parameters of the PROSPECT-4-INFORM model used for the generation of a Look-Up-Table (LUT) of 30000 simulated spectra. (*μ = mean, σ = standard deviation).

		Variable	Unit	Range	Distribution
PROSPECT-4	LCC	Leaf chlorophyll content	$\mu g\,cm^{-2}$	10-70	Gaussian (μ = 40, σ = 25)
	LWC	Leaf water content	cm	0.006-0.015	Sobol
	LDMC	Dry matter content	$g\,cm^{-2}$	0.003-0.015	Sobol
	N	Leaf structural parameter	-	1.5	-
INFORM	LAI	Leaf Area Index	m^2m^{-2}	1.5-8	Gaussian (μ = 4, σ = 2)
	LAIu	Leaf area index of understory	m^2m^{-2}	0.5-2.5	Sobol
	sd	Stem density	$trees\,ha^{-1}$	200-400	Sobol
	cd	Crown diameter	m	3-9	Sobol
	h	Tree height	m	20	-
	ALA	Average leaf inclination	deg	45	-
	θ_s	Sun zenith angle	deg	31	-
	θ_o	Observer zenith angle	deg	0	-
	ϕ	Azimuth angle	deg	128	-
	skyl	Fraction of diffuse radiation	-	0.1	-

metrics selected in this study is reported in Table 4. For a more detailed description of the cost function families and of each estimator refer to Leonenko, Los, and North (2013). Gaussian noise ranging from 0 to 10% (with step 1%) was added to the simulated reflectance spectra in order to consider the uncertainties affecting the model and the measured data, and 0 to 20 (with step 1) solutions of the best matching modelled spectra were averaged to mitigate the effect of ill-posedness.

The retrieval workflow was performed within ARTMO v. 3.23 (Automated Radiative Transfer Models Operator; http://ipl.uv.es/artmo/) (Rivera et al., 2013; Verrelst et al., 2011), a graphic user interface software package running in MATLAB (The MathWorks, Inc., Natick, USA) that includes a suite of leaf and canopy RTMs. ARTMO streamlines the model configuration, running and output storage, thus facilitating the handling and processing of high dimensional spectral data.

The standard fitting statistics such as coefficient of determination (r^2), root mean square error (RMSE), relative RMSE (rRMSE) (*i.e.*, RMSE/mean of measured values), bias (*i.e.*, mean of estimated values – mean of observed values) and relative bias (rbias) (*i.e.*, bias/mean of estimated values) between measured and simulated LCC and LAI were computed to evaluate the performances of the different RTM inversion strategies tested. The leave-one-out cross-validated statistics (r^2_{CV}; $RMSE_{CV}$) were also computed to compare the prediction performance of the different model implementations.

3.2.4.3 *BESS parameterisation strategy and GPP, APAR & LUE estimation*

The Breathing Earth System Simulator (BESS) (Jiang and Ryu, 2016; Ryu et al., 2011) was used to derive a snapshot of instantaneous GPP over the study area at the time of the *HyPlant* overflight.

BESS is a biophysical model developed to monitor carbon and water fluxes using multi-source remotely sensed data at moderate spatial resolution (1-5 km). The model couples a 1-dimensional atmospheric radiative transfer module to compute direct and diffuse radiation in the PAR and NIR spectral regions (Kobayashi and Iwabuchi, 2008; Ryu et al., 2018), a two-leaf and two-stream canopy radiative transfer model to compute the absorbed PAR and NIR radiation by sunlit and shaded leaves, respectively (Pury and Farquhar, 1997; Ryu et al., 2011), and an integrated carbon assimilation-stomatal conductance-energy balance model (Ball, 1988; Paw and Gao, 1988) to compute GPP and ET. In its original configuration, BESS uses as input MODIS atmosphere (*e.g.*, cloud optical thickness, aerosol optical thickness, water vapour, ozone) and land products (*e.g.*, LAI, land cover, albedo in the PAR and NIR spectral regions) as well as other satellite data (*e.g.*, OCO-2-NOAA data to derive CO_2 concentration maps; Shuttle Radar Topography Mission (SRTM) data to take into account the effect of altitude on the incoming radiation).

Table 4: Selected cost functions (CF) for the description of the distance $D[M,S]$ between measured ($M = (m(\lambda_1), m(\lambda_2), \ldots, m(\lambda_n))$) and simulated ($S = (s(\lambda_1), s(\lambda_2), \ldots, s(\lambda_n))$) reflectance spectra. The CFs are grouped in three broad families: information measures, M-estimates and minimum contrast estimates.

CF family	CF	Formula
M-est.	RMSE	$D[M,S] = \sqrt{\frac{\sum_{\lambda_i=1}^{\lambda_n}(m(\lambda_i)-s(\lambda_i))^2}{n}}$
	Geman-McClure	$D[M,S] = \sum_{\lambda_i=1}^{\lambda_n} \frac{(m(\lambda_i)-s(\lambda_i))^2}{1+(m(\lambda_i)-s(\lambda_i))^2}$
Information measures	Kullback-Leibler	$D[M,S] = \sum_{\lambda_i=1}^{\lambda_n} m(\lambda_i) ln \frac{(m(\lambda_i)}{s(\lambda_i)}$
	Jeffreys-Kullback-Leibler	$D[M,S] = \sum_{\lambda_i=1}^{\lambda_n} (m(\lambda_i) - (s(\lambda_i))(ln(m(\lambda_i)) - ln(s(\lambda_i)))$
	Neyman χ-square	$D[M,S] = \sum_{\lambda_i=1}^{\lambda_n} \frac{(m(\lambda_i)-s(\lambda_i))^2}{s(\lambda_i)}$
	K-divergence Lin	$D[M,S] = \sum_{\lambda_i=1}^{\lambda_n} m(\lambda_i) ln \frac{(2m(\lambda_i))}{m(\lambda_i)+s(\lambda_i)}$
	L-divergence Lin	$D[M,S] = \sum_{\lambda_i=1}^{\lambda_n} m(\lambda_i) ln(m(\lambda_i) + s(\lambda_i) ln(s(\lambda_i) - m(\lambda_i) + s(\lambda_i)) ln \frac{(m(\lambda_i)+s(\lambda_i))}{2}$
	Harmonique Toussaint	$D[M,S] = \sum_{\lambda_i=1}^{\lambda_n} m(\lambda_i) - \frac{(2m(\lambda_i)s(\lambda_i))}{m(\lambda_i)+s(\lambda_i)}$
	Negative exponential disparity	$D[M,S] = \sum_{\lambda_i=1}^{\lambda_n} s(\lambda_i)(exp(-\frac{(m(\lambda_i)-s(\lambda_i)}{s(\lambda_i)}) - 1)$
	Bhattacharyya divergence	$D[M,S] = -log(1 + \sum_{\lambda_i=1}^{\lambda_n} \sqrt{m(\lambda_i)s(\lambda_i)} - \frac{1}{2}(m(\lambda_i) + s(\lambda_i)))$
	Shannon	$D[M,S] = -\sum_{\lambda_i=1}^{\lambda_n} \frac{m(\lambda_i)+s(\lambda_i)}{2} log \frac{m(\lambda_i)+s(\lambda_i)}{2} + \frac{1}{2}(\sum^{\lambda_n} \lambda_i = 1 m(\lambda_i) log(m(\lambda_i)) + \sum_{\lambda_i=1}^{\lambda_n} s(\lambda_i) log(s(\lambda_i)))$
Min contr. est.	$K(x) = (log(x))^2$	$D[M,S] = \sum_{\lambda_i=1}^{\lambda_n} (log(m(\lambda_i)) - log(s(\lambda_i)))^2$
	$K(x) = log(x) + 1/x$	$D[M,S] = \sum_{\lambda_i=1}^{\lambda_n} (log \frac{s(\lambda_i)}{m(\lambda_i)} + \frac{m(\lambda_i)}{s(\lambda_i)}) - 1$
	$K(x) = -log(x) + x$	$D[M,S] = \sum_{\lambda_i=1}^{\lambda_n} (-log \frac{s(\lambda_i)}{m(\lambda_i)} + \frac{s(\lambda_i)}{m(\lambda_i)}) - 1$
	$K(x) = x(log(x)) - x$	$D[M,S] = 1 + \sum_{\lambda_i=1}^{\lambda_n} \frac{s(\lambda_i)}{m(\lambda_i)} (log \frac{s(\lambda_i)}{m(\lambda_i)} - 1)$

For this study, BESS was customised to ingest *HyPlant* high-resolution (1 m) products and atmospheric constraints obtained from meteorological data collected in the field, outputting a BESS-GPP map at the time of *HyPlant*'s overflight at high spatial resolution.

Four *HyPlant*-derived spatially resolved products were used to feed BESS: two broadband reflectance maps and two key plant trait maps. Broadband reflectance was calculated from the DUAL hyperspectral reflectance cube with a weighted average after a regular spectral resampling (1 nm spectral interval) in the VIS (400-700 nm) and NIR (841-876 nm) spectral regions, respectively. Maximum carboxylation rate normalised to 25°C ($Vcmax_{25}$) and LAI were derived from the RTM inversion. While LAI is a direct output of the RTM, $Vcmax_{25}$ was empirically inferred from LCC using a linear relationship for broadleaved forest species found by Croft et al. (2017). This study found a strong linear relationship (r^2 = 0.78, $p < 0.001$) between the two variables across three growing seasons considering four different deciduous tree species, demonstrating that LCC can be a reliable proxy for modelling Vcmax. $Vcmax_{25}$ map was then derived from the LCC map obtained as output of the RTM inversion according to Eq. 1 (Croft et al., 2017):

$$Vcmax_{25} = 1.3 * LCC + 3.72 \quad (1)$$

Additionally, atmospheric forcings such as air temperature, pressure, column water vapour, relative humidity and aerosol optical thickness were obtained from punctual measurements acquired with a Microtops II sunphotometer (Solar Light Company, Glenside, USA). The incident solar irradiance during the overpass was collected in the spectral region 350-2500 nm with a calibrated FieldSpec 4 (ASD Inc., Longmont, USA) measuring over a levelled white Spectralon (Labsphere, North Sutton, USA).

3.2.5 HyPlant data product comparison

The outputs obtained from *HyPlant* DUAL and FLUO images (*e.g.*, GPP, F_{687}, F_{760}) were inter-compared by fitting regression models between pairs of variables. The statistical analysis was performed in R (R Core Team, 2018) and aimed at testing different models to find the best fit. The independency of observations condition required in regression analysis is not met in case of spatial-autocorrelation in the data, meaning that clusters of data points present numerical similarity because of their spatial proximity (Haining, 1980). The spatial dependency implicates that part of the information within the dataset is repeated and therefore redundant. In order to detect a possible violation of the independency assumption, an analysis of the semivariograms of the images was performed. Based on the results of this anal-

ysis, all the airborne-derived products were aggregated at tree crown level (*i.e.*, all the pixels belonging to the same tree crown were averaged) for spatial comparison instead of performing a pixel by pixel comparison. Besides overcoming the issues related to the spatial dependency, this approach allowed reducing noise in the data and mitigating the slight geometric mismatch between the images recorded from the *HyPlant* DUAL and FLUO modules.

3.3 RESULTS

3.3.1 HyPlant data products

3.3.1.1 *Red & far-red F maps*

The high-spatial resolution F_{687} and F_{760} maps obtained over the forest using the SFM implemented for the processing of *HyPlant* imagery are shown in Figure 6.

Overall, the magnitude of F_{760} ranged from 0 to 2.5 $mW\ m^{-2}\ sr^{-1}\ nm^{-1}$, with a frequency peak around 1.5 $mW\ m^{-2}\ sr^{-1}\ nm^{-1}$, while F_{687} ranged from 0 to 2 $mW\ m^{-2}\ sr^{-1}\ nm^{-1}$, with values around 0.8 $mW\ m^{-2}\ sr^{-1}\ nm^{-1}$ occurring most frequently. These values were consistent throughout the image and coherent with the ones usually observed in forested areas using ground-based measurements. The spatial patterns were meaningful for both F_{687} and F_{760}: higher fluorescence was observed in the sunlit part of the canopy, lower fluorescence was observed in the inter-crown gaps and non-fluorescing targets such as bare soil and asphalt exhibited near-zero values. On the other hand, F_{687} was characterised by a higher noise in the retrieval which resulted into a remarkable 'salt-and-pepper' effect on the map. A quantitative evaluation of the SFM performance in estimating F was carried out comparing the airborne with the ground-based retrievals measured in correspondence of six selected targets (Figure 7).

The comparison showed consistency between airborne and ground F measured both in the red and far-red regions of the spectrum for different canopies. The linear models fitted between airborne and ground-based observations were statistically significant ($p < 0.05$) and showed the effectiveness of the SFM in F_{687} ($r^2 = 0.75$; RMSE = 0.42 $mW\ m^{-2}\ sr^{-1}\ nm^{-1}$) and F_{760} ($r^2 = 0.74$; RMSE = 0.43 $mW\ m^{-2}\ sr^{-1}\ nm^{-1}$) retrievals. In terms of absolute values, a systematic overestimation of F_{687} measured from *HyPlant* compared to the ground references was recorded (bias = 0.41 $mW\ m^{-2}\ sr^{-1}\ nm^{-1}$; rbias = 52%). This effect was smaller in F_{760} retrieval (bias = 0.27 $mW\ m^{-2}\ sr^{-1}\ nm^{-1}$; rbias = 17%).

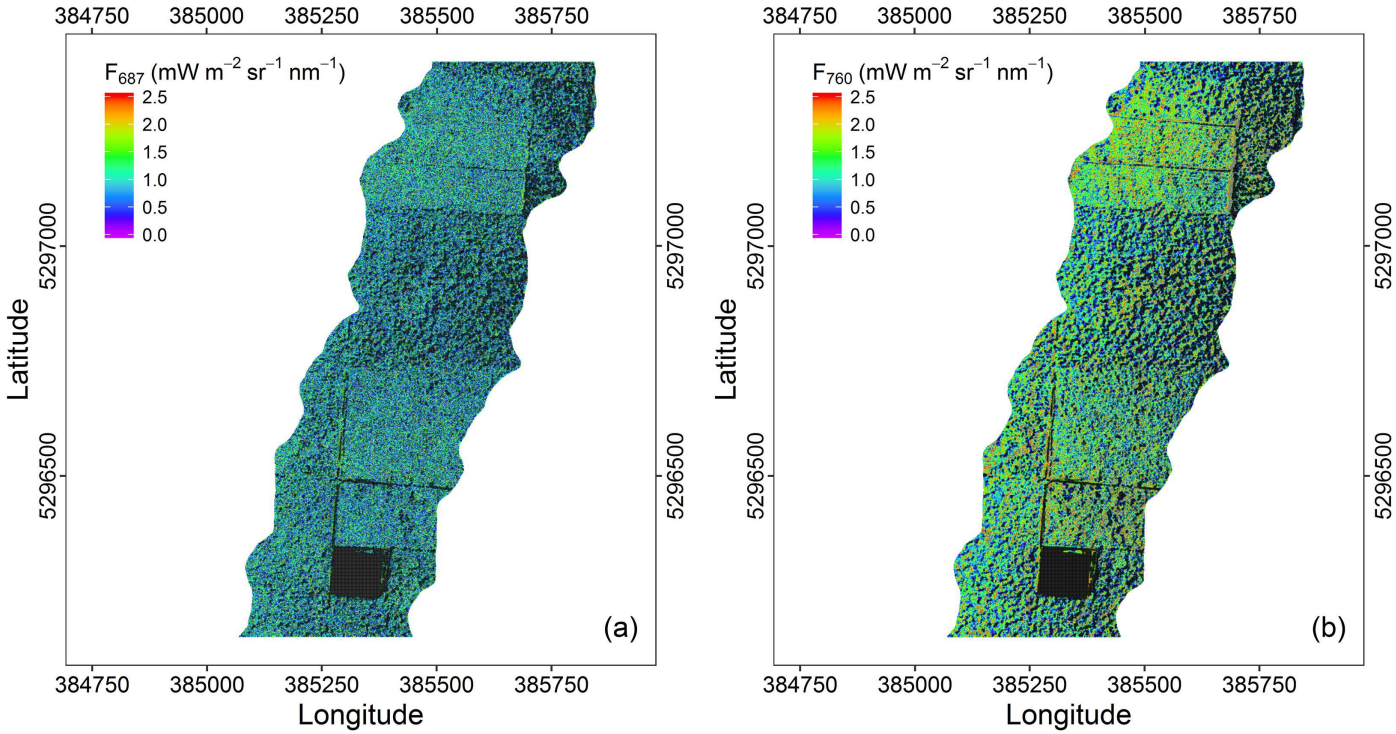

Figure 6: a) F_{687} and b) F_{760} maps obtained from *HyPlant* FLUO hyperspectral radiance using the spectral fitting method (SFM).

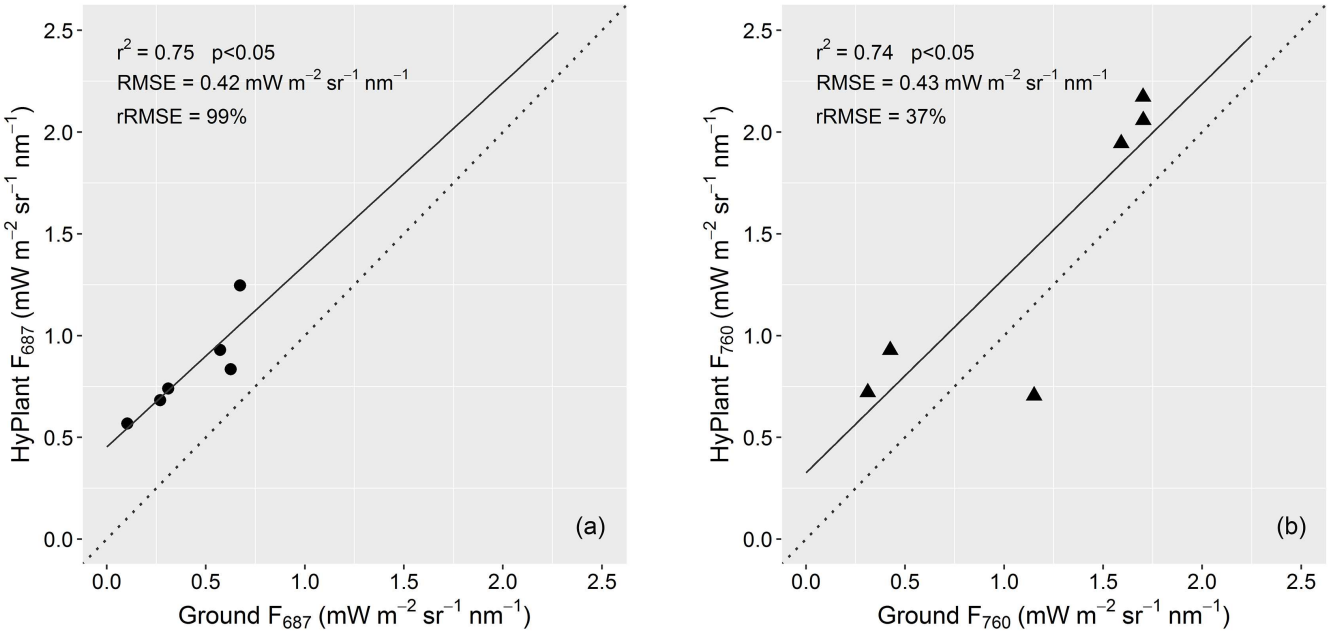

Figure 7: Comparison between ground-based and airborne a) F_{687} and b) F_{760} retrievals in correspondence of different forest species. The solid line corresponds to the linear model fitted between the paired variables. The dotted line represents the 1:1 line.

3.3.1.2 *Plant trait maps*

The results of the GSA performed on the coupled PROSPECT-4-INFORM model are shown in Figure 8. For each input parameter of the RTM, the obtained total-order sensitivity index (SI) was expressed in percentage as a function of the wavelength. The analysis revealed a small influence of the leaf structural parameter (N), tree height (h) and average leaf inclination (ALA) across the entire spectrum. These parameters were therefore set to constant values in order to allow maximising the variability of the other input variables.

The LCC and LAI maps at high spatial resolution obtained as output of the RTM-based retrieval from *HyPlant* DUAL imagery are shown in Figure 9.

Strong correlations were found between measured and predicted values of LCC and LAI (Table 5, Figure 10), demonstrating that the inversion of the INFORM model constrained with various regularisation techniques yields accurate retrievals of plant traits in forest ecosystems.

LCC was most accurately retrieved using a logarithmic minimum contrast cost function based on the minimisation of the distance (contrast) between a parametric model and a non-parametric spectral density (Leonenko, Los, and North, 2013). The best fitting (r^2 = 0.65, $p < 0.001$; n = 21) was obtained using the mean of the ten best solutions and no addition of random noise to the simulations. The use of a divergence measure cost function formalised by Kullback and Leibler (1951), based on the minimisation of the distance between two probability distributions, showed the best performances in the retrieval of LAI. As for the retrieval of LCC, the best results were obtained using ten best solutions and no addition of random noise (r^2 = 0.72, $p < 0.001$; n = 14). The summary statistics in fitting and cross-validation of the linear regressions between measured and estimated LCC and LAI are reported in Table 5. The scatterplots showing the measured LCC and LAI values against the predicted ones are reported in Figure 10.

Overall, LCC and LAI showed reasonable value distributions and meaningful spatial patterns within the complex mixed forest ecosystem (Figure 9). The LCC and LAI spatial patterns showed some similarities, but they were not totally correlated (r^2 = 0.5, $p < 0.001$). Based on the species distribution in the study area obtained from the classification performed in Tagliabue et al. (2016) using APEX airborne data, it was observed that field maple and small-leaved linden were the species characterised by the highest LCC values, even though the differences compared to the other species were not significant. LAI showed a larger inter-species variability, with the highest value for small-leaved linden and the lowest for Scots pine. In general, LCC did not differ significantly in regeneration and mature stands, while LAI was higher in regeneration stands.

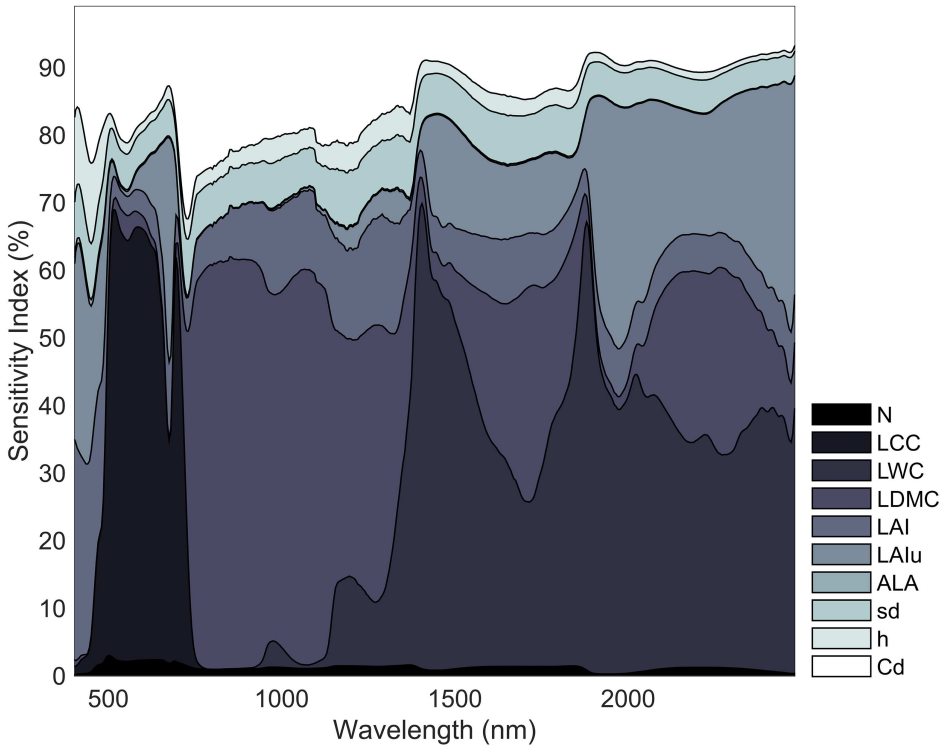

Figure 8: Results of the GSA of the coupled PROSPECT-4-INFORM radiative transfer model. The total-order sensitivity index (SI) is expressed in % for each input parameter as a function of the wavelength. The acronyms in the legend correspond to leaf structural parameter (N), leaf chlorophyll content (LCC), leaf water content (LWC), leaf dry matter content (LDMC), leaf area index (LAI), leaf area index of the understory (LAIu), average leaf inclination (ALA), stem density (sd), tree height (h) and crown diameter (Cd).

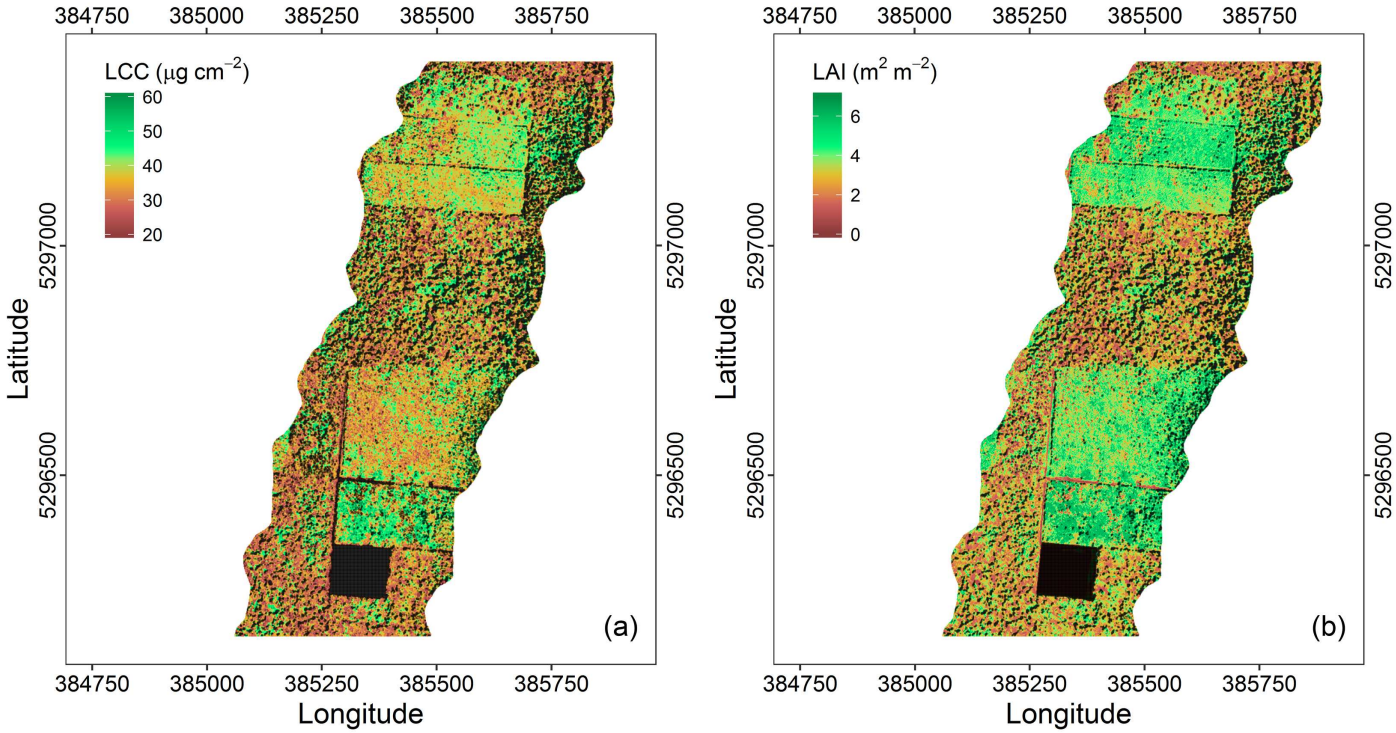

Figure 9: a) LCC and b) LAI high-resolution maps obtained from *HyPlant* DUAL data through LUT-based inversion of the coupled PROSPECT-4-INFORM radiative transfer model using the optimal inversion strategy.

Table 5: Summary of statistics in fitting (r^2, RMSE, rRMSE, bias, rbias) and cross-validation (r^2_{CV}; $RMSE_{CV}$) of the comparison between measured and estimated LCC and LAI values.

Plant trait	r^2	r^2_{CV}	RMSE	$RMSE_{CV}$	rRMSE	bias	rbias
LCC	0.65	0.58	5.66 ($\mu g\,cm^{-2}$)	3.96 ($\mu g\,cm^{-2}$)	15 (%)	2.61 ($\mu g\,cm^{-2}$)	7 (%)
LAI	0.72	0.47	0.51 (m^2m^{-2})	0.57 (m^2m^{-2})	14 (%)	0.04 (m^2m^{-2})	1 (%)

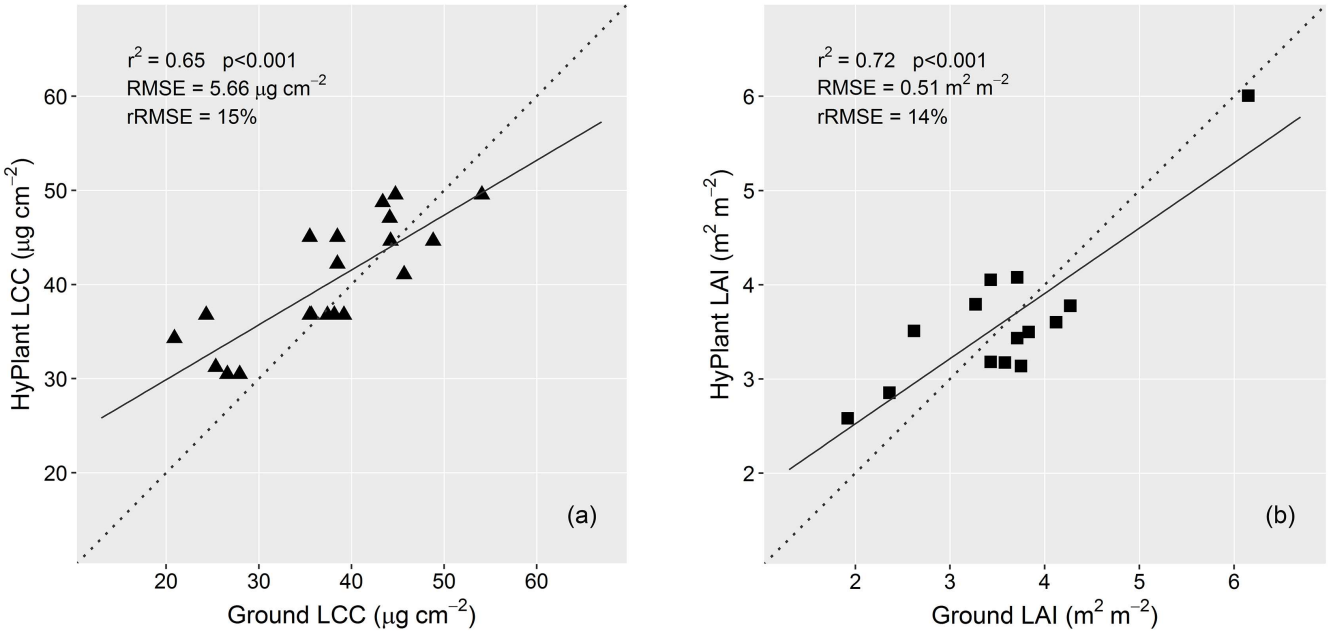

Figure 10: Comparison between ground-based measurements and *HyPlant* estimates of a) LCC and b) LAI. The solid lines correspond to a linear model fitted between the paired variables. The dotted lines represent the 1:1 lines.

3.3.1.3 *GPP, APAR & LUE maps*

The incorporation of spatialised maps of key plant traits into the process-based BESS model allowed obtaining spatial maps of GPP, APAR and LUE at high spatial resolution (Figure 11).

The map of instantaneous GPP showed values ranging from 0 $\mu mol\, CO_2\, m^{-2}\, s^{-1}$ for bare soil up to ~30 $\mu mol\, CO_2\, m^{-2}\, s^{-1}$ for dense vegetation. The regeneration areas, where trees were planted with higher density and both LCC and LAI were higher, were clearly distinguishable in the image due to their larger CO_2 assimilation. In the mature stands, the crown-shadow patterns were more evident and the GPP values were generally lower, even though with a noticeable variability across the image. It is worth noting that, due to the nature of the model and the available input data, the obtained modelled GPP was considerably driven by LAI and $Vcmax_{25}$ (r^2 = 0.94 and r^2 = 0.68, respectively, $p < 0.001$). However, LAI and $Vcmax_{25}$ were only weakly related (r^2 = 0.5, $p < 0.001$).

APAR varied from 0 to ~1900 $\mu mol\, photon\, m^{-2}\, s^{-1}$ and showed consistent patterns with GPP (r^2 = 0.82, $p < 0.001$), despite a lower variability for high APAR values. LUE, obtained as the ratio between modelled GPP and APAR, ranged from 0 to ~0.018 $\mu mol\, CO_2\, \mu mol\, photon^{-1}$ and appeared strongly related to both the GPP (r^2 = 0.76, $p < 0.001$) and APAR maps (r^2 = 0.8, $p < 0.001$).

3.3.2 Linking measured F and modelled BESS-GPP, -APAR & -LUE

The analysis of the semivariograms of the images obtained from *HyPlant* revealed the presence of a clear spatial autocorrelation in the data. This effect exists within a range from 0 to 10-15 m, as it can be gathered from the range (*i.e.*, the distance expressed in meters at which the semivariogram levels) of the semivariogram function showed in Figure 12. This distance corresponds to the average diameter of the tree crowns, indicating that there is a high similarity among pixels of the same crown. For this reason, the spatial relationships between the airborne-derived outputs showed hereafter refer to the data aggregated at tree crown level.

The spatial relationships between F_{687} and F_{760} retrieved from *HyPlant* ultra-fine spectral resolution radiance data and GPP, APAR and LUE obtained as outputs of the BESS model driven with airborne-derived data are shown in Figure 13. In the scatterplots, each data point is the average of all the sunlit pixels of the same tree crown.

Different regression models were tested between the paired variables. Overall, the best fit was found when using a logarithmic model, that allowed describing the nonlinearity of the relationships. A positive logarithmic relationship was found between F_{760} and GPP (r^2 = 0.46, $p < 0.001$), F_{760} and APAR (r^2 = 0.43, $p < 0.001$)

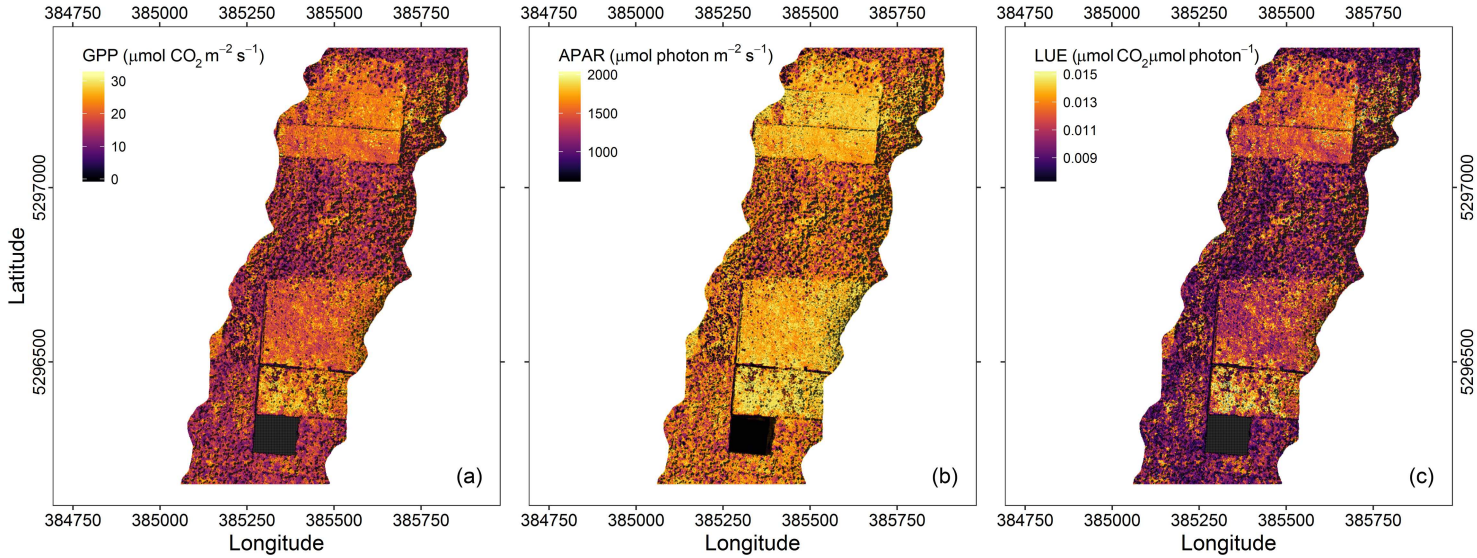

Figure 11: a) GPP, b) APAR and c) LUE maps obtained from the BESS model driven with airborne-derived high-resolution maps.

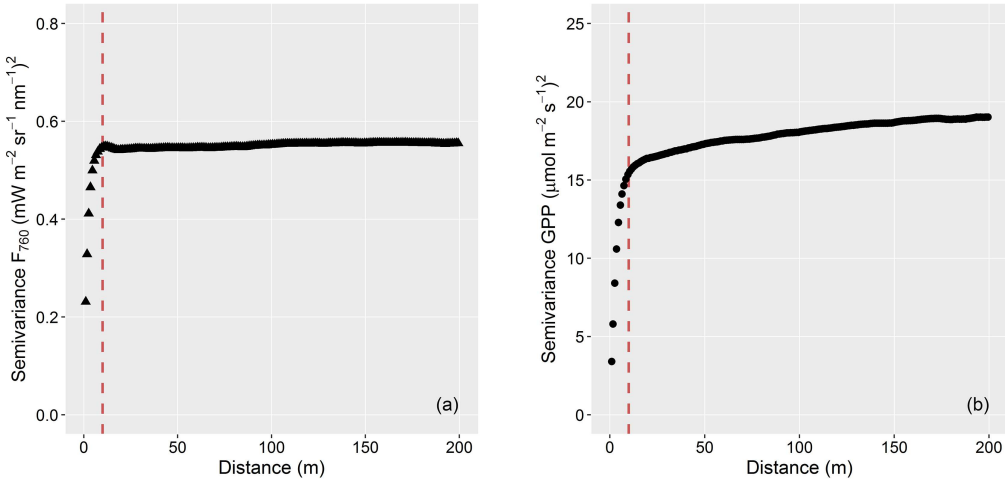

Figure 12: Semivariogram functions of the a) F_{760} and b) GPP images expressed as a function of the distance (m). The red dashed lines represent the range of the semivariogram functions.

and between F_{760} and $Vcmax_{25}$ (r^2 = 0.17, $p < 0.001$). Conversely, no significant relationship was found between F_{687} and GPP, F_{687} and APAR or F_{687} and $Vcmax_{25}$ ($p > 0.05$). The analysis of the logarithmic regression between LUE and the red (Fy_{687}) and far-red (Fy_{760}) F yields revealed an opposite nature of the two relationships: Fy_{760} showed a positive correlation with LUE (r^2 = 0.19, $p < 0.001$), while Fy_{687} and LUE were found to be negatively correlated (r^2 = 0.25, $p < 0.001$) (Figure 13 d, h).

3.4 DISCUSSION

The quantitative estimation of vegetation traits is required in a variety of ecological applications. Regardless the considerable advances achieved through the development and testing of a wide range of leaf as well as canopy-level retrieval methods (Verrelst et al., 2015a), their quantification from remotely sensed data remains challenging. The inference of these traits is in fact concealed by confounding factors related to the canopy (*e.g.*, canopy structure, background influence, illumination effects), the atmosphere (Houborg, Fisher, and Skidmore, 2015; Malenovský et al., 2013) and the sun-sensors geometries, that might introduce large inaccuracies in the retrieved traits. The inversion of physically based RTMs is generally recognised as a reliable and accurate approach (Atzberger et al., 2015; Dorigo

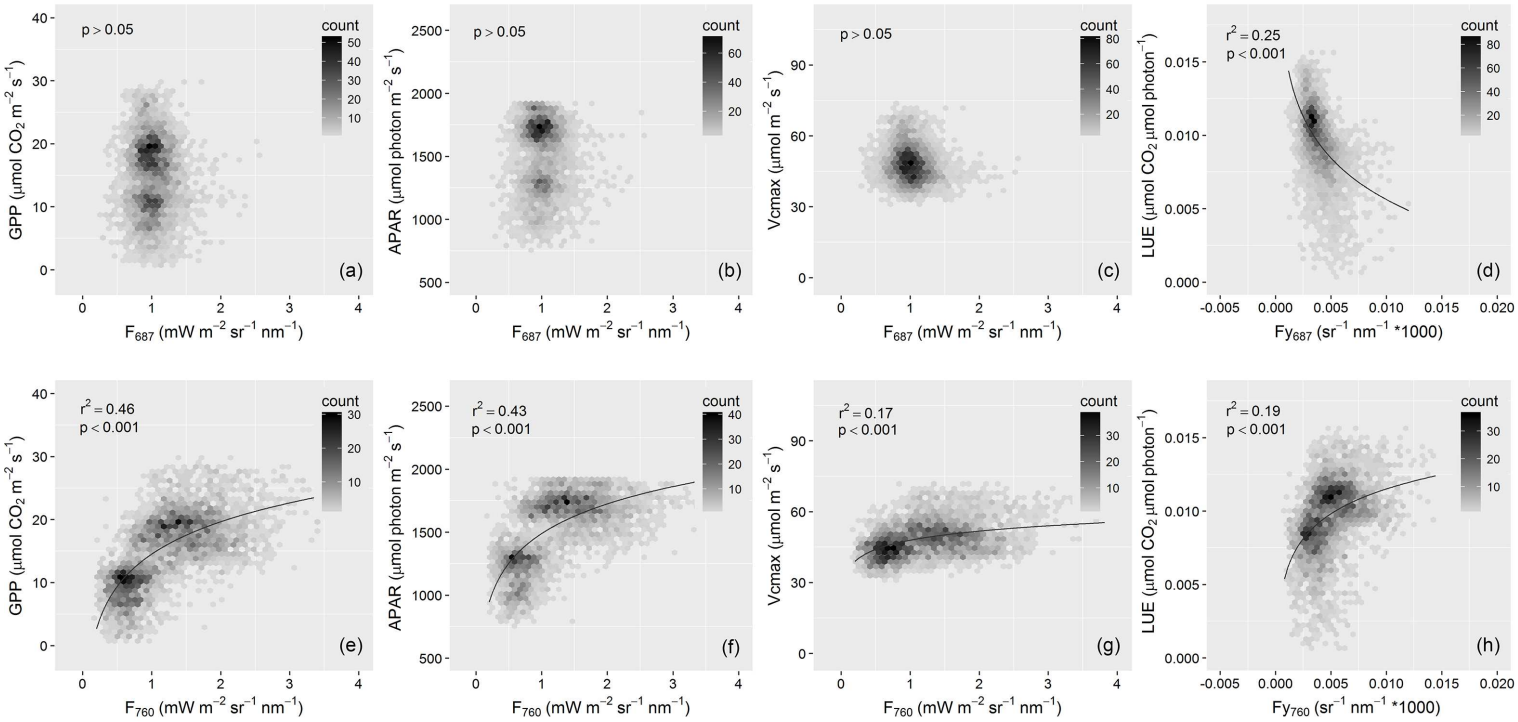

Figure 13: Relationships at tree crown level between: a) F_{687} and GPP, b) F_{687} and APAR, c) F_{687} and $Vcmax_{25}$, d) Fy_{687} and LUE, e) F_{760} and GPP, f) F_{760} and APAR, g) F_{760} and $Vcmax_{25}$ and h) Fy_{760} and LUE. The colour scale represents the point density. The solid curves correspond to a logarithmic model fitted between the paired variables.

et al., 2007). However, the use of regularisation strategies is critical to mitigate the drawbacks of ill-posedness and to obtain trustworthy results (Combal et al., 2002; Verrelst et al., 2014). In this study, LCC was accurately estimated with an r^2 of 0.65 and RMSE of 5.66 $\mu g\,cm^{-2}$ (refer to Table 5 for the complete summary of statistics) by inverting the canopy-level INFORM model coupled with the leaf-level PROSPECT-4 model. Previous studies conducted in similar contexts showed estimation accuracies ranging from ~4.5 to ~13.5 $\mu g\,cm^{-2}$ depending on the inversion strategy, sensor configuration and study site characteristics. Croft et al. (2013) obtained an accuracy of 6.42 $\mu g\,cm^{-2}$ (r^2 = 0.62) inverting the PROSPECT-4Scale model (Chen and Leblanc, 1997) in a mixed forest site using MERIS satellite data, that degraded to 10.45 $\mu g\,cm^{-2}$ (r^2 = 0.41) when inverting the model on CASI airborne hyperspectral data. Croft et al. (2015) further achieved an accuracy of 7.05-13.40 $\mu g\,cm^{-2}$ (r^2 = 0.79-0.38) using the same model in a follow-up study. Inverting the PROSPECT-DART model (Gastellu-Etchegorry et al., 1996) in coniferous sites, Hernández-Clemente, Navarro-Cerrillo, and Zarco-Tejada (2014) and Malenovský et al. (2013) obtained LCC estimates with an RMSE of 5.03 $\mu g\,cm^{-2}$ (r^2 = 0.54) and of 2.27-12.30 $\mu g\,cm^{-2}$ (r^2 = 0.72-0.41), respectively. It is worth noting that none of the aforementioned studies tested the use of regularisation options to constrain the model inversion apart from the use of prior information to restrict the variability of the model input parameters. In this study, LAI was estimated using the same LUT-parameterisation as for LCC of the coupled PROSPECT-4-INFORM model, obtaining an r^2 of 0.72 and RMSE of 0.5 $m^2\,m^{-2}$ (refer to Table 5 for the complete summary of statistics) compared to the ground measurements. Similar results were obtained inverting the INFORM model in broadleaved as well as coniferous forests by Wang et al. (2018) (RMSE = 0.43 $m^2\,m^{-2}$; r^2 = 0.63), Yang et al. (2011) (RMSE = 0.41 $m^2\,m^{-2}$; r^2 = 0.74), Atzberger (2000) (r^2 = 0.57) and Schlerf and Atzberger (2006) (RMSE = 0.58 $m^2\,m^{-2}$; r^2 = 0.73). The latter authors achieved lower accuracies (RMSE = 0.58 $m^2\,m^{-2}$; r^2 = 0.51-0.57) using the same model applied on multi-directional CHRIS-PROBA satellite data Schlerf and Atzberger (2012). Similar results were achieved using different RTMs, *e.g.* Omari et al. (2013) inverted the PROFLAIR model (White, Miller, and Chen, 2001) in a broadleaf-dominated forest obtaining an estimation accuracy of 0.47 $m^2\,m^{-2}$ (r^2 = 0.59) and Banskota et al. (2015) used DART to estimate LAI in a deciduous forest with an accuracy of 0.5-0.74 $m^2\,m^{-2}$ (r^2 = 0.6-0.64). Overall, the LAI estimation accuracy reported in literature ranges between ~0.4 and ~0.9 $m^2\,m^{-2}$. A systematic assessment of using different strategies for minimising the ill-posedness of the inversion has not been performed in studies conducted in forest ecosystems yet. However, it can be grasped from the previous works that the use of even few regularisation options (*e.g.*, prior information about the input parameters, multiple best solutions of the inversion, ecological rules to exclude unrealistic solutions) usually

leads to more accurate LAI retrievals. In this study, the coupled PROSPECT-4-INFORM model was successfully inverted providing reliable LCC and LAI spatialised maps in a mixed forest site. Besides the representativeness of the model, which provides a fair compromise between realism and simplicity, the parameterisation of the model to generate the LUT and the recourse to regularisation options were found to be advisable to obtain accurate retrievals, as highlighted in analogous studies conducted on crops (Verrelst et al., 2015c). The prior knowledge about the variability of the model input parameters allowed excluding unlikely combinations that constitute a source of error and unnecessarily increase the LUT size. Likewise, the global sensitivity analysis allowed an optimised model parameterisation: redundant information in the LUT due to multiple combinations carrying the same information was avoided, while the variability of most sensitive model parameters was maximised.

Consistently with the findings of Wang et al. (2018), who performed a sensitivity analysis of the PROSPECT-5-INFORM model, the leaf water content and leaf dry matter content showed a great influence on the modelled canopy reflectance (Figure 8). In addition, a great contribution of LCC to the variation of canopy reflectance was observed in the visible part of the spectrum, which was not considered in Wang et al. (2018). At the canopy level, the most affecting variables across the spectrum were LAI (understory and overstory) and crown diameter, while the stem density had a moderate influence on the output. This is not in complete agreement with the aforementioned study, but the authors suggested a mutual compensation between the three canopy structural parameters. Since the stem density did not vary much in our study site, it is likely that this resulted into a larger influence of LAI. Leaf structural parameters, canopy height and average leaf inclination, which showed a negligible effect on the reflectance variation, were fixed to maximise the predictive power of the model. Regarding the LUT-based inversion strategy, various optimisation options were tested in this work, including the use of different cost functions to match measured and modelled spectra, the addition of gaussian noise to the simulated data and the use of multiple solutions of the inversion. Our results showed a considerable impact of the choice of the cost function used to minimise the distance between the measured and simulated spectra on the retrieval of both LCC and LAI. As observed by Verrelst et al. (2014) in a study focused on the LUT-based retrieval of LCC and LAI in crops, we found that the use of the classical RMSE always led to sub-optimal results. The use of multiple best solutions also improved the estimates, although not being as impacting as the choice of the cost function. The addition of random noise to the simulations did not affect the retrieval in our case.

Beyond focusing on the retrieval of reflectance-based products, this work aimed at analysing the spatial variability of red and far-red sun-induced chlorophyll flu-

orescence across the study site, which constitutes a more direct proxy of the vegetation functional state (Wieneke et al., 2016). F_{687} and F_{760} were estimated using the spectral fitting methods with an r^2 of 0.75 and 0.74 ($p < 0.05$), respectively, as assessed from the comparison against the ground-based measurements. The SFM was exploited for the first time in this study to map the distribution of F at both the emission peaks over a forest area. F quantification using the SFM offers several advantages compared to other retrieval methods, *e.g.*, the exploitation of the oxygen absorption bands, where the signal is proportionally stronger than in the solar Fraunhofer lines, and the physically-based nature that makes it independent from the observed scene. On the other hand, the SFM approach requires a rigorous atmospheric correction scheme, which is not needed when using other methods (*e.g.*, Singular Vector Decomposition, improved Fraunhofer Line Discrimination) exploiting the dark lines in the solar spectrum (*e.g.*, Damm et al. 2014; Guanter et al. 2012).

The recognised challenges posed by the retrieval of red F (*e.g.*, the narrower shape of the O_2-B band compared to O_2-A and the overall lower signal detectable from above due to the reabsorption within the leaf and the canopy) resulted into a higher uncertainty in the retrieval of F_{687}, which appeared noisier than F_{760} at full resolution (1 m). However, the aggregation of the data at crown level for further analysis reduced this issue as a consequence of noise averaging.

Recently, F has been exploited to study photosynthetic activity of vegetation from RS. This is based on the mechanistic link between F emission, photochemistry and heat dissipation. However, this relationship is multifaceted and multiple gaps still need to be filled to have an unbiased understanding of the link between F and GPP. In particular, it remains unclear what is the nature of the relationship between far-red F and GPP at high spatial resolution. The relationship between red F and GPP remains even more ambiguous. To address these questions, we used the BESS model to derive GPP, APAR and LUE over the study site and to get insights into the relationships between red, far-red F and these variables at the tree crown level.

The high-resolution GPP, APAR and LUE maps obtained driving the model with airborne-derived inputs, taking into account inevitable model simplifications, are representative of the instantaneous carbon uptake, light absorption and light use efficiency at the time of *HyPlant*'s overpass. BESS is a process-based model, and its performances in predicting GPP were comprehensively evaluated in Ryu et al. (2011), Jiang and Ryu (2016) and Whitley et al. (2016). Ryu et al. (2011) validated the model at the global scale against eddy covariance (EC) tower flux data from 33 FLUXNET sites covering a broad range of plant functional types. The strong linear relationship found with modelled GPP (r^2 = 0.86, rbias = 5%) at annual composite provided experimental evidence of the model capacity to produce accurate

GPP estimates. Further evaluation of the model was carried out in Jiang and Ryu (2016) by means of a comparison against a set of 113 FLUXNET sites distributed worldwide in the period 2000-2015. The results at both 8-daily and annual composites confirmed the reliability of the model in predicting GPP (r^2 = 0.67 and r^2 = 0.93, respectively, compared to flux measurements). In Whitley et al. (2016), BESS was benchmarked against a set of models of increasing complexity, showing consistent performances with other terrestrial biosphere models. With respect to the ordinary BESS implementation, the differences in our study mainly reside in the high-spatial resolution data used to feed the model and in the snapshot nature of the analysis. The unavailability of EC tower data in the study site limited our possibility to directly compare *HyPlant*-BESS outputs with ground-based flux estimates, anyhow, a proper validation would have not been feasible even in case of their availability. The flux tower information is in fact a point measurement, which is valuable for monitoring the temporal variation of the carbon fluxes but is difficult to exploit for assessing their spatial variability. Because of the high-detail nature of this snapshot analysis and the data available, a more feasible option to check the model performances was the comparison between modelled variables and proxies of these variables that can be remotely sensed. As shown in Figure 14, BESS-fAPAR (*i.e.*, fraction of APAR, calculated as ratio between BESS-APAR and incoming PAR) was found to be highly correlated to VIs which are well-known to be related to the fraction of absorbed PAR. BESS-fAPAR showed the strongest correlation with VIs such as NDVI (Rouse, Haas, and Deering, 1974) (r^2 = 0.86, $p < 0.001$) and NDVIre (Gitelson and Merzlyak, 1994) (r^2 = 0.86, $p < 0.001$), which are sensitive to the photosynthetic component of the canopy. Conversely, the correlation with VIs related to the totality of the canopy such as NDSI (Inoue et al., 2008) was found to be lower (r^2 = 0.63, $p < 0.001$). This further supports the correct representation of the carbon fluxes by the model, since the modelled APAR that is used to estimate GPP is representative of canopy component which is effectively involved in photosynthesis.

The soundness of *HyPlant*-BESS results was made possible by the accurate spatial representation of LAI and LCC (from which $Vcmax_{25}$ was empirically derived) obtained through RTM inversion. These two variables constitute the two main drivers of BESS according to the sensitivity analysis performed in Ryu et al. (2011). Some potential uncertainties in GPP modelling can be associated with the use of LCC to infer $Vcmax_{25}$.

The relationship between far-red F and GPP has been shown to be strong in several studies conducted at different spatio-temporal scales over different vegetation types. Multiple studies exploiting satellite data showed a linear relationship between global scale annual averages of spaceborne F retrievals and data-driven upscalings of GPP from EC tower measurements (Frankenberg et al., 2011; Guan-

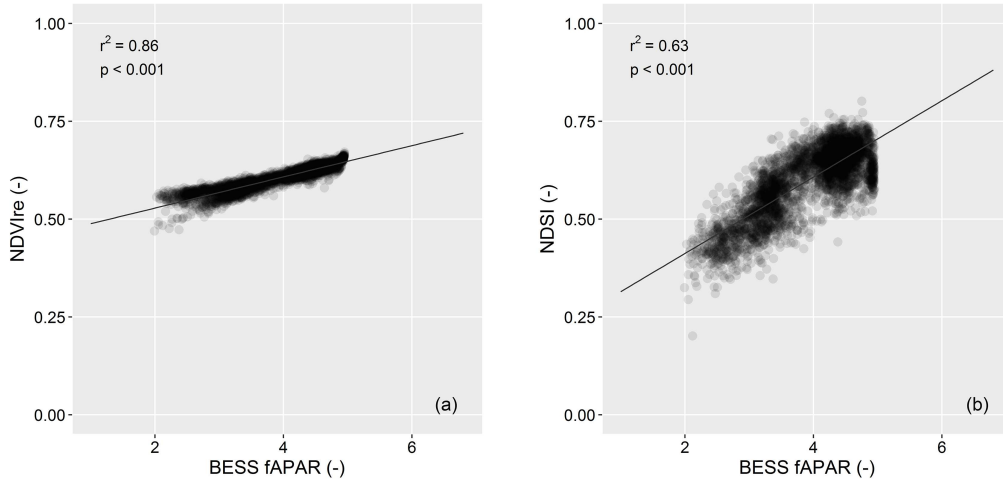

Figure 14: Relationships at tree crown level between BESS derived fAPAR and VIs: a) BESS-fAPAR and NDVIre; b) BESS-fAPAR and NDSI.

ter et al., 2014; Joiner et al., 2011). However, different results were obtained in studies conducted at local and regional scales as well as modelled data. Several authors found nonlinear and ecosystem-specific relationships (*e.g.*, Damm et al. 2015; Goulas et al. 2017; Zhang et al. 2016), revealing that this link is more complex at finer spatial resolution. As a matter of fact, this relation is the reflection of a complex interplay between species-specific functional traits and of the different functional strategies used to balance the photochemical and non-photochemical light dissipation (Tol et al., 2014). In addition, the distribution of the absorbing and scattering elements within the canopy determines the canopies to act as photon traps (Knyazikhin et al., 2013; Lewis and Disney, 2007). As a consequence, the escape probability of photons is a function of the complexity of the canopy architecture. All these factors modulate the F signal detected by the sensor, that in turn might be nonlinearly correlated with GPP when the scale of observation allows appreciating these effects.

Working at individual tree crown scale, we found a statistically significant positive nonlinear relationship between measured F_{760} and modelled GPP (r^2 = 0.46, $p < 0.001$), confirming the previous findings and demonstrating that even in a snapshot case an empirical relationship between the spatial variation of the two variables exists. However, the pronounced scattering of the data points suggests that there are other factors affecting the relationship that are apparently masked when working at broader spatial and/or temporal scales. To understand whether this actually depends on the scale of observation, the effect of spatial degradation

was tested on our data by aggregating *HyPlant* high resolution images at increasing spatial resolutions (*i.e.*, 10 m-20 m-40 m-80 m) (Figure 15). In contrast with the results showed in Figure 13, where the data were aggregated at crown level, the spatial aggregation exercise showed in Figure 15 provides an insight on situations that could be potentially observed at satellite scale, where the coarser spatial resolution does not allow working at individual crown level anymore.

The clear progressive decrease of the scattering along with the increase of the correlation (*i.e.*, r^2 = 0.29 at 10 m resolution and r^2 = 0.52 at 80 m resolution) suggests that the averaging of the spatial heterogeneity effectively improves the relationship between F and GPP. It can be also noticed that the relationship tends to become more linear as the spatial resolution increases, which is somewhat similar to what Damm et al. (2015) and Zhang et al. (2016) observed in the temporal dimension and might be explained by the reduction of the variability across the study site and by the changing impact of the confounding effects of canopy structure at coarser spatial resolution. A similar correlation was observed between F_{760} and APAR (r^2 = 0.43, $p < 0.001$). APAR has been shown to be the main driver of F_{760} temporal variability because of its large variation (Koffi et al., 2015; Li, Xiao, and He, 2018; Miao et al., 2018; Rossini et al., 2010; Yang et al., 2018; Yang et al., 2015). To disentangle such influence of APAR in the relation between F_{760} and GPP, the relationship between Fy_{760} (F_{760} /APAR) and LUE (GPP/APAR) was examined, revealing a significant positive nonlinear correlation (r^2 = 0.19, $p < 0.001$) between the two variables. This result is consistent with the findings of Verma et al. (2017), Yang et al. (2015), and Zhang et al. (2016), supporting the hypothesis that F_{760} contains information not only on APAR, but on both the terms that constitutes the equation GPP = APAR $\times$ LUE. Other studies conducted in the temporal domain found an opposite behaviour. For example, a recent work conducted by Yang et al. (2018) in a rice paddy site found that far-red F is a better proxy of APAR than GPP at high temporal resolution, suggesting a different meaning of the relationship between F, GPP and APAR in the spatial and temporal domain. Regarding F emitted in the red region, some studies suggested that it might be a more sensitive indicator of plants' photosynthetic activity due to the greater contribution of photosystem II in this region (Baker, 2008; Porcar-Castell et al., 2014; Verrelst et al., 2015b). Following this hypothesis, simulation studies conducted using the SCOPE model (Tol et al., 2009) showed that the relationship between red F and GPP should be similar or even better than the one observed between far-red F and GPP (Verrelst et al., 2016; Zhang et al., 2016). However, the few studies that exploited real red F observations to validate this finding showed contradictory results. While in Cheng et al. (2013) red F performed better than far-red F in predicting GPP, Goulas et al. (2017) and Liu et al. (2017) concluded that far-red F is a better proxy of GPP, especially when considering canopies with

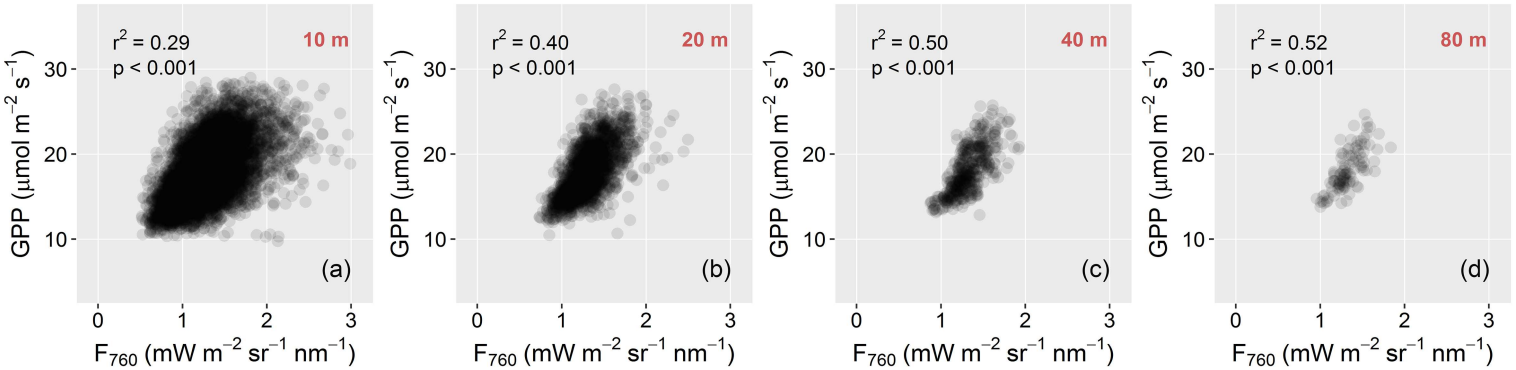

Figure 15: Relationship between F_{760} and BESS-GPP at increasing spatial aggregation: a) 10 m, b) 20 m, c) 40 m and d) 80 m.

varying biochemical and structural composition. This is supported by the modelling results of Du et al. (2017) and Liu et al. (2018), that show a heavily scattered relationship between red F and APAR compared to the one between far-red F and APAR, because of the greater influence of LCC and LAI variation. In our study, no significant correlation was found between the spatial variability of F_{687} and GPP and APAR. Yet, interestingly a statistically significant negative correlation emerged when normalising both red F and GPP by APAR ($r^2 = 0.25$, $p < 0.001$). To the best of our knowledge, whilst both positive and negative correlations were shown to be possible between Fy_{760} and LUE depending on the energy partitioning (Miao et al., 2018), no previous study investigated the relationship between Fy_{687} and LUE. Hence, further studies need to be performed in order to be able to interpret this finding. A possible explanation could be related to the role of reabsorption within the canopy, which has a strong effect on red F while almost not affecting far-red F.

3.5 CONCLUSIONS

In this study, *HyPlant* airborne high-resolution images acquired over a mixed forest ecosystem were exploited to obtain and analyse the spatial intra- and inter-variability of different variables related to vegetation biochemical, structural and functional state. Firstly, LCC and LAI, two key variables in vegetation-related studies, were estimated with accuracy of 5.66 $\mu g\,cm^{-2}$ and 0.51 $m^2\,m^{-2}$, respectively, by inverting the coupled PROSPECT-4-INFORM radiative transfer model. The high accuracy of the two spatialised products as well as their consistent spatial patterns were made possible by an optimal parameterization and inversion strategy applied on *HyPlant* hyperspectral data. Secondly, high-resolution maps of sun-induced chlorophyll fluorescence, an indicator of plants' photosynthetic activity, were obtained for the first time at both the red and far-red peaks over a forested area. The comparison against top-of-canopy measurements acquired at the same time of the overpass highlighted the accuracy of the estimates, demonstrating the reliability of the SFM retrievals ($r^2 = 0.73$ at O_2-B band; $r^2 = 0.74$ at O_2-A). Third, the spatialised plant traits obtained through RTM inversion were successfully exploited to drive a customised version of the Breathing Earth System Simulator (BESS), which provided GPP, APAR and LUE maps. These maps constitute an independent measure of the spatial variability of the instantaneous carbon fluxes and light absorption at the time of *HyPlant* overflight. BESS-GPP and APAR showed a nonlinear positive - even though scattered - correlation with F_{760} ($r^2 = 0.46$ and $r^2 = 0.43$, respectively). In addition, a positive nonlinear correlation was found between Fy_{760} and LUE ($r^2 = 0.19$). This result showed that this relationship,

usually observed in the temporal domain, can hold in the spatial domain at the scale of individual tree crowns. At the same time, it entailed the need of taking into account the spatial variability, since it revealed that the relationship between F and GPP can be more complex at more detailed scale. BESS-GPP, APAR and LUE were also compared against F in the red region, showing more unexpected results. No significant correlation was in fact found between F_{687} and GPP or APAR, while a negative correlation was observed between Fy_{687} and LUE ($r^2 = 0.25$).

Jointly, our results provided insights into the critical role of the spatial heterogeneity in controlling the carbon fluxes, highlighting the importance of using high spatial resolution RS data to grasp the complexity of the terrestrial ecosystem dynamics. Furthermore, they pointed out the need to integrate different RS derived products to obtain a comprehensive picture of the vegetation related processes. Further research in this direction constitutes a high priority for advancing the understanding of terrestrial ecosystem dynamics and prediction of their future responses to a changing climate.

4 SUN-INDUCED CHLOROPHYLL FLUORESCENCE AS A PROXY OF FUNCTIONAL DIVERSITY

ABSTRACT

[1] Over the last decades, the increasing anthropogenic pressure and the climate change deeply modified the ecosystems functioning impacting biodiversity. Because of the ecological relevance of biodiversity loss, understanding the relationship between biodiversity and ecosystem functioning as well as monitoring biodiversity changes became key research objectives. In this framework, the development of tools capable of providing repeated and spatially-resolved information about biodiversity appears critical. Due to its inherent capacity of providing large-scale and temporally continuous information in a time- and cost-effective way, remotely sensed surface reflectance data have been used increasingly for this purpose over the last years. However, the objective is still far to be reached. In this work, we examined for the first time the potential of sun-induced chlorophyll fluorescence (F) as a novel indicator of the functional diversity of terrestrial ecosystems. This was achieved exploiting high spatial resolution images acquired with the FLEX airborne demonstrator *HyPlant*. *HyPlant* was flown in 2013 over a temperate forest ecosystem characterized by a relevant variability in terms of forest species and management stages. Different approaches were tested to quantify the functional diversity based on reflectance and fluorescence data. We used the Shannon's index and the Rao's Q diversity to measure the heterogeneity across the study site. The two metrics, which differ from each other due to the fact that the Rao's Q diversity explicitly takes into account the numeric value of each

1 The content of this Chapter belongs to a manuscript that is currently in preparation and will be submitted to Remote Sensing of Environment as: Tagliabue, G., Panigada, C., Celesti, M., Cogliati, S., Colombo, R., Migliavacca, M., Rascher, U., Rocchini, D., Schüttemeyer, D., Rossini, M. "Sun-induced fluorescence as a proxy of functional diversity".

pixel, were calculated likewise from a traditional reflectance-based vegetation index (*i.e.*, Normalised Difference Vegetation Index (NDVI)) and from F retrieved at 760 nm using the spectral fitting method. The entropy patterns obtained were compared against a functional diversity map used as a reference. Results showed a strong underestimation of the functional diversity when using NDVI as input for the entropy calculation. In particular, the low NDVI-based entropy observed in the regeneration stands of the forest evidenced that NDVI cannot grasp the variability of the functional diversity. Conversely, F-based entropy showed a fair agreement with the patterns observed in the reference map. The results obtained demonstrated that F might be a powerful tool for assessing the ecosystem functional diversity, opening new perspectives for monitoring biodiversity at different spatial and temporal scales.

4.1 INTRODUCTION

Anthropogenic activities and climate change are impacting biodiversity causing so called "global biodiversity crisis". This is of particular interest because of the ecosystem capacity of providing services (Cardinale et al., 2011; Koh et al., 2004; Lausch et al., 2016) and of the relationship between biodiversity and ecosystem functioning (Balvanera et al., 2006; Schulze and Mooney, 1993; Tilman, Isbell, and Cowles, 2014), stability (Isbell et al., 2015; Musavi et al., 2017) and resilience (Schwalm et al., 2017), despite contrasting positions in literature (Grossiord et al., 2014). For this reason, the international community is engaging urgent action to avert biodiversity loss and degradation of ecosystem services, as framed *e.g.* in the European Biodiversity Strategy for 2020. In this context, the capacity of monitoring biodiversity across space and over time in a reliable and consistent way is critical, but this objective is still far to be reached (Pettorelli et al., 2017).

In the last few years, the usefulness of passive remote sensing (RS) observations has been largely investigated (Kuenzer et al., 2014; Nagendra, 2001; Schweiger et al., 2018). RS, due to its capacity of providing large-scale, long-term consistent information about the Earth, is inherently characterised by a huge potential in the detection, quantification, assessment and forecasting of biodiversity at the global scale Kuenzer et al., 2014; Pettorelli et al., 2016. So far, research has mainly focused on three approaches: i) mapping plant species or functional types; ii) mapping habitats and iii) establishing a direct relationship between biodiversity (either taxonomic or to less extent functional) and RS data (Asner et al., 2017; Gholizadeh et al., 2019, 2018; Nagendra, 2001; Schneider et al., 2017). The latter approach is usually either based i) on the use of inverse radiative transfer modelling and dimensionality reduction methods (Asner et al., 2017; Schneider et al., 2017) or

ii) on the concept of spectral variation hypothesis (Palmer et al., 2002). This theory states that the biodiversity signal is encoded in the spectral variability, and therefore the larger is the spectral heterogeneity across space, the higher is biodiversity. Based on this hypothesis, different approaches were proposed to quantify the spatial heterogeneity and thus biodiversity.

During the last decade, the relationship between biodiversity and ecosystem functioning emerged as a central issue in ecological studies (Loreau et al., 2001). The link has been established based on experimental studies showing a positive relationship between ecosystem productivity and plant diversity (Balvanera et al., 2006; Cardinale et al., 2011; Hooper et al., 2005), and underlies a broad definition of biodiversity, *i.e.*, refers to the functional diversity. In particular, conversely to the traditional concept of biodiversity which refers to the taxonomic diversity (*i.e.*, the diversity in terms of species composition and abundance), the functional diversity considers the variability of plant traits (PTs), which varies within species and constitutes a determinant of the ecosystem functioning (Diaz et al., 2007; Musavi et al., 2015; Ruiz-Benito et al., 2014; Tilman et al., 1997).

The exploitation of the link between functional diversity and ecosystem functioning depends on the efficient mapping of the functional diversity across space. To this purpose, various measures have been proposed over the last years (Mouchet et al., 2010; Petchey and Gaston, 2006; Schneider et al., 2017). These approaches are primarily based on continuous mapping the PTs variability, which is justified by the relationship between PTs and ecosystem functional properties (EFPs), which are descriptors of the ecosystem functioning (Reichstein et al., 2014). In this direction, due to its close relationship with both the variability of PTs and the vegetation functioning, sun-induced chlorophyll fluorescence (F) might be a novel and powerful synthetic metric for inferring the functional diversity.

In this framework, the objective of this study was to test the potential of a novel approach based on the use of remotely sensed F for the assessing the functional diversity. As far as we know, this is the first attempt trying to couple F with the concept of spectral variation hypothesis. We aimed at answering the following research question:

- Is sun-induced chlorophyll fluorescence a valuable information to improve functional diversity mapping compared to state of the art measures based on reflectance?

To achieve this objective, high-resolution airborne images acquired with the *HyPlant* airborne imaging sensor (Rascher et al., 2015) over a temperate mixed forest ecosystem were used to map the functional diversity using different approaches: the potential of F was compared against the use of a traditional vegetation indices

(VIs) commonly used in ecology (Rouse, Haas, and Deering, 1974). In addition, different metrics for the estimation of the spatial heterogeneity were tested, and their advantages and drawbacks discussed.

4.2 DATA AND METHODS

4.2.1 Study Site

The site selected for this study is the Hardt Forest, a temperate forest located in France (47°48′29" N, 7°26′53" E; Mulhouse; Alsace). The analysis was limited to a subset of the forest (*i.e.*, ~90 ha) covered by the *HyPlant* overpasses.

The Hardt Forest is dominated by the presence of broadleaved species (~90%), with a sparse presence of deciduous and evergreen coniferous ones (~10%). The most common species in the main canopy layer are: European hornbeam (*Carpinus betulus* L.), pedunculate and sessile oak (*Quercus robur* L., *Quercus petraea* (Matt.) Liebl.), field maple (*Acer campestre* L.), small-leaved linden (*Tilia cordata* Mill.), Scots pine (*Pinus sylvestris* L.) and European larch (*Larix decidua* Mill.). As a result of the management, the forest is structured in stands of at least 500 m minimum dimension which are characterised by a relative variability in terms of management stages.

The region where the forest is located is temperate, with an average temperature of 22°C in summer and of 4°C in winter. The mean annual rainfall is 680 mm, with a maximum typically between May and August.

A field campaign aiming at collecting spectral measurements, PTs and ancillary meteorological data in the time window of the airborne acquisitions was conducted in the summer of 2013. For a detailed description of the ground and airborne data acquisition and pre-processing refer to Paragraphs 3.2.2 and 3.2.3 of Chapter 3, respectively.

4.2.2 Forest species mapping

The reflectance cube obtained from the DUAL module of *HyPlant* was used to map the forest species distribution over the study site. The classification was performed with a supervised machine learning method, targeting seven different tree species (*i.e.*, *Carpinus betulus* L., *Quercus robur* L., *Quercus petraea* (Matt.) Liebl., *Acer campestre* L., *Tilia cordata* Mill., *Pinus sylvestris* L., *Larix decidua* Mill.) grouped into six classes: ”Hornbeam”, ”Oak”, ”Maple”, ”Linden”, ”Pine” and ”Larch”. An additional class named ”Defoliated trees” was defined in order to detect trees,

mainly hornbeams and maples, affected by crown defoliation due to an infestation of caterpillars at the time of the campaign. Mature and regeneration patches of the forest were classified separately. This choice was motivated by the high variability of the spectral signal among trees of the same species at different development stage, caused by differences in the leaf biochemical properties as well as in the canopy architecture. The classification scheme described hereafter was repeated likewise for both, masking out alternatively either the mature or the regeneration stands.

The training set was prepared selecting pure spectral endmembers for each class by integrating the knowledge derived from the field surveys and the visual interpretation of high resolution orthophotos and RGB images acquired from UAV. These endmembers consisted of polygons targeting pure tree crowns over a wide patch of the study area in order to capture the intra-specific spatial variability. Depending on the occurrence of the species and the crown size, 15 to 30 polygons, each consisting of 6 to 10 pixels, were collected for each class, constituting a training set of ~700 pixels.

The training set was used to train a support vector machine (SVM) algorithm with a radial basis function kernel (Vapnik, 1995) at clustering the pixels into the defined classes. The SVM is a non-parametric classifier based on the statistical learning theory proposed by Vapnik and Chervonenkis (1971). The rationale of the classifier is to try to separate the classes by defining an optimal n-dimensional hyperplane that maximises the distance from the closest data points, referred to as support vectors, through the minimisation of a cost function (Vapnik, 1995). The SVM algorithms have been used increasingly in RS in the last few years because of their effectiveness and suitability in handling high-dimensional data (Melgani and Bruzzone, 2004; Mountrakis, Im, and Ogole, 2011; Pal and Mather, 2005). In particular, they have been extensively applied for tree species classification in different biomes using hyperspectral data, showing outperforming accuracies compared to other classification methods (Dalponte et al., 2009, 2013; Feret and Asner, 2013; Melgani and Bruzzone, 2004; Pal and Mather, 2004). A relevant property of the SVMs, making them suitable for hyperspectral data classification, is their low sensitivity to the so-called Hughes phenomenon (Hughes, 1968). This effect consists in a decrease of the classification accuracy when the ratio between the number of input features and training samples outreaches a certain threshold, due to the fact that the estimation of the classifier parameters (*e.g.*, the estimation of the covariance matrices in the case of the Maximum Likelihood classifier) becomes complicated. This phenomenon, which is frequent in RS applications because the availability of training samples is usually limited, is critical when using hyperspectral data since it requires using feature reduction techniques at the cost of a loss of information and time. The SVMs proved to be unaffected by this issue

(Camps-valls and Bruzzone, 2005; Melgani and Bruzzone, 2004; Pal and Mather, 2004; Waske and Benediktsson, 2010), hence, all the features were used as input for the classifier.

For the accuracy assessment, a testing set composed of ~400 pixels was selected on the image using a random stratified sampling scheme. In order to ensure the representativeness of the testing sample for all the classes, the number of testing samples was defined for each class according to the relevance of the class. Each testing sample was labelled through visual interpretation and used as ground truth in the validation process. The standard accuracy metrics (*i.e.*, overall accuracy (OA), producer's accuracy (PA) and user's accuracy (UA)) were calculated from the confusion matrix generated by crossing the classification result with the ground truths.

4.2.3 Far-red F retrieval

F was retrieved at the far-red emission peak (*i.e.*, 760 nm) from *HyPlant* ultra-fine resolution observations using a dedicated processing-chain. The retrieval is based on the SFM approach (Cogliati et al., 2015) adapted to *HyPlant* data to derive a F at the O_2-A absorption band (*i.e.*, F_{760}). The rationale behind the SFM relies on the exploitation of mathematical functions to model the canopy reflectance and fluorescence spectra at the different wavelengths in order to decouple the F signal from the reflected radiance. In the current implementation, the spectral function parameters used to model reflectance and fluorescence were estimated directly comparing *HyPlant* at-sensor radiance with forward RT simulations. Conversely, the atmospheric input parameters were derived from sunphotometer measurements collected synchronously to the *HyPlant* overpasses. The maps were ground-validated by comparing the airborne retrievals with ground-based spectral measurements collected over six selected forest targets. For a detailed description of the retrieval scheme refer to Paragraph 3.2.4.1 of Chapter 3.

4.2.4 Diversity measures from reflectance and fluorescence RS data

The heterogeneity across the study area was measured using three different metrics related to the diversity: the species richness, the Shannon's index (Shannon, 1948) and the Rao's Q diversity (Rao, 1982). The species richness was calculated as number of different tree species within the considered kernel based on the species classification map. The Shannon's index (H) was calculated as in Eq. 2, where p is the relative proportion of the *i-th* value within the considered kernel.

$$H = -\sum_{i=1}^{n} p_i \ln p_i \tag{2}$$

The Shannon's entropy is non-dimensional, namely it just accounts for the relative abundance of pixel values, without considering their distance in a spectral space. To solve this issue, the Rao's Q diversity (Q) has been proposed in RS applications (Rocchini, Marcantonio, and Ricotta, 2017), since it discriminates between different *i* values and was calculated as in Eq. 3, where *dij* is the dissimilarity between two values *i* and *j* based on the Euclidean distance.

$$Q = \sum_{i=1}^{n} \sum_{j=1}^{n} d_{ij} p_i p_j \tag{3}$$

The two entropy measures (*i.e.*, H and Q) were calculated likewise from the reflectance and fluorescence-based maps of the study area. The NDVI index (Rouse, Haas, and Deering, 1974) was selected as a synthetic descriptor of vegetation based on reflectance, while F_{760} was used as fluorescence-based metric. In addition, the Shannon's index was calculated from the species classification map.

The NDVI and F_{760} maps were converted to 8 bits and re-scaled between 0 and 1 before calculating entropy to harmonize the range and variability of the two variables. Moreover, the inter-crown shadows were masked using a threshold on red and near-infrared reflectance. A moving kernel approach was used to derive the Shannon and Rao's indices over the whole NDVI and F_{760} images: the metrics were calculated within a kernel of 3×3, 5×5 and 9×9 pixels iteratively for each pixel of the matrices. The coding was performed in R (R Core Team, 2018) using a user-defined function for the Shannon's index and the `spectralrao` function stored in the GitHub repository `https://github.com/mattmar/spectralrao` for the Rao's Q calculation (Rocchini, Marcantonio, and Ricotta, 2017).

4.2.5 Functional diversity metrics

To obtain an independent measure of the functional diversity over the study area, four key PTs were selected and mapped using the airborne hyperspectral data. Based on their ecological relevance, we selected leaf chlorophyll content (LCC), leaf area index (LAI), leaf water content (LWC) and leaf dry matter content (LDMC). The selected traits were retrieved from the DUAL hyperspectral reflectance cube through a Look-Up-Table (LUT) based inversion of the coupled leaf and canopy PROSPECT-4-INFORM radiative transfer model (RTM) (Atzberger, 2000; Jacquemoud and Baret, 1990). The RTM was parameterised based on previous knowledge about the variability of the model input parameters in the forest

and on the results of a global sensitivity analysis. The model was run in forward to generate a LUT of 30000 simulated spectra. Hence, the traits of interest were retrieved by inverting the model with a LUT-based approach. Regularisation options were used to minimise the drawbacks of ill-posedness: LCC was retrieved using a logarithmic minimum contrast cost function (Leonenko, Los, and North, 2013) and averaging the first ten solutions of the inversion; LAI was retrieved with a divergence measure cost function formalised by Kullback and Leibler (1951) and averaging the ten best solutions; LWC and LDMC were obtained using the Root Mean Square Error (RMSE) as cost function and averaging the ten best solutions. For a thorough description of the RT model and of the retrieval strategy refer to Paragraph 3.2.4.2 of Chapter 3.

A Principal Component Analysis (PCA) was used to combine LCC, LAI, LWC and LDMC and to remove the statistical redundancy in the multiple selected traits. Because of the different units, the traits were re-scaled between 0 and 1 before applying the PCA. Following the same approach as for NDVI and F_{760}, the Rao's Q diversity was calculated over the entire image using the R `spectralrao` function. The mode `multidimension` was set to use multiple matrices as input for the diversity calculation. We selected the first three PC, that together explained 96% of the total variance of the four selected PTs.

4.3 RESULTS

4.3.1 Forest species map and species diversity

The classification process applied on *HyPlant* high-resolution imagery enabled to produce a thematic map of the distribution of the main tree species in the Hardt forest (Figure 16a).

Table 6 shows the confusion matrix obtained crossing the ground truths with the classification results. The overall accuracy (OA) obtained was 75.1%, while the producer's (PA) and user's (UA) accuracies ranged between 60-93% and 63-97%, respectively, depending on the considered class. Scots pine was mapped with the highest accuracy due to its spectral dissimilarity compared with the broadleaves, which were characterised by a higher misclassification. The defoliated tree class showed a high UA (89.2%), but the low PA (58.6%) highlighted that the defoliated trees were sometimes not identified, probably depending on the degree of defoliation.

The thematic product obtained highlighted a non-homogeneous abundance and distribution of the different forest species. Overall, the most common species were oak and hornbeam, but the two species were characterised by a different spatial

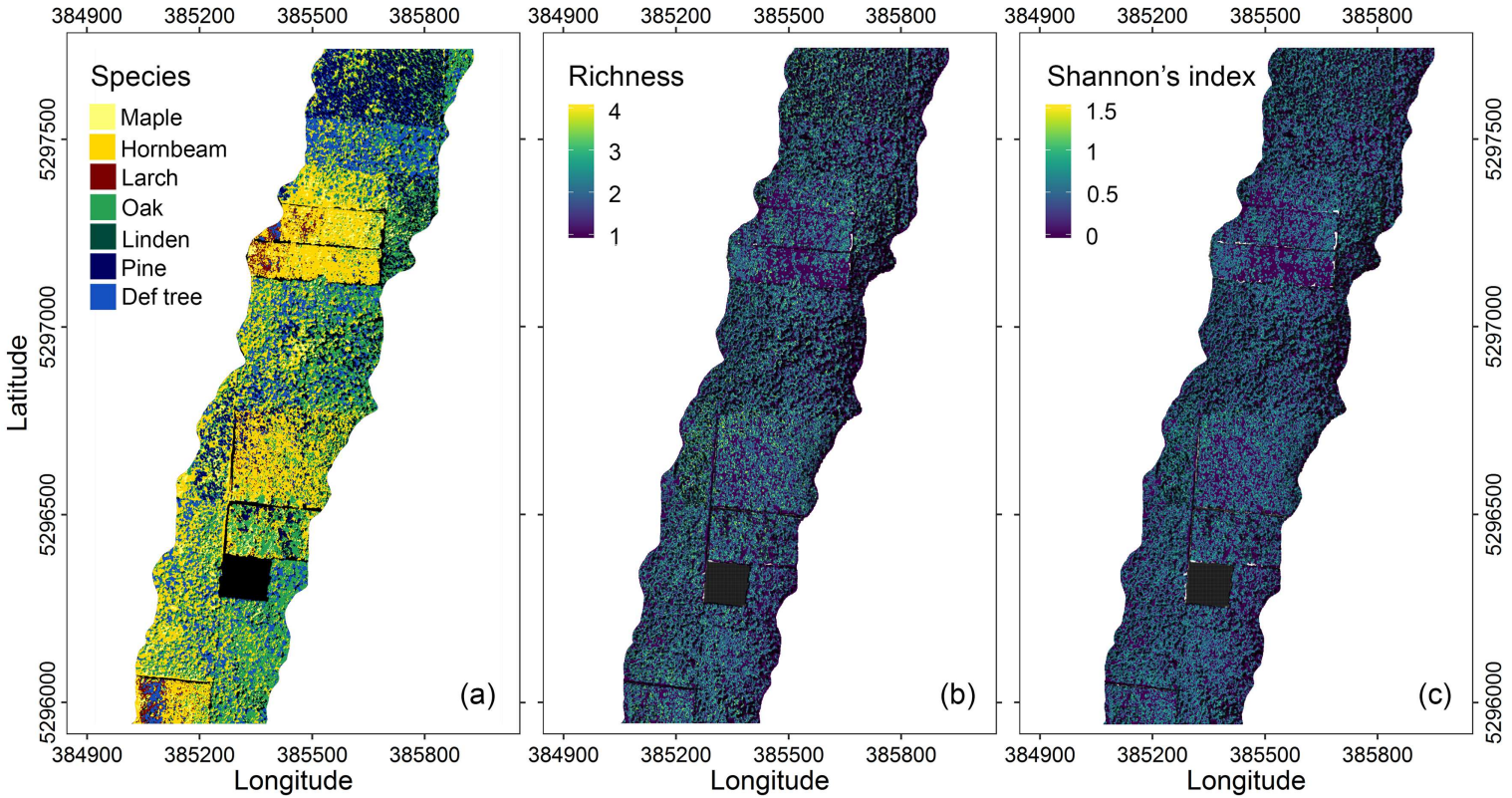

Figure 16: a) Thematic map of the dominant tree species in the Hardt forest obtained with the support vector machine (SVM) algorithm; b) Species richness calculated from the species map using a kernel of 3 × 3 pixels; c) Shannon's index calculated from the species map using a kernel of 3 × 3 pixels.

Table 6: Confusion matrix obtained from the validation scheme. Columns represent the true classes while rows represent the classification results. The user's (UA) and producer's (PA) accuracies are reported in the last column and row, respectively. The overall accuracy (OA) is also displayed.

		Ground Truth							
		Hornbeam	Oak	Linden	Maple	Pine	Def. trees	Tot	UA
SVM classification	Hornbeam	78.4%	4.9%	0%	0%	0%	14%	19%	75.3%
	Oak	16.2%	77.5%	12.5%	0%	7.1%	24%	30.9%	63.2%
	Linden	1.3%	8.8%	76.8%	6.2%	0%	0%	13.6%	78.2%
	Maple	2.7%	5.9%	10.7%	93.7%	0%	2%	11.4%	65.2%
	Pine	0%	0%	0%	0%	85.7%	1%	9.1%	97.3%
	Def. trees	1.3%	2.9%	0%	0%	7.1%	58.6%	16.1%	89.2%
	Tot	100%	100%	100%	100%	100%	100%	100%	
	PA	78.4%	77.5%	76.8%	93.7%	85.7%	58.6%		OA = 75.1%

distribution. While oaks were found to prevail over hornbeams in the mature forest, the regeneration areas were overwhelmingly dominated by hornbeam. Pine was fairly common but mainly limited to confined patches of the forest (*e.g.*, the managed patch in the northern patch of the study area). Maple, linden and larch presented a scattered distribution throughout the entire forest. The defoliated trees were widespread across the mature forest, while almost absent in the regeneration stands.

The species richness and the Shannon's index calculated from the species map are shown in Figure 16b and Figure 16c, respectively. Both these diversity metrics based on the spatial distribution of the tree species across the site showed a low heterogeneity and range of variation across space. The patterns are consistent in the two images and reflect a poor biodiversity in the study site in terms of species composition.

4.3.2 Shannon's diversity

The Shannon's index maps obtained from NDVI and F_{760} using a kernel of 3 $\times$ 3 pixels are shown in Figure 17a and Figure 17b, respectively. In both cases, a low variability of the index was observed, with generally high entropy values all over the forest. Such a relative homogeneity is the result of a low sensitivity of the Shannon's index due to the large variability of NDVI and F_{760} values across space. This is particularly evident in the Shannon's entropy calculation based on F_{760}, where the index is nearly everywhere close to saturation.

4.3.3 Rao's Q diversity

An RGB composite of the principal components (PCs) obtained from the PCA analysis calculated on the PTs (*i.e.*, LCC, LAI, LWC and LDMC) is shown in Figure 18a. LCC, LAI, LWC and LDMC used as input of the PCA have a mean and standard deviation of 0.48±0.10, 0.46±0.18, 0.50±0.08 and 0.48±0.06, respectively, when scaled between 0 and 1. The frequency histograms of the re-scaled traits are shown in Figure 18b, Figure 18c, Figure 18d and Figure 18e.

Different patterns in the forest were clearly distinguishable in the map (Figure 18). These patterns are related to the diversity in terms of the biochemical and structural traits mapped and reflect the differences in the ecological functioning. Magenta-orange areas correspond to high values in the first PC, which is strongly related to LAI and moderately correlated with LCC and LWC. These patches correspond to regeneration areas of the forest, where trees are younger and the canopy density is higher. The mature part of the forest is dominated by green-bluish

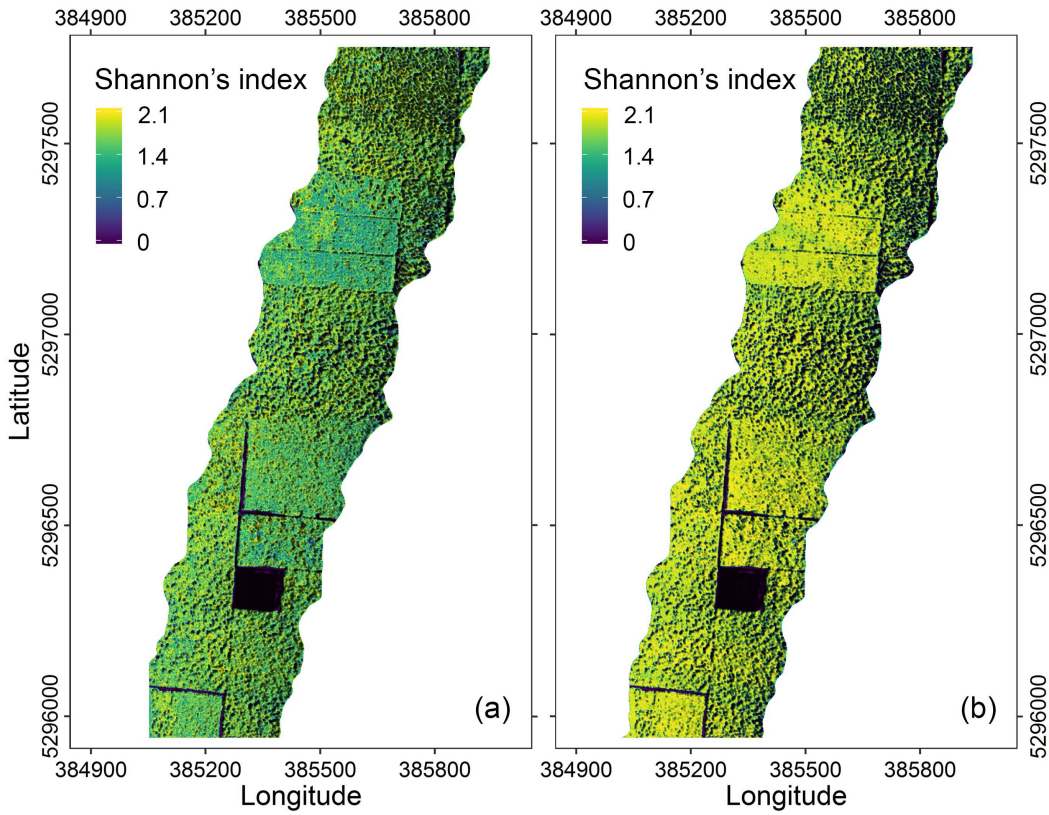

Figure 17: Shannon's index maps calculated from a) NDVI and b) F_{760} using a kernel of 3×3 pixels.

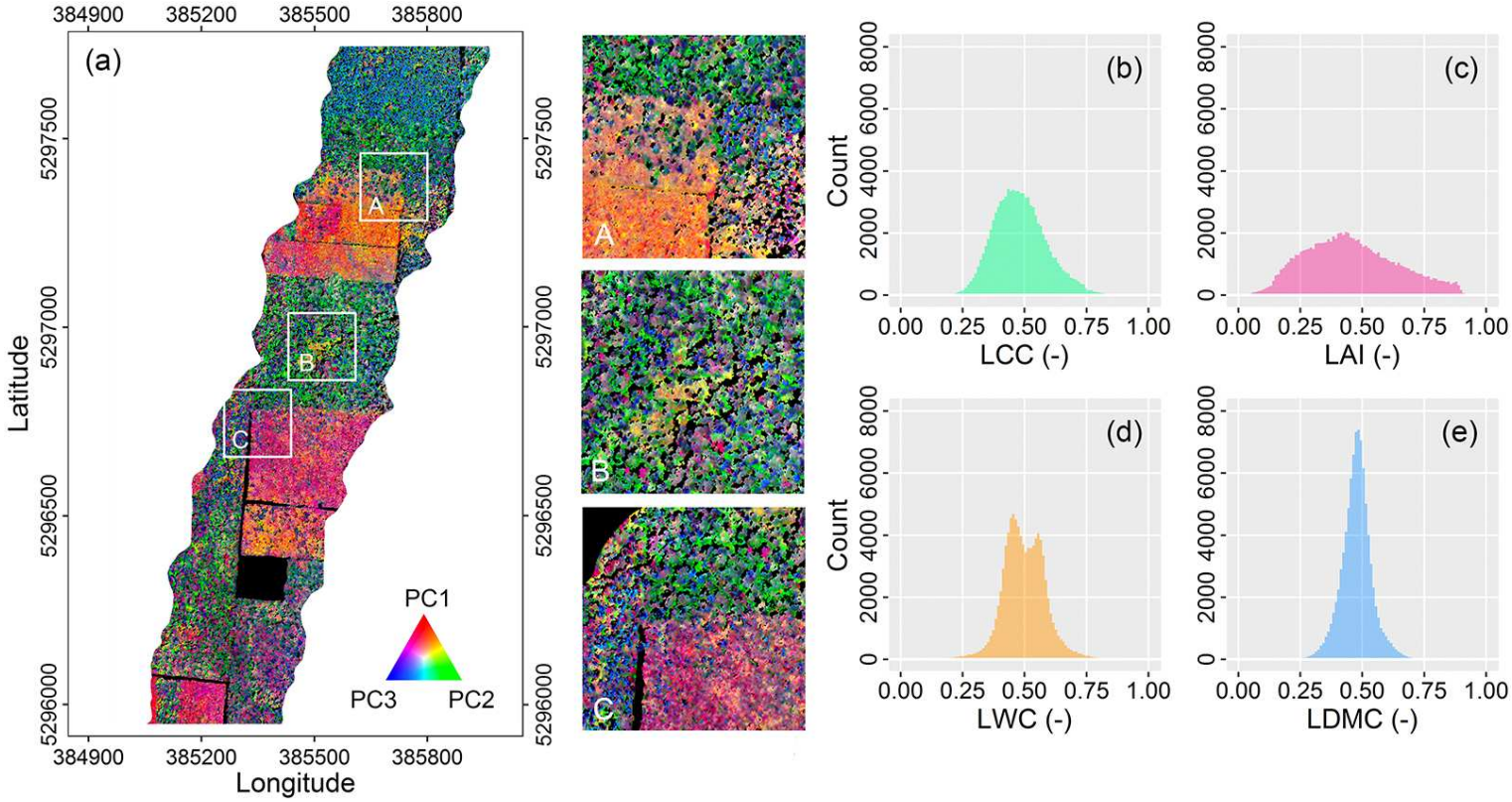

Figure 18: a) RGB composite of the first three Principal Components (PC) derived from the analysis performed on leaf chlorophyll content (LCC), leaf area index (LAI), leaf water content (LWC) and leaf dry matter content (LDMC) derived from the airborne imaging spectroscopy. The colours are the result of the combination of the first (PC1), second (PC2) and third (PC3) principal component in the R, G and B channels, respectively. The histograms show the distribution of b) LCC, c) LAI, d) LWC and e) LDMC scaled between 0 and 1 across the entire image.

colours, indicating a high influence of the second and partly the third PC. The second PC is positively correlated with LCC and negatively correlated with LWC and LDMC, while it is not correlated with LAI. The third PC is strongly driven by the LDMC alone. The effect of the third PC is dominant in the conifers, which appear light-blue in the image. The subregions marked in the image are representative of three different conditions encountered across the area: subset A marks an area at the edge between the regeneration and mature forest, where the managed plantation is characterised by high values in the first and second PC; subset B is a 100% mature forest area where the canopy is complexly structured and subset C marks a mixed regeneration/mature forest area where the regeneration stand presents high values in the first and third PC and the mature stand has a different species composition compared to subset A.

The functional diversity map obtained applying the Rao's Q diversity metric to the first three PC is shown in Figure 19a. The patterns reveal a high diversity in the forest, highlighting the presence of patches characterised by different entropy. The highest Rao's Q values are observed in the regeneration stands of the forest, which are also characterised by a considerable spatial variability. In contrast, the mature forest appears in general more homogeneous, but high diversity spots can also be observed. The use of kernels of increasing size (up to 9 × 9 pixels) to calculate the Rao's Q diversity did not significantly affect the observed entropy patterns (r^2 = 0.92 and r^2 = 0.71 comparing the Rao's Q calculated using a kernel of 3 × 3 against kernels of 5 × 5 and 9 × 9, respectively).

The diversity maps obtained calculating the Rao's Q diversity from the NDVI and F_{760} maps are shown in Figure 19b and Figure 19c, respectively. NDVI-based Rao's Q was characterised by generally low values across the entire image. In particular, very low entropy was observed in the regeneration stands, with Rao's Q values of ~5000. The highest diversity was observed in correspondence of the mature areas of the forest characterised by a significant presence of coniferous species, *e.g.*, the stand in the northern part of the image and the area on the left respect to the regeneration patch in the central part of the image. In these areas, the Rao's Q diversity reached values up to ~35000. F_{760}-based Rao's Q presented a larger heterogeneity across the image. The regeneration stands showed the highest entropy (~150000), while the lowest entropy was observed in the coniferous stands (~50000). Overall, the diversity was considerably higher compared to NDVI-based Rao's Q.

Figure 20 shows a zoom of the Rao's Q diversity based on PC, NDVI and F_{760} in correspondence of subsets A, B and C. In addition, for a more quantitative evaluation of the patterns observed in the images, the spatialised residuals of the linear models fitted between NDVI and PC based Rao's Q, and between F_{760} and PC based Rao's Q were plotted. The distribution of negative (blue bubbles) and pos-

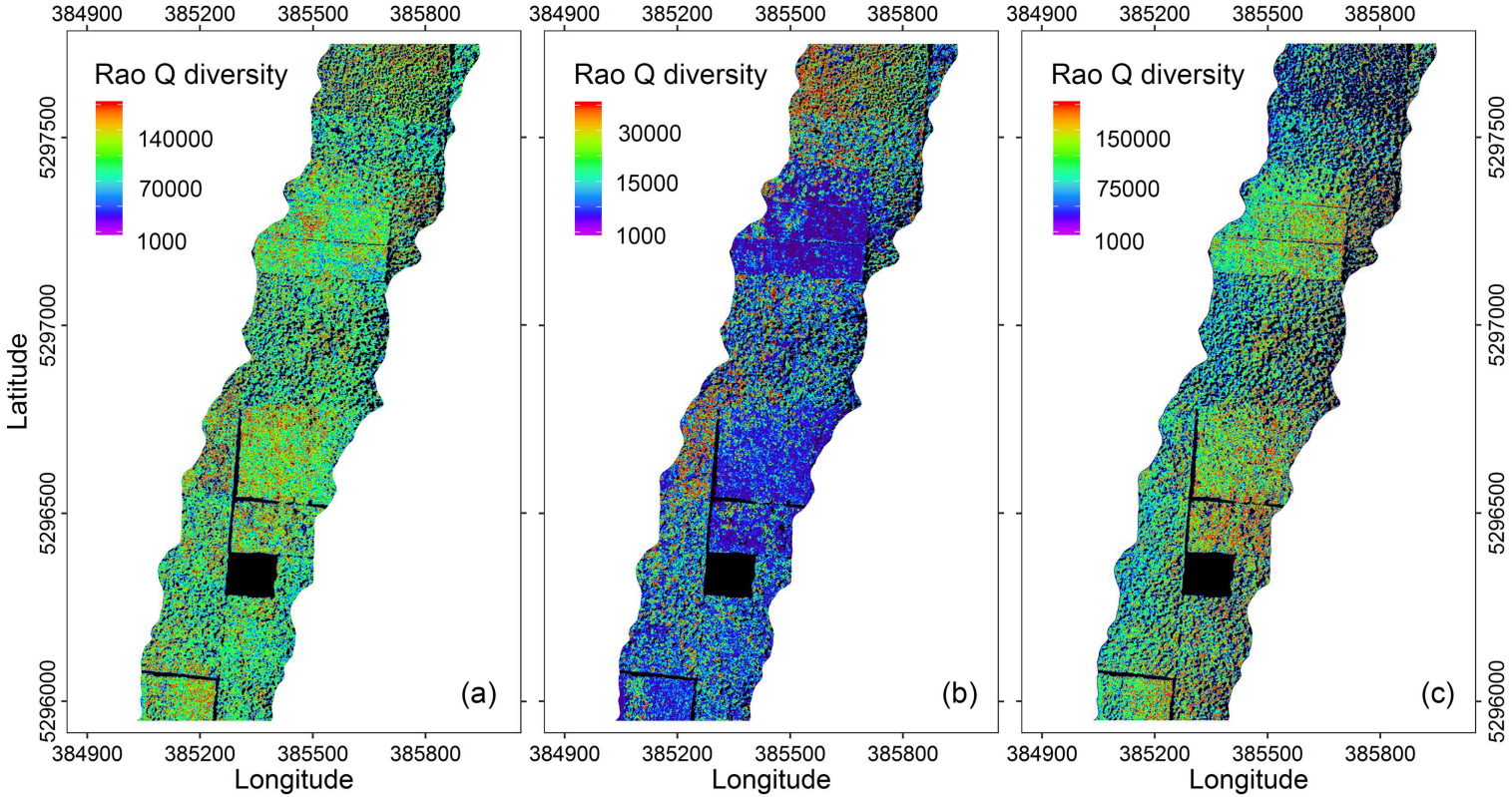

Figure 19: Rao's Q diversity metric calculated from a) PC, b) NDVI and c) F_{760} using a kernel of 3×3 pixels.

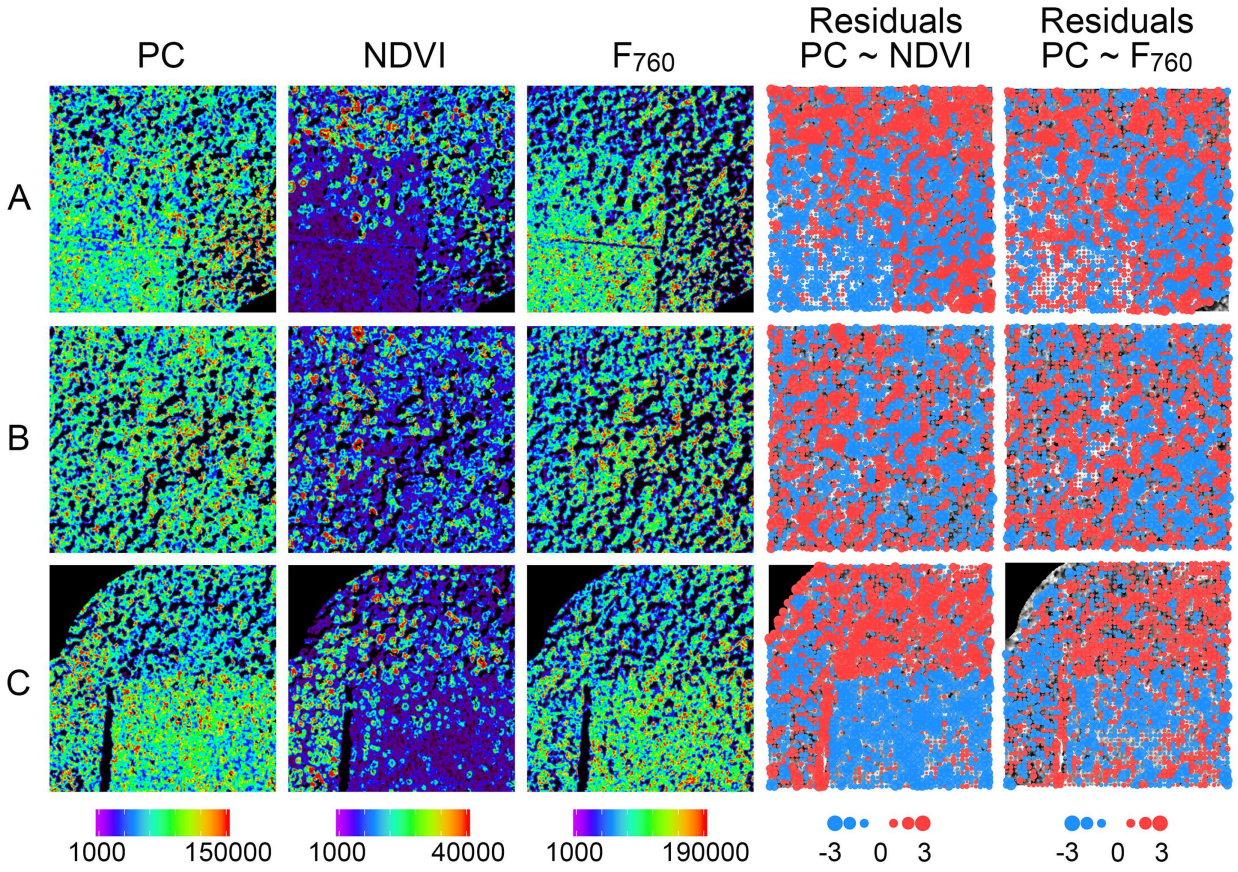

Figure 20: Rao's Q diversity calculated from PC, NDVI and F_{760} in correspondence of subset A, B and C using a 3×3 pixels kernel. In the last two columns, the spatialised residuals between NDVI and PC-based Rao's Q and between F_{760} and PC-based Rao's Q are plotted. The bubbles (blue for negative residuals, red for positive residuals) are overlaid to a grey-scale image of the corresponding subset.

itive (red bubbles) residuals in the three subsets was generally consistent in the two models fitted, however, a significant difference in terms of absolute residuals was observed. The model fitted between the Rao's Q diversities calculated on PC and NDVI was overall characterised by larger residuals (*i.e.*, bigger bubbles) compared to the one fitted between PC and F_{760}-based Rao's Q diversities (*i.e.*, smaller bubbles). The residuals were mainly negative for both NDVI and F_{760}-based Rao's Q diversity in correspondence of the regeneration stands of the forest, while both positive and negative residuals were observed in the mature forest. The correlation between PC and NDVI-based diversity was statistically significant in subset B ($r = 0.30$, $p < 0.001$), whereas it was non-significant in subset A and C ($p > 0.1$). Conversely, the correlation between PC and F_{760}-based diversity was statistically significant in all the subsets ($r = 0.46$, $r = 0.57$ and $r = 0.56$ in subset A, B and C, respectively).

4.4 DISCUSSION AND CONCLUSIONS

Measuring biodiversity across space and over time is a pivotal objective in ecology. In this respect, RS can be a powerful tool as it provides the means to overcome several drawbacks related to the traditional biodiversity estimation from field data. However, there is no agreement yet on the RS data and metrics to be used to infer biodiversity from remote, as well as the pros and cons of different products (*i.e.*, reflectance, VIs and F) to map biodiversity. In this study, we tested different approaches based on the exploitation of different kinds of RS data as well as on the use of different metrics to quantify biodiversity.

Firstly, a traditional approach based on the semi-automatic classification of airborne images was used to map the tree species in the study area. The classification allowed a proper discrimination of the different forest species in the area, as emerged from the accuracy assessment. An OA of 75.1% was obtained, indicating a solid performance of the SVM algorithm in discriminating the different forest species in a complex environment characterised by a large spatial heterogeneity. In this regard, the high spatial resolution of *HyPlant* data (1 m) was critical to help dealing with the spatial variability by reducing the occurrence of spectral mixing among the classes. Based on the classification results, the species richness and the Shannon's index were calculated to evaluate the taxonomic diversity across the study area. This traditional approach of assessing biodiversity provides information about the distribution of species based on their taxonomic identity and can be relevant for *e.g.* monitoring the biodiversity patterns and detect species changes or losses over time. However, it cannot provide any information about the intra-specific variability in functional traits, which constitute a determinant of

the functional diversity and it is more related to ecosystem stability rather than taxonomic diversity alone. As a matter of fact, the functional traits might vary within the same species as much as between different species; vice versa, different species might be characterised by similar functional traits thus not contributing to the functional diversity (Schneider et al., 2017). Therefore, disregarding the intra-specific variability might strongly either masking or emphasizing the functional diversity. Schneider et al. (2017) further suggested that in relatively species-poor temperate forests, such as the one analysed in this study, ignoring the functional diversity typically leads to a strong underestimation of biodiversity. This statement was confirmed by our findings, which showed that the use of diversity metrics based on the species composition led to diametrically opposed results compared to their application to remotely sensed spatially continuous variables grasping the intra-specific variability of PTs.

However, applying the entropy metrics to continuous RS data under the spectral variation hypothesis (Palmer et al., 2002) only partially allows overcoming the limitations related to neglecting the intra-specific variability of functional traits. Two other critical aspects must be considered for properly mapping the functional diversity: the entropy metric to be used to infer the functional diversity and the RS data to be used as input for the calculation.

Concerning the first point, the possible drawbacks related to the entropy metric selected need to be addressed. As it can be observed in Figure 17, the Shannon's index was overall characterised by high values all over the images and the diversity patterns were not easily inferable. This depends upon the fact that the Shannon's index only relies on the relative proportion of each value encountered within the kernel, without considering its numerical value. Therefore, values that are similar but numerically different are considered different in the calculation, so that the index quickly tends to saturate. In our case, this issue was emphasised by the high spatial heterogeneity of the input data (*i.e.*, NDVI and F_{760}), that is related to both the high resolution of the data and the complexity of the forest canopy.

Consistently with the findings of Rocchini, Marcantonio, and Ricotta (2017) and Rocchini et al. (2018), we found the Rao's Q diversity to be a better indicator of the spatial heterogeneity over simpler diversity metrics. The Rao's Q takes into account the pairwise numerical difference between the values encountered within the kernel, thus allowing to assign a different entropy to two values that are not identical but similar from two values that are numerically distant. Respect to the Shannon's index, the Rao's Q diversity allowed to meaningfully emphasize the entropy patterns in the images by flattening the high entropy values determined by small variations of the values encountered within the kernel while amplifying the real differences.

As regards the second point, it must be considered that RS offers a variety of different tools. So far, different approaches have been proposed to synthesize the intra-specific variability of PTs, *e.g.*, the use of VIs related to the vegetation structure and greenness (Rocchini et al., 2018; Rocchini, Marcantonio, and Ricotta, 2017) and the use of spatialised retrievals of PTs (Schneider et al., 2017). Regardless of the methodology used to quantify biodiversity, both the approaches are essentially based on reflectance, *i.e.*, on the amount of radiation reflected by vegetation as a function of its biochemical and structural properties. In this study, we tested a completely novel approach for assessing biodiversity based on the exploitation of the F signal emitted by vegetation. The potential of using F compared to a traditional VI such as NDVI was strongly demonstrated by the results obtained. As a matter of fact, the functional diversity patterns obtained calculating entropy on F_{760} were found to be significantly related to the ones obtained applying the metric on the PC synthesizing the variability of PTs ($r = 0.52$, $p < 0.001$). Conversely, the patterns obtained applying the metric on NDVI were not significantly correlated ($p > 0.1$) with the functional diversity map used as a reference. In terms of patterns, the comparison between the Rao's Q calculated on PC, NDVI and F_{760} clearly shows that NDVI strongly underestimates the functional diversity across all the study area. This is particularly evident in the regeneration areas, where the low entropy based on NDVI calculation shows that NDVI cannot grasp the variability of the functional diversity. This effect is emphasized in these regeneration patches of the forest probably due to the saturation of NDVI. This suggests that F760 might be a powerful tools for estimating the functional diversity especially in contexts where vegetation is characterised by a high biomass and greenness (*e.g.*, forest ecosystems).

The potential of F_{760} in predicting the functional diversity is partially explained by the strong influence of the variability of PTs on the F signal. However, the fact that F is also an indicator of the plant functional activity suggests that F might be an even most powerful tool for studying the link biodiversity-ecosystem productivity compared to the use of PTs.

5 CONCLUSIONS

The main objective of this Ph.D. was to advance the understanding of vegetation functioning by using multi-source remotely sensed data in the optical domain. The link between vegetation optical properties, PTs and EFPs was analysed and fully explained exploiting multi-source high-spectral and spatial resolution remotely sensed data acquired on the same focus area (*i.e.*, a forest ecosystem).

To achieve this objective, I addressed different approaches for studying vegetation remotely, from a more traditional one based on the mapping of the forest species using semi-automatic classification techniques, to innovative ones based on the exploration of the potential of F for inferring information about the ecosystem functioning. These works were presented in Chapter 2, 3 and 4 of this thesis, respectively. The main outcomes of each chapter are summarised below, together with some concluding remarks and potential future perspectives of this work.

5.1 MAIN RESULTS

The use of multi-temporal hyperspectral images acquired with the APEX airborne sensor allows an accurate and operational mapping of the species distribution in complex forest ecosystems.

This result is the main outcome of the study presented in Chapter 2, aimed at mapping the spatial distribution of the dominant forest species in the Hardt forest based on APEX hyperspectral airborne data. In this study, the forest species were mapped using a maximum likelihood classifier applied to spectral indices calculated on APEX reflectance. The combination of multi-temporal images improved the classification accuracy. As a matter of fact, the highest accuracy (74.4%) was obtained combining the APEX images acquired in June and September 2013,

while the accuracy significantly decreased when using one image at a time (< 60%). This is explained by the fact that the use of images acquired in different phenological stages allows capturing characteristic spectral responses related to species-specific phenological behaviours. For this reason, it is useful to exploit images acquired in different phenological stages in order to enhance the differences among spectrally similar forest species and better discriminate them using semi-automatic routines. Results highlighted the possibility of obtaining accurate thematic maps of the species distribution in a rather straightforward way. This methodology might be operationally used to monitor the variation of the forest composition over time, allowing to detect changes and track the evolution of the forest.

The spatial patterns of far-red F derived from high-spatial and spectral resolution airborne data are non-linearly correlated to process-based GPP estimates obtained driving an ecophysiological model with airborne-derived PTs.

These results emerged from the study presented in Chapter 3, which explored the spatial relationship between two independent measures of photosynthesis: F on the one hand, GPP on the other. In this study, a comprehensive analysis of the forest optical and functional properties was carried out, allowing a full explanation of the spatial variability of the forest functioning. Firstly, this study demonstrated the feasibility of obtaining reliable F retrievals at both the red and far-red emission peaks ($r^2 = 0.74$, $p < 0.001$ and $r^2 = 0.73$, $p < 0.001$, respectively, compared to ground-based retrievals) over a forested area using spectral fitting methods. Secondly, it showed the possibility of obtaining accurate retrievals of key PTs (RMSE = 5.66 $\mu g\, cm^{-2}$, RMSE = 0.51 $m^2 m^{-2}$ for LCC and LAI, respectively) using an optimised inversion of a forest radiative transfer model and of using these forest traits to drive the estimation of GPP and APAR using a process-based model. Thirdly, it demonstrated that the spatial relationship between far-red F and GPP and APAR is statistically significant and nonlinear ($r^2 = 0.46$, $p < 0.001$ and $r^2 = 0.43$, $p < 0.001$, respectively), while the spatial relationship between red F and GPP or APAR is non-significant ($p > 0.1$). These results constitute a valuable and novel insight into the spatial variability of the forest ecosystem functions, providing evidence of the critical role of the spatial heterogeneity in controlling the carbon uptake. Despite being mostly neglected in previous studies due to the coarse spatial scale imposed by the spaceborne F retrievals currently available, this aspect is key to unravel the complex relationship between F and photosynthesis.

The heterogeneity of far-red F derived from high-spatial and spectral resolution airborne data is significantly related to functional diversity.

This result is the outcome of the study presented in Chapter 4, which investigated the possibility of exploiting F heterogeneity as a measure of the functional diversity of terrestrial ecosystems from remote. In this study, different approaches to quantify biodiversity were evaluated. Firstly, traditional metrics describing species richness and abundance were calculated on the species distribution map. When repeated images are acquired over the same area, this information might be valuable to monitor changes in the forest composition over time. However, this kind of approach has strong inherent limitations related to impossibility of providing information about the intra-specific variability of the functional traits, which is a determinant of the functional diversity. Being the functional diversity a relevant aspect in ecology due to its relation to the ecosystem functioning, as a second step entropy metrics calculated on reflectance and fluorescence were tested to quantify it. Results showed the Rao's Q diversity is a powerful measure of the spatial heterogeneity compared to simpler metrics which only take into account the relative proportion of different numerical values. In addition and more interestingly, results showed that the functional diversity patterns obtained calculating the Rao's Q diversity on F are better related to the functional map used as reference compared to the ones obtained applying the same metric on a traditional reflectance-based vegetation index (*i.e.*, NDVI). In particular, results showed a strong underestimation of the functional diversity based on NDVI across the juvenile stands of the forest, evidencing that NDVI cannot grasp the variability of functional diversity. The results obtained in this study demonstrated for the first time the potential of F as a measure of ecosystem functional diversity, opening new interesting perspectives for the investigation of the relationship between biodiversity and ecosystem productivity at multiple spatial and temporal scales.

5.2 CONCLUDING REMARKS AND OUTLOOK

In this Ph.D. thesis, multiple approaches for assessing vegetation functioning were evaluated and discussed. Through the three studies carried out, vegetation was characterised from the structural, biochemical and functional point of view, providing a thorough understanding of the forest status. This was made possible by the integration of multi-source RS data, as well as by the exploitation of different RS techniques and physically-based models. Overall, the results obtained effectively demonstrated the strength of hyperspectral remotely sensed imagery for inferring information about vegetation. In particular, results foster the use of F as a measure of plant functional status in light of the positive relations found between F and ecosystem productivity as well as between F and functional diversity, which is potentially another way of inferring information about the ecosystem

productivity. While the majority of the studies analysed the relation between F and photosynthesis in the temporal dimension, this thesis focused on the spatial one, adding a small contribution towards the complete understanding of the multifaceted nature of the relationship between F and ecosystem functioning. This aspect is particularly important in perspective of the actual (*e.g.*, OCO-2) and future (*e.g.*, FLEX) availability of spaceborne sensors capable of providing spatially resolved F retrievals at finer resolution (up to 300 m) compared to the ones exploited so far.

The enhanced understanding of the link between vegetation optical properties measured from remote, PTs and descriptors of the ecosystem processes will allow a more operational use of remotely sensed data for observing vegetation functioning, which is a key challenge for establishing feedbacks between the biosphere and climate systems.

BIBLIOGRAPHY

Alonzo, M., B. Bookhagen, and D. A. Roberts (2014). "Urban tree species mapping using hyperspectral and lidar data fusion". In: *Remote Sensing of Environment* 148, pages 70–83. DOI: 10.1016/j.rse.2014.03.018 (cited on page 8).

Asner, G. P., R. Martin, D. E. Knapp, R. Tupayachi, C. B. Anderson, F. Sinca, N. Vaughn, and W. Llactayo (2017). "Airborne laser-guided imaging spectroscopy to map forest trait diversity and guide conservation". In: *Science* 355.6323, pages 385–389. DOI: 10.1126/science.aaj1987 (cited on page 58).

Atzberger, C. (2000). "Development of an invertible forest reflectance model: The INFORM-Model". In: *Proceedings of the 20th EARSeL Symposium: A decade of trans-European Remote Sensing Cooperation, 14-16 June 2000, Dresden (Germany)*. Edited by Buchroithner, pages 39–44 (cited on pages 30, 48, 63).

Atzberger, C., R. Darvishzadeh, M. Immitzer, M. Schlerf, A. K. Skidmore, and G. le Maire (2015). "Comparative analysis of different retrieval methods for mapping grassland leaf area index using airborne imaging spectroscopy". In: *International Journal of Applied Earth Observation and Geoinformation* 43, pages 19–31. DOI: 10.1016/j.jag.2015.01.009 (cited on pages 23, 24, 46).

Atzberger, C. and K. Richter (2012). "Spatially constrained inversion of radiative transfer models for improved LAI mapping from future Sentinel-2 imagery". In: *Remote Sensing of Environment* 120, pages 208–218. DOI: 10.1016/j.rse.2011.10.035 (cited on page 24).

Baker, N. R. (2008). "Chlorophyll Fluorescence: A Probe of Photosynthesis In Vivo". In: *Annual Review of Plant Biology* 59.1, pages 89–113. DOI: 10.1146/annurev.arplant.59.032607.092759 (cited on pages 2, 22, 53).

Baldeck, C. A., G. P. Asner, R. E. Martin, C. B. Anderson, D. E. Knapp, J. R. Kellner, and J. S. Wright (2015). "Operational tree species mapping in a diverse tropical forest with airborne imaging spectroscopy". In: *PLoS ONE* 10.7. DOI: 10.1371/journal.pone.0118403 (cited on pages 8, 15).

Ball, J. T. (1988). "An analysis of stomatal conductance". PhD thesis (cited on page 33).

Balvanera, P., A. B. Pfisterer, N. Buchmann, J.-S. He, T. Nakashizuka, D. Raffaelli, and B. Schmid (2006). "Quantifying the evidence for biodiversity effects on ecosystem functioning and services". In: *Ecology Letters* 9, pages 1146–1156. DOI: 10.1111/j.1461-0248.2006.00963.x (cited on pages 4, 58, 59).

Banskota, A., S. P. Serbin, R. H. Wynne, V. A. Thomas, M. J. Falkowski, N. Kayastha, and P. A. Townsend (2015). "An LUT-Based Inversion of DART Model to Estimate Forest LAI from Hyperspectral Data". In: *IEEE Journal of Selected Topics in Applied Earth Observations and Remote Sensing* 8.6, pages 3147–3160 (cited on page 48).

Baret, F. and S. Buis (2008). "Estimating canopy characteristics from remote sensing observations: review of methods and associated problems". In: *Advances in Land Remote Sensing. New York, USA.* Pages 173–201. DOI: 10.1007/978-1-4020-6450-0_7 (cited on pages 3, 24).

Beer, C., M. Reichstein, E. Tomelleri, P. Ciais, M. Jung, N. Carvalhais, C. Roedenbeck, M. A. Arain, D. D. Baldocchi, G. B. Bonan, A. Bondeau, A. Cescatti, G. Lasslop, A. Lindroth, M. Lomas, S. Luyssaert, H. A. Margolis, K. W. Oleson, O. Roupsard, E. Veenendaal, N. Viovy, C. Williams, F. I. Woodward, and D. Papale (2010). "Terrestrial Gross Carbon Dioxide Uptake: Global Distribution and Covariation with Climate". In: *Science* 329.August, pages 834–839 (cited on pages 1, 22, 23).

Bodegom, P. M. van, J. C. Douma, J. Witte, J. Ordoñez, R. Bartholomeus, and R. Aerts (2012). "Going beyond limitations of plant functional types when predicting global ecosystem-atmosphere fluxes: Exploring the merits of traits-based approaches". In: *Global Ecology and Biogeography* 21.6, pages 625–636. DOI: 10.1111/j.1466-8238.2011.00717.x (cited on page 23).

Boschetti, M., L. Boschetti, S. Oliveri, L. Casati, and I. Canova (2007). "Tree species mapping with Airborne hyperspectral MIVIS data: the Ticino Park study case". In: *International Journal of Remote Sensing* 28.6, pages 1251–1261. DOI: 10.1080/01431160600928542 (cited on pages 8, 11, 15).

Butler, E. E., A. Datta, H. Flores-Moreno, M. Chen, K. R. Wythers, F. Fazayeli, A. Banerjee, O. K. Atkin, J. Kattge, B. Amiaud, B. Blonder, G. Boenisch, B. Bond-Lamberty, K. A. Brown, C. Byun, G. Campetella, B. E. Cerabolini, J. H. Cornelissen, J. M. Craine, D. Craven, F. T. de Vries, S. Díaz, T. F. Domingues, E. Forey, A. González-Melo, N. Gross, W. Han, W. N. Hattingh, T. Hickler, S. Jansen, K. Kramer, N. J. Kraft, H. Kurokawa, D. C. Laughlin, P. Meir, V. Minden, Ü. Niinemets, Y. Onoda, J. Peñuelas, Q. Read, L. Sack, B. Schamp, N. A. Soudzilovskaia, M. J. Spasojevic, E. Sosinski, P. E. Thornton, F. Valladares, P. M. van Bodegom, M. Williams, C. Wirth, and P. B. Reich (2017). "Mapping local and global variability in plant trait distributions". In: *Proceedings of the National Academy of Sciences*, page 201708984. DOI: 10.1073/pnas.1708984114. arXiv: 1711.07918 (cited on page 23).

Camps-valls, G. and L. Bruzzone (2005). "Kernel-Based Methods for Hyperspectral Image Classification". In: *IEEE Transactions on Geoscience and Remote Sensing* 43.6, pages 1–12 (cited on page 62).

Cao, M. and F. I. Woodward (1998). "Dynamic responses of terrestrial ecosystem carbon cycling to global climate change". In: *Nature* 393.May, pages 249–252 (cited on page 22).

Cardinale, B. J., K. L. Matulich, D. U. Hooper, J. E. Byrnes, E. Duffy, L. Gamfeldt, P. Balvanera, M. I. Connor, and A. Gonzalez (2011). "The functional role of producer diversity in ecosystems". In: *American Journal of Botany* 98.3, pages 572–592. DOI: 10.3732/ajb.1000364 (cited on pages 4, 58, 59).

Chapin, F., E. Zavaleta, V. Eviner, R. Naylor, P. Vitousek, H. Reynolds, D. Hooper, S. Lavorel, O. Sala, S. Hobbie, M. Mack, and S. Díaz (2000). "Consequences of changing biodiversity". English (US). In: *Nature* 405.6783, pages 234–242. DOI: 10.1038/35012241 (cited on page 3).

Chen, J. M. and S. G. Leblanc (1997). "A Four-Scale Bidirectional Reflectance Model Based on Canopy Architecture". In: *IEEE Transactions on Geoscience and Remote Sensing* 35.5, pages 1316–1337 (cited on page 48).

Chen, J. and T. Black (1992). "Defining leaf area index for non-flat leaves". In: *Plant, Cell and Environment* 15, pages 421–429 (cited on page 28).

Cheng, Y. B., E. M. Middleton, Q. Zhang, K. F. Huemmrich, P. K. Campbell, L. A. Corp, B. D. Cook, W. P. Kustas, and C. S. Daughtry (2013). "Integrating solar induced fluorescence and the photochemical reflectance index for estimating gross primary production in a cornfield". In: *Remote Sensing* 5.12, pages 6857–6879. DOI: 10.3390/rs5126857 (cited on page 53).

Cho, M. A., R. Mathieu, G. P. Asner, L. Naidoo, J. van Aardt, A. Ramoelo, P. Debba, K. Wessels, R. Main, I. P. Smit, and B. Erasmus (2012). "Mapping tree species composition in South African savannas using an integrated airborne spectral and LiDAR system". In: *Remote Sensing of Environment* 125, pages 214–226. DOI: 10.1016/j.rse.2012.07.010. eprint: z0024 (cited on page 8).

Ciais, P., J. Willem, P. Friedlingstein, and G. Munhoven (2013). "Carbon and Other Biogeochemical Cycles". In: *Climate Change 2013: The Physical Science Basis. Contribution of Working Group I to the Fifth Assessment Report of the Intergovernmental Panel on Climate Change*. Chapter 6 (cited on pages 1, 22).

Clark, M. L., D. A. Roberts, and D. B. Clark (2005). "Hyperspectral discrimination of tropical rain forest tree species at leaf to crown scales". In: *Remote Sensing of Environment* 96.3-4, pages 375–398. DOI: 10.1016/j.rse.2005.03.009 (cited on pages 8, 15).

Cogliati, S., R. Colombo, M. Celesti, G. Tagliabue, U. Rascher, A. Schickling, P. Rademske, L. Alonso, N. Sabater, M. Drusch, and D. Schüttemeyer (2018). "Retrieval of the fluorescence emission by atmospheric forward modelling and spectral fitting". In: *Proceedings of the International Geoscience and Remote Sensing Symposium 2018, 22-27 July 2018, Valencia, Spain* (cited on page 29).

Cogliati, S., W. Verhoef, S. Kraft, N. Sabater, L. Alonso, J. Vicent, J. Moreno, M. Drusch, and R. Colombo (2015). "Retrieval of sun-induced fluorescence using advanced spectral fitting methods". In: *Remote Sensing of Environment* 169, pages 344–357. DOI: 10.1016/j.rse.2015.08.022 (cited on pages 25, 27, 29, 62).

Colgan, M. S., C. A. Baldeck, J. baptiste Féret, and G. P. Asner (2012). "Mapping savanna tree species at ecosystem scales using support vector machine classification and BRDF correction on airborne hyperspectral and LiDAR data". In: *Remote Sensing* 4.11, pages 3462–3480. DOI: 10.3390/rs4113462 (cited on page 8).

Colombo, R., M. Celesti, R. Bianchi, P. K. Campbell, S. Cogliati, B. D. Cook, L. A. Corp, A. Damm, J. C. Domec, L. Guanter, T. Julitta, E. M. Middleton, A. Noormets, C. Panigada, F. Pinto, U. Rascher, M. Rossini, and A. Schickling (2018). "Variability of sun-induced chlorophyll fluorescence according to stand age-related processes in a managed loblolly pine forest". In: *Global Change Biology* August 2017, pages 1–17. DOI: 10.1111/gcb.14097 (cited on page 2).

Combal, B., F. Baret, M. Weiss, A. Trubuil, D. Macé, A. Pragnère, R. Myneni, Y. Knyazikhin, and L. Wang (2002). "Retrieval of canopy biophysical variables from bidirectional reflectance using prior information to solve the ill-posed inverse problem". In: *Remote Sensing of Environment* 84.1, pages 1–15. DOI: 10.1016/S0034-4257(02)00035-4 (cited on pages 3, 24, 48).

Croft, H., J. M. Chen, N. Froelich, B. Chen, and R. M. Staebler (2015). "Seasonal controls of canopy chlorophyll content on forest carbon uptake: Implications for GPP modeling". In: *Journal of Geophysical Research G: Biogeosciences* 120.8, pages 1576–1586. DOI: 10.1002/2015JG002980 (cited on page 48).

Croft, H., J. M. Chen, X. Luo, P. Barlett, B. Chen, and R. M. Staebler (2017). "Leaf chlorophyll content as a proxy for leaf photosynthetic capacity". In: *Global Change Biology*, pages 1–12. DOI: 10.1111/gcb.13599 (cited on page 35).

Croft, H., J. M. Chen, Y. Zhang, and A. Simic (2013). "Modelling leaf chlorophyll content in broadleaf and needle leaf canopies from ground , CASI , Landsat TM 5 and MERIS reflectance data". In: *Remote Sensing of Environment* 133, pages 128–140. DOI: 10.1016/j.rse.2013.02.006 (cited on page 48).

Dalponte, M., L. Bruzzone, and D. Gianelle (2008). "Fusion of Hyperspectral and LiDAR Remote Sensing Data for Classification of Complex Forest Areas". In: *IEEE Transactions on Geoscience and Remote Sensing* 46.5, pages 1416–1427. DOI: 10.1109/TGRS.2008.916480 (cited on page 8).

Dalponte, M., L. Bruzzone, and D. Gianelle (2012). "Tree species classification in the Southern Alps based on the fusion of very high geometrical resolution multispectral/hyperspectral images and LiDAR data". In: *Remote Sensing of Environment* 123, pages 258–270. DOI: 10.1016/j.rse.2012.03.013 (cited on page 8).

Dalponte, M., L. Bruzzone, L. Vescovo, and D. Gianelle (2009). "The role of spectral resolution and classifier complexity in the analysis of hyperspectral images of

forest areas". In: *Remote Sensing of Environment* 113.11, pages 2345–2355. DOI: 10.1016/j.rse.2009.06.013 (cited on page 61).

Dalponte, M., H. O. Ørka, T. Gobakken, D. Gianelle, and E. Næsset (2013). "Tree species classification in boreal forests with hyperspectral data". In: *IEEE Transactions on Geoscience and Remote Sensing* 51.5, pages 2632–2645. DOI: 10.1109/TGRS.2012.2216272 (cited on pages 8, 15, 61).

Damm, A., J. Elber, A. Erler, B. Gioli, K. Hamdi, R. Hutjes, M. Kosvancova, M. Meroni, F. Miglietta, A. Moersch, J. Moreno, A. Schickling, R. Sonnenschein, T. Udelhoven, S. van der Linden, P. Hostert, and U. Rascher (2010). "Remote sensing of sun-induced fluorescence to improve modeling of diurnal courses of gross primary production (GPP)". In: *Global Change Biology* 16.1, pages 171–186. DOI: 10.1111/j.1365-2486.2009.01908.x (cited on page 2).

Damm, A., L. Guanter, V. Laurent, M. E. Schaepman, A. Schickling, and U. Rascher (2014). "FLD-based retrieval of sun-induced chlorophyll fluorescence from medium spectral resolution airborne spectroscopy data". In: *Remote Sensing of Environment* 147, pages 256–266. DOI: 10.1016/j.rse.2014.03.009 (cited on pages 2, 50).

Damm, A., L. Guanter, E. Paul-Limoges, C. van der Tol, A. Hueni, N. Buchmann, W. Eugster, C. Ammann, and M. E. Schaepman (2015). "Far-red sun-induced chlorophyll fluorescence shows ecosystem-specific relationships to gross primary production: An assessment based on observational and modeling approaches". In: *Remote Sensing of Environment* 166, pages 91–105. DOI: 10.1016/j.rse.2015.06.004 (cited on pages 52, 53).

Darvishzadeh, R., A. K. Skidmore, M. Schlerf, C. Atzberger, F. Corsi, and M. A. Cho (2008). "LAI and chlorophyll estimation for a heterogeneous grassland using hyperspectral measurements". In: *ISPRS Journal of Photogrammetry and Remote Sensing* 63.4, pages 409–426. DOI: 10.1016/j.isprsjprs.2008.01.001 (cited on page 24).

Diaz, S., S. Lavorel, F. de Bello, F. Quetier, K. Grigulis, and M. T. Robson (2007). "Incorporating plant functional diversity effects in ecosystem service assessments". In: *Proceedings of the National Academy of Sciences* 104.52, pages 20684–20689. DOI: 10.1073/pnas.0704716104 (cited on page 59).

Dorigo, W. A., R. Zurita-Milla, A. de Wit, J. Brazile, R. Singh, and M. E. Schaepman (2007). "A review on reflective remote sensing and data assimilation techniques for enhanced agroecosystem modeling". In: *International Journal of Applied Earth Observation and Geoinformation* 9.2, pages 165–193. DOI: 10.1016/j.jag.2006.05.003 (cited on pages 24, 46).

Drusch, M., J. Moreno, U. Del Bello, R. Franco, Y. Goulas, A. Huth, S. Kraft, E. M. Middleton, F. Miglietta, G. H. Mohammed, L. Nedbal, U. Rascher, D. Schüttemeyer, and W. Verhoef (2017). "The FLuorescence EXplorer mission concept -

ESA's Earth Explorer 8". In: *IEEE Trans. Geosci. Remote Sens.* 55.3, pages 1273–1284 (cited on page 24).

Du, S., L. Liu, X. Liu, and J. Hu (2017). "Response of canopy solar-induced chlorophyll fluorescence to the absorbed photosynthetically active radiation absorbed by chlorophyll". In: *Remote Sensing* 9.9. DOI: 10.3390/rs9090911 (cited on page 55).

Feret, J.-B. and G. P. Asner (2013). "Tree Species Discrimination in Tropical Forests using Airborne Imaging Spectroscopy". In: *IEEE Journal of Selected Topics in Applied Earth Observations and Remote Sensing* 51.1, pages 73–84 (cited on page 61).

Feret, J.-B., C. François, G. P. Asner, A. A. Gitelson, R. E. Martin, L. P. Bidel, S. L. Ustin, G. le Maire, and S. Jacquemoud (2008). "PROSPECT-4 and 5: Advances in the leaf optical properties model separating photosynthetic pigments". In: *Remote Sensing of Environment* 112.6, pages 3030–3043. DOI: 10.1016/j.rse.2008.02.012 (cited on page 30).

Filella, I. and J. Penuelas (1994). *The red edge position and shape as indicator of plant chlorophyll content, biomass and hydric status*. DOI: 10.1080/01431169408954177 (cited on page 11).

Fournier, A., F. Daumard, S. Champagne, A. Ounis, Y. Goulas, and I. Moya (2012). "Effect of canopy structure on sun-induced chlorophyll fluorescence". In: *ISPRS Journal of Photogrammetry and Remote Sensing* 68.1, pages 112–120. DOI: 10.1016/j.isprsjprs.2012.01.003 (cited on page 2).

Frankenberg, C., J. B. Fisher, J. Worden, G. Badgley, S. Saatchi, J.-E. Lee, G. C. Toon, A. Butz, M. Jung, A. Kuze, and T. Yokota (2011). "New global observations of the terrestrial carbon cycle from GOSAT: Patterns of plant fluorescence with gross primary productivity". In: *Geophysical Research Letters* 38.17, pages 1–6. DOI: 10.1029/2011GL048738 (cited on pages 2, 23, 51).

Frankenberg, C., R. Pollock, R. Lee, R. Rosenberg, J. Blavier, D. Crisp, C. Dell, G. Osterman, C. Roehl, P. Wennberg, and D. Wunch (2015). "The Orbiting Carbon Observatory (OCO-2): spectrometer performance evaluation using pre-launch direct sun measurements". In: *Atmospheric Measurement Techniques* 8, pages 301–313. DOI: 10.5194/amt-8-301-2015 (cited on page 23).

Franklin, S. E. (2001). *Remote sensing for sustainable forest management*, page 407. DOI: 10.1201/9781420032857.ch2 (cited on page 8).

Friedlingstein, P., M. Meinshausen, V. K. Arora, C. D. Jones, A. Anav, S. K. Liddicoat, and R. Knutti (2014). "Uncertainties in CMIP5 Climate Projections due to Carbon Cycle Feedbacks". In: *American Meteorological Society*, pages 511–526. DOI: 10.1175/JCLI-D-12-00579.1 (cited on page 23).

Gao, B. C., M. J. Montes, and C. O. Davis (2004). "Refinement of wavelength calibrations of hyperspectral imaging data using a spectrum-matching technique".

In: *Remote Sensing of Environment* 90.4, pages 424–433. DOI: 10.1016/j.rse.2003.09.002 (cited on page 9).

Garzonio, R., B. Di Mauro, R. Colombo, and S. Cogliati (2017). "Surface Reflectance and Sun-Induced Fluorescence Spectroscopy Measurements Using a Small Hyperspectral UAS". In: *Remote Sensing* 9.472, pages 1–24. DOI: 10.3390/rs9050472 (cited on page 2).

Gastellu-Etchegorry, J., V. Demarez, V. Pinel, and F. Zagolski (1996). "Modeling Radiative Transfer in Heterogeneous 3-D Vegetation Canopies". In: *Remote Sensing of Environment* 156.July 1995, pages 131–156 (cited on page 48).

Genty, B., J. M. Briantais, and N. R. Baker (1989). "The relationship between the quantum yield of photosynthetic electron transport and quenching of chlorophyll fluorescence". In: *Biochimica et Biophysica Acta - General Subjects* 990.1, pages 87–92. DOI: 10.1016/S0304-4165(89)80016-9 (cited on pages 2, 22).

Gholizadeh, H., J. A. Gamon, P. A. Townsend, A. I. Zygielbaum, C. J. Helzer, G. Y. Hmimina, R. Yu, R. M. Moore, A. K. Schweiger, and J. Cavender-Bares (2019). "Detecting prairie biodiversity with airborne remote sensing". In: *Remote Sensing of Environment* 221.October 2018, pages 38–49. DOI: 10.1016/j.rse.2018.10.037 (cited on page 58).

Gholizadeh, H., J. A. Gamon, A. I. Zygielbaum, R. Wang, A. K. Schweiger, and J. Cavender-Bares (2018). "Remote sensing of biodiversity: Soil correction and data dimension reduction methods improve assessment of α-diversity (species richness) in prairie ecosystems". In: *Remote Sensing of Environment* 206.June 2017, pages 240–253. DOI: 10.1016/j.rse.2017.12.014 (cited on page 58).

Ghosh, A., F. E. Fassnacht, P. Joshi, and B. Koch (2014). "A framework for mapping tree species combining hyperspectral and LiDAR data: Role of selected classifiers and sensor across three spatial scales". In: *International Journal of Applied Earth Observation and Geoinformation* 26, pages 49–63. DOI: 10.1016/j.jag.2013.05.017 (cited on page 8).

Gitelson, A. and M. N. Merzlyak (1994). "Spectral Reflectance Changes Associated with Autumn Senescence of Aesculus hippocastanum L. and Acer platanoides L. Leaves. Spectral Features and Relation to Chlorophyll Estimation". In: *Journal of Plant Physiology* 143.3, pages 286–292. DOI: 10.1016/S0176-1617(11)81633-0 (cited on page 51).

Goulas, Y., A. Fournier, F. Daumard, S. Champagne, A. Ounis, O. Marloie, and I. Moya (2017). "Gross Primary Production of a Wheat Canopy Relates Stronger to Far Red Than to Red Solar-Induced Chlorophyll Fluorescence". In: *Remote Sensing* 9.1, page 97. DOI: 10.3390/rs9010097 (cited on pages 52, 53).

Grossiord, C., A. Granier, S. Ratcliffe, O. Bouriaud, H. Bruelheide, E. Checko, D. Forrester, S. Dawud, L. Finer, M. Pollastrini, M. Scherer-Lorenzen, F. Valladares, D. Bonal, and A. Gessler (2014). "Tree diversity does not always improve resis-

tance of forest ecosystems to drought". In: *Proceedings of the National Academy of Sciences* 111.41, pages 14812–14815. DOI: 10.1073/pnas.1411970111. arXiv: arXiv:1408.1149 (cited on page 58).

Guanter, L., C. Frankenberg, A. Dudhia, P. E. Lewis, J. Gómez-Dans, A. Kuze, H. Suto, and R. G. Grainger (2012). "Retrieval and global assessment of terrestrial chlorophyll fluorescence from GOSAT space measurements". In: *Remote Sensing of Environment* 121, pages 236–251. DOI: 10.1016/j.rse.2012.02.006 (cited on pages 2, 23, 50).

Guanter, L., M. Rossini, R. Colombo, M. Meroni, C. Frankenberg, J.-E. Lee, and J. Joiner (2013). "Using field spectroscopy to assess the potential of statistical approaches for the retrieval of sun-induced chlorophyll fluorescence from ground and space". In: *Remote Sensing of Environment* 133, pages 52–61. DOI: 10.1016/j.rse.2013.01.017 (cited on page 2).

Guanter, L., Y. Zhang, M. Jung, J. Joiner, M. Voigt, J. a. Berry, C. Frankenberg, A. R. Huete, P. J. Zarco-Tejada, J.-E. Lee, M. S. Moran, G. Ponce-Campos, C. Beer, G. Camps-Valls, N. Buchmann, D. Gianelle, K. Klumpp, A. Cescatti, J. M. Baker, and T. J. Griffis (2014). "Global and time-resolved monitoring of crop photosynthesis with chlorophyll fluorescence". In: *Proceedings of the National Academy of Sciences of the United States of America* 111.14, E1327–33. DOI: 10.1073/pnas.1320008111 (cited on pages 2, 51).

Haining, R. (1980). "Spatial autocorrelation problems". In: *Geography and the Urban Environment*, pages 1–44 (cited on page 35).

Hamazaki, T., Y. Kaneko, and A. Kuze (2004). "Carbon dioxide monitoring from the GOSAT satellite". In: *Proceedings of the XXth ISPRS conference, Istanbul, Turkey, 12–23 July 2004* (cited on page 23).

Heimann, M. and M. Reichstein (2008). "Terrestrial ecosystem carbon dynamics and climate feedbacks". In: *Nature* 451.7176, pages 289–292. DOI: 10.1038/nature06591 (cited on pages 1, 22).

Hernández-Clemente, R., R. M. Navarro-Cerrillo, and P. J. Zarco-Tejada (2014). "Deriving Predictive Relationships of Carotenoid Content at the Canopy Level in a Conifer Forest Using Hyperspectral Imagery and Model Simulation". In: *IEEE Transactions on Geoscience and Remote Sensing* 52.8, pages 5206–5217 (cited on page 48).

Homolová, L., Z. Malenovský, J. G. Clevers, G. García-Santos, and M. E. Schaepman (2013). "Review of optical-based remote sensing for plant trait mapping". In: *Ecological Complexity* 15, pages 1–16. DOI: 10.1016/j.ecocom.2013.06.003 (cited on page 23).

Hooper, D. U., F. Chapin, J. Ewel, A. Hector, P. Inchausti, S. Lavorel, J. Lawton, D. Lodge, M. Loreau, S. Naeem, B. Schmid, H. Setala, A. Symstad, J. Vandermeer, and D. Wardle (2005). "Effects of biodiversity on ecosystem functioning: a con-

sensus of current knowledge". In: *Ecological Monographs* 75.July 2004, pages 3–35 (cited on pages 4, 59).

Horler, D., M. Dockray, and J. Barber (1983). "The red edge of plant leaf reflectance". In: *International Journal of Remote Sensing* 4.2, pages 273–288. DOI: 10.1080/01431168308948546 (cited on page 11).

Houborg, R., J. B. Fisher, and A. K. Skidmore (2015). "Advances in remote sensing of vegetation function and traits". In: *International Journal of Applied Earth Observation and Geoinformation* 43, pages 1–6. DOI: 10.1016/j.jag.2015.06.001 (cited on pages 24, 46).

Houborg, R., M. McCabe, A. Cescatti, F. Gao, M. A. Schull, and A. Gitelson (2015). "Joint leaf chlorophyll content and leaf area index retrieval from Landsat data using a regularized model inversion system (REGFLEC)". In: *Remote Sensing of Environment* 159, pages 203–221. DOI: 10.1016/j.rse.2014.12.008 (cited on pages 3, 23, 24).

Hu, B., J. R. Miller, P. Zarco-Tejada, J. Freemantle, and H. Zwick (2008). "Boreal forest mapping at the BOREAS study area using seasonal optical indices sensitive to plant pigment content". In: *Canadian Journal of Remote Sensing* 34, S158–S171. DOI: 10.5589/m07-066 (cited on page 11).

Hughes, G. F. (1968). "On the Mean Accuracy of Statistical Pattern Recognizers". In: *IEEE Transactions on Information Theory* 14.1, pages 55–63 (cited on pages 11, 61).

Inoue, Y., J. Peñuelas, A. Miyata, and M. Mano (2008). "Normalized difference spectral indices for estimating photosynthetic efficiency and capacity at a canopy scale derived from hyperspectral and CO_2 flux measurements in rice". In: *Remote Sensing of Environment* 112, pages 156–172. DOI: 10.1016/j.rse.2007.04.011 (cited on page 51).

Isbell, F., D. Craven, J. Connolly, M. Loreau, B. Schmid, C. Beierkuhnlein, T. M. Bezemer, C. Bonin, H. Bruelheide, E. De Luca, A. Ebeling, J. N. Griffin, Q. Guo, Y. Hautier, A. Hector, A. Jentsch, J. Kreyling, V. Lanta, P. Manning, S. T. Meyer, A. S. Mori, S. Naeem, P. A. Niklaus, H. W. Polley, P. B. Reich, C. Roscher, E. W. Seabloom, M. D. Smith, M. P. Thakur, D. Tilman, B. F. Tracy, W. H. Van Der Putten, J. Van Ruijven, A. Weigelt, W. W. Weisser, B. Wilsey, and N. Eisenhauer (2015). "Biodiversity increases the resistance of ecosystem productivity to climate extremes". In: *Nature* 526.7574, pages 574–577. DOI: 10.1038/nature15374 (cited on page 58).

Jacquemoud, S. and F. Baret (1990). "PROSPECT: A model of leaf optical properties spectra". In: *Remote Sensing of Environment* 34.2, pages 75–91. DOI: 10.1016/0034-4257(90)90100-Z (cited on pages 30, 63).

Jiang, C. and Y. Ryu (2016). "Multi-scale evaluation of global gross primary productivity and evapotranspiration products derived from Breathing Earth System

Simulator (BESS)". In: *Remote Sensing of Environment* 186, pages 528–547. DOI: 10.1016/j.rse.2016.08.030 (cited on pages 25, 33, 50, 51).

Joiner, J., Y. Yoshida, A. Vasilkov, Y. Yoshida, L. A. Corp, and E. M. Middleton (2011). "First observations of global and seasonal terrestrial chlorophyll fluorescence from space". In: *Biogeosciences* 8.3, pages 637–651. DOI: 10.5194/bg-8-637-2011 (cited on pages 2, 52).

Joiner, J., Y. Yoshida, L. Guanter, and E. M. Middleton (2016). "New methods for the retrieval of chlorophyll red fluorescence from hyperspectral satellite instruments: Simulations and application to GOME-2 and SCIAMACHY". In: *Atmospheric Measurement Techniques* 9.8, pages 3939–3967. DOI: 10.5194/amt-9-3939-2016 (cited on page 2).

Jones, T. G., N. C. Coops, and T. Sharma (2010). "Assessing the utility of airborne hyperspectral and LiDAR data for species distribution mapping in the coastal Pacific Northwest, Canada". In: *Remote Sensing of Environment* 114.12, pages 2841–2852. DOI: 10.1016/j.rse.2010.07.002 (cited on page 8).

Jung, M., M. Reichstein, H. A. Margolis, A. Cescatti, A. D. Richardson, M. A. Arain, A. Arneth, C. Bernhofer, D. Bonal, J. Chen, D. Gianelle, N. Gobron, G. Kiely, W. Kutsch, G. Lasslop, B. E. Law, A. Lindroth, L. Merbold, L. Montagnani, E. J. Moors, D. Papale, M. Sottocornola, F. Vaccari, and C. Williams (2011). "Global patterns of land-atmosphere fluxes of carbon dioxide, latent heat, and sensible heat derived from eddy covariance, satellite, and meteorological observations". In: *Journal of Geophysical Research: Biogeosciences* 116.3, pages 1–16. DOI: 10.1029/2010JG001566 (cited on page 23).

Jung, M., M. Vetter, M. Herold, G. Churkina, M. Reichstein, S. Zaehle, P. Ciais, N. Viovy, A. Bondeau, Y. Chen, K. Trusilova, F. Feser, and M. Heimann (2007). "Uncertainties of modeling gross primary productivity over Europe : A systematic study on the effects of using different drivers and terrestrial biosphere models". In: *Global Biogeochemical Cycles* 21, pages 1–12. DOI: 10.1029/2006GB002915 (cited on page 23).

Kempeneers, P., F. Vancoillie, W. Liao, F. Devriendt, and K. Vandekerkhove (2014). "Tree species mapping by combining hyperspectral with LiDAR data". eng. In: *Geoscience and Remote Sensing, IEEE International symposium, Proceedings*. Edited by M. Bernier, J. Lévesque, J.-M. Garneau, and E. LeDrew. Québec, QC, Canada: IEEE, page 4 (cited on page 8).

Knorr, W. (2000). "Annual and interannual CO2 exchanges of the terrestrial biosphere: process-based simulations and uncertainties". In: *Global Ecology and Biogeography* 9, pages 225–252 (cited on page 23).

Knyazikhin, Y., M. A. Schull, P. Stenberg, M. Mottus, M. Rautiainen, Y. Yang, A. Marshak, P. Latorre Carmona, R. K. Kaufmann, P. E. Lewis, M. I. Disney, V. Vanderbilt, A. B. Davis, F. Baret, S. Jacquemoud, A. Lyapustin, and R. B. Myneni

(2013). "Hyperspectral remote sensing of foliar nitrogen content". In: *Proceedings of the National Academy of Sciences* 110.3, E185–E192. DOI: 10.1073/pnas.1210196109 (cited on page 52).

Kobayashi, H. and H. Iwabuchi (2008). "A coupled 1-D atmosphere and 3-D canopy radiative transfer model for canopy reflectance , light environment , and photosynthesis simulation in a heterogeneous landscape". In: *Remote Sensing of Environment* 112, pages 173–185. DOI: 10.1016/j.rse.2007.04.010 (cited on page 33).

Koffi, E. N., P. J. Rayner, A. J. Norton, C. Frankenberg, and M. Scholze (2015). "Investigating the usefulness of satellite-derived fluorescence data in inferring gross primary productivity within the carbon cycle data assimilation system". In: *Biogeosciences* 12.13, pages 4067–4084. DOI: 10.5194/bg-12-4067-2015 (cited on page 53).

Koh, L. P., R. R. Dunn, S. S. Navjot, R. K. Colwell, H. C. Proctor, and V. S. Smith (2004). "Species Coextinctions and the Biodiversity Crisis". In: *Science* 305.5690, pages 1632–1634. DOI: 10.1126/science.1101101 (cited on page 58).

Kötz, B., F. Baret, H. Poilvé, and J. Hill (2005). "Use of coupled canopy structure dynamic and radiative transfer models to estimate biophysical canopy characteristics". In: *Remote Sensing of Environment* 95.1, pages 115–124. DOI: 10.1016/j.rse.2004.11.017 (cited on page 24).

Kuenzer, C., M. Ottinger, M. Wegmann, H. Guo, C. Wang, J. Zhang, S. Dech, and M. Wikelski (2014). "Earth observation satellite sensors for biodiversity monitoring: potentials and bottlenecks". In: *International Journal of Remote Sensing* 35.18, pages 6599–6647. DOI: 10.1080/01431161.2014.964349 (cited on page 58).

Kullback, S. and R. Leibler (1951). "On information and sufficiency". In: *Annals of Mathematical Statistics* 22, pages 79–86 (cited on pages 39, 64).

Kuusk, A. (1991). "The Hot Spot Effect in Plant Canopy Reflectance". In: *Photon-Vegetation Interactions*. DOI: 10.1007/978-3-642-75389-3_5 (cited on page 30).

Lang, A. and X. Yueqin (1986). "Estimation of Leaf Area Index from transmission of direct sunlight in discontinuous canopies". In: *Agricultural and Forest Meteorology* 37, pages 229–243 (cited on page 28).

Lausch, A., G. Bannehr, M. Beckmann, C. Boehm, H. Feilhauer, J. M. Hacker, M. Heurich, A. Jung, R. Klenke, C. Neumann, M. Pause, D. Rocchini, M. E. Schaepman, S. Schmidtlein, K. Schulz, P. Selsam, J. Settele, A. K. Skidmore, and A. F. Cord (2016). "Linking Earth Observation and taxonomic, structural and functional biodiversity: Local to ecosystem perspectives". In: *Ecological Indicators* 70, pages 317–339. DOI: 10.1016/j.ecolind.2016.06.022 (cited on page 58).

Leonenko, G., S. O. Los, and P. R. North (2013). "Statistical distances and their applications to biophysical parameter estimation: Information measures, m-estimates,

and minimum contrast methods". In: *Remote Sensing* 5.3, pages 1355–1388. DOI: 10.3390/rs5031355 (cited on pages 31, 33, 39, 64).

Lewis, P. E. and M. I. Disney (2007). "Spectral invariants and scattering across multiple scales from within-leaf to canopy". In: *Remote Sensing of Environment* 109.2, pages 196–206. DOI: 10.1016/j.rse.2006.12.015 (cited on page 52).

Li, X., J. Xiao, and B. He (2018). "Chlorophyll fluorescence observed by OCO-2 is strongly related to gross primary productivity estimated from flux towers in temperate forests". In: *Remote Sensing of Environment* 204.October 2017, pages 659–671. DOI: 10.1016/j.rse.2017.09.034 (cited on pages 2, 23, 53).

Lichtenthaler, H. K. and C. Buschmann (2001). "Chlorophylls and Carotenoids : Measurement and Characterization by UV-VIS Spectroscopy". In: *Current Protocols in Food Analytical Chemistry* 4.3, pages 1–8 (cited on page 28).

Linke, J., M. C. Betts, M. B. Lavigne, and S. E. Franklin (2006). "Introduction: Structure, Function, and Change of Forest Landscapes". In: *Understanding Forest Disturbance and Spatial Pattern* (cited on page 8).

Liu, L., X. Liu, J. Hu, and L. Guan (2017). "Assessing the wavelength-dependent ability of solar-induced chlorophyll fluorescence to estimate the GPP of winter wheat at the canopy level". In: *International Journal of Remote Sensing* 38.15, pages 4396–4417. DOI: 10.1080/01431161.2017.1320449 (cited on pages 2, 53).

Liu, X., L. Guanter, L. Liu, A. Damm, U. Rascher, D. Peng, S. Du, and J.-p. Gastellu-etchegorry (2018). "Downscaling of solar-induced chlorophyll fluorescence from canopy level to photosystem level using a random forest model". In: *Remote Sensing of Environment* 9. DOI: 10.1016/j.rse.2018.05.035 (cited on page 55).

Loreau, M., S. Naeem, P. Inchausti, J. Bengtsson, J. Grime, A. Hector, D. U. Hooper, M. Huston, D. Raffaelli, B. Schmid, D. Tilman, and D. A. Wardle (2001). "Biodiversity and Ecosystem Functioning: Current Knowledge and Future Challenges". In: *Science* 294.October, pages 804–808. DOI: 10.1126/science.1064088. arXiv: 088 (cited on pages 4, 59).

Malenovský, Z., J. Albrechtová, Z. Lhotáková, R. Zurita-Milla, J. G. Clevers, M. E. Schaepman, and P. Cudlín (2006). "Applicability of the PROSPECT model for Norway spruce needles". In: *International Journal of Remote Sensing* 27.24, pages 5315–5340. DOI: 10.1080/01431160600762990 (cited on page 24).

Malenovský, Z., L. Homolová, R. Zurita-Milla, P. Lukeš, V. Kaplan, J. Hanuš, J. P. Gastellu-Etchegorry, and M. E. Schaepman (2013). "Retrieval of spruce leaf chlorophyll content from airborne image data using continuum removal and radiative transfer". In: *Remote Sensing of Environment* 131, pages 85–102. DOI: 10.1016/j.rse.2012.12.015 (cited on pages 3, 46, 48).

Marcinkowska, A., B. Zagajewski, A. Ochtyra, A. Jarocińska, E. Raczko, L. Kupková, P. Stych, and K. Meuleman (2014). "Mapping vegetation communities of the Karkonosze National Park using APEX hyperspectral data and Support Vec-

tor Machines". In: *Miscellanea Geographica - Regional Studies on Development* 18.2, pages 1–7. DOI: 10.2478/mgrsd-2014-0007 (cited on pages 8, 15).

Melgani, F. and L. Bruzzone (2004). "Classification of Hyperspectral Remote Sensing Images with Support Vector Machines". In: *IEEE Transactions on Geoscience and Remote Sensing* 42.8, pages 1778–1790 (cited on pages 61, 62).

Meroni, M., A. Barducci, S. Cogliati, F. Castagnoli, M. Rossini, L. Busetto, M. Migliavacca, E. Cremonese, M. Galvagno, R. Colombo, and U. Morra Di Cella (2011). "The hyperspectral irradiometer, a new instrument for long-term and unattended field spectroscopy measurements". In: *Review of Scientific Instruments* 82, pages 1–10. DOI: 10.1063/1.3574360 (cited on page 27).

Meroni, M., L. Busetto, R. Colombo, L. Guanter, J. Moreno, and W. Verhoef (2010). "Performance of Spectral Fitting Methods for vegetation fluorescence quantification". In: *Remote Sensing of Environment* 114.2, pages 363–374. DOI: 10.1016/j.rse.2009.09.010 (cited on page 27).

Meroni, M. and R. Colombo (2009). "3S: A novel program for field spectroscopy". In: *Computers and Geosciences* 35.7, pages 1491–1496. DOI: 10.1016/j.cageo.2009.01.005 (cited on page 27).

Meroni, M., R. Colombo, and C. Panigada (2004). "Inversion of a radiative transfer model with hyperspectral observations for LAI mapping in poplar plantations". In: *Remote Sensing of Environment* 92.2, pages 195–206. DOI: 10.1016/j.rse.2004.06.005 (cited on page 24).

Miao, G., K. Guan, X. Yang, C. J. Bernacchi, J. A. Berry, E. H. DeLucia, J. Wu, C. E. Moore, K. Meacham, Y. Cai, B. Peng, H. Kimm, and M. D. Masters (2018). "Sun-Induced Chlorophyll Fluorescence, Photosynthesis, and Light Use Efficiency of a Soybean Field from Seasonally Continuous Measurements". In: *Journal of Geophysical Research: Biogeosciences* 123.2, pages 610–623. DOI: 10.1002/2017JG004180 (cited on pages 53, 55).

Mouchet, M. A., S. Villeger, N. W. Mason, and D. Mouillot (2010). "Functional diversity measures: an overview of their redundancy and their ability to discriminate community assembly rules". In: *Functional Ecology* 24, pages 867–876. DOI: 10.1111/j.1365-2435.2010.01695.x (cited on pages 4, 59).

Mountrakis, G., J. Im, and C. Ogole (2011). "Support vector machines in remote sensing: A review". In: *ISPRS Journal of Photogrammetry and Remote Sensing* 66.3, pages 247–259. DOI: 10.1016/j.isprsjprs.2010.11.001 (cited on page 61).

Moya, I., L. Camenen, G. Latouche, C. Mauxion, S. Evain, and Z. Cerovic (1998). "An instrument for the measurement of sunlight excited plant fluorescence". In: *Photosynthesis: Mechanisms and Effects*. Volume 5, pages 4265–4266 (cited on page 2).

Munro, R., R. Lang, D. Klaes, G. Poli, C. Retscher, R. Lindstrot, R. Huckle, A. Lacan, M. Grzegorski, A. Holdak, A. Kokhanovsky, J. Livschitz, and M. Eisinger

(2016). "The GOME-2 instrument on the Metop series of satellites: instrument design, calibration, and level 1 data processing - an overview". In: *Atmospheric Measurement Techniques* 9, pages 1279–1301. DOI: 10.5194/amt-9-1279-2016 (cited on page 23).

Musavi, T., M. D. Mahecha, M. Migliavacca, M. Reichstein, M. J. van de Weg, P. M. van Bodegom, M. Bahn, C. Wirth, P. B. Reich, F. Schrodt, and J. Kattge (2015). "The imprint of plants on ecosystem functioning: A data-driven approach". In: *International Journal of Applied Earth Observation and Geoinformation* 43, pages 119–131. DOI: 10.1016/j.jag.2015.05.009 (cited on pages 4, 59).

Musavi, T., M. Migliavacca, M. Reichstein, J. Kattge, C. Wirth, T. A. Black, I. Janssens, A. Knohl, D. Loustau, O. Roupsard, A. Varlagin, S. Rambal, A. Cescatti, D. Gianelle, H. Kondo, R. Tamrakar, and M. D. Mahecha (2017). "Stand age and species richness dampen interannual variation of ecosystem-level photosynthetic capacity". In: *Nature Ecology and Evolution* 1.2, pages 1–6. DOI: 10.1038/s41559-016-0048 (cited on page 58).

Nagendra, H. (2001). "Using remote sensing to assess biodiversity". In: *International Journal of Remote Sensing* 22.12, pages 2377–2400. DOI: 10.1089/ast.2015.1406. arXiv: arXiv:1011.1669v3 (cited on page 58).

Omari, K., H. P. White, K. Staenz, and D. J. King (2013). "Retrieval of Forest Canopy Parameters by Inversion of the PROFLAIR Leaf-Canopy Re fl ectance Model Using the LUT Approach". In: *IEEE Journal of Selected Topics in Applied Earth Observations and Remote Sensing* 6.2, pages 715–723 (cited on page 48).

Pal, M. and P. M. Mather (2004). "Assessment of the effectiveness of support vector machines for hyperspectral data". In: *Future Generation Computer Systems* 20, pages 1215–1225. DOI: 10.1016/j.future.2003.11.011 (cited on pages 61, 62).

Pal, M. and P. M. Mather (2005). "Support vector machines for classification in remote sensing". In: *International Journal of Remote Sensing* 26.5, pages 1007–1011. DOI: 10.1080/01431160512331314083 (cited on page 61).

Palmer, M. W., P. G. Earls, B. W. Hoagland, P. S. White, and T. Wohlgemuth (2002). "Quantitative tools for perfecting species lists". In: *Environmetrics* 13.2, pages 121–137. DOI: 10.1002/env.516 (cited on pages 59, 74).

Pandey, P. C., N. J. Tate, and H. Balzter (2014). "Mapping tree species in coastal portugal using statistically segmented principal component analysis and other methods". In: *IEEE Sensors Journal* 14.12, pages 4434–4441. DOI: 10.1109/JSEN.2014.2335612 (cited on page 8).

Panigada, C., M. Rossini, L. Busetto, M. Meroni, F. Fava, and R. Colombo (2010). "Chlorophyll concentration mapping with MIVIS data to assess crown discoloration in the Ticino Park oak forest". In: *International Journal of Remote Sensing* 31.12, pages 3307–3332. DOI: 10.1080/01431160903193497 (cited on page 8).

Papageorgiou, G. C. and G. Govindjee (2004). "Chlorophyll Fluorescence: A Signature of Photosynthesis". In: *Chlorophyll Fluorescence: A Signature of Photosynthesis*, pages 1–42 (cited on pages 1, 22).

Paw, K. T. and W. Gao (1988). "Applications of solutions to non-linear energy budget equations". In: *Agricultural and Forest Meteorology* 43, pages 121–145 (cited on page 33).

Petchey, O. L. and K. J. Gaston (2006). "Functional diversity: back to basics and looking forward". In: *Ecology Letters* 9, pages 741–758. DOI: 10.1111/j.1461-0248.2006.00924.x (cited on pages 4, 59).

Pettorelli, N., H. Nagendra, D. Rocchini, M. Rowcliffe, R. Williams, J. Ahumada, C. D. Angelo, C. Atzberger, D. Boyd, G. Buchanan, M. Haklay, K. S. He, N. Horning, N. Kelly, H. D. Klerk, X. Liu, J. Swenson, and M. Wegmann (2017). "Remote Sensing in Ecology and Conservation : three years on". In: *Remote Sensing in Ecology and Conservation* 3.2, pages 53–56. DOI: 10.1002/rse2.53 (cited on page 58).

Pettorelli, N., M. Wegmann, A. K. Skidmore, S. Mücher, T. P. Dawson, M. Fernandez, R. Lucas, M. E. Schaepman, T. Wang, B. O'Connor, R. H. Jongman, P. Kempeneers, R. Sonnenschein, A. K. Leidner, M. Böhm, K. S. He, H. Nagendra, G. Dubois, T. Fatoyinbo, M. C. Hansen, M. Paganini, H. M. de Klerk, G. P. Asner, J. T. Kerr, A. B. Estes, D. S. Schmeller, U. Heiden, D. Rocchini, H. M. Pereira, E. Turak, N. Fernandez, A. Lausch, M. A. Cho, D. Alcaraz-Segura, M. A. McGeoch, W. Turner, A. Mueller, V. St-Louis, J. Penner, P. Vihervaara, A. Belward, B. Reyers, and G. N. Geller (2016). "Framing the concept of satellite remote sensing essential biodiversity variables: challenges and future directions". In: *Remote Sensing in Ecology and Conservation*, n/a–n/a. DOI: 10.1002/rse2.15 (cited on page 58).

Plascyk, J. (1975). "The MK II Fraunhofer Line Discriminator (FLD -II) for Airborne and Orbital Remote Sensing of Solar-Stimulated Luminescence". In: *Optical Engineering* 14.4. DOI: 10.1117/12.7971842 (cited on page 2).

Porcar-Castell, A., E. Tyystjärvi, J. Atherton, C. Van Der Tol, J. Flexas, E. E. Pfündel, J. Moreno, C. Frankenberg, and J. A. Berry (2014). "Linking chlorophyll a fluorescence to photosynthesis for remote sensing applications: Mechanisms and challenges". In: *Journal of Experimental Botany* 65.15, pages 4065–4095. DOI: 10.1093/jxb/eru191 (cited on pages 1–3, 22, 53).

Pury, D. de and G. Farquhar (1997). "Simple scaling of photosynthesis from leaves to canopies without the errors of big-leaf models". In: *Plant Cell and Environment* 20, pages 537–557 (cited on page 33).

R Core Team (2018). *R: A Language and Environment for Statistical Computing*. R Foundation for Statistical Computing. Vienna, Austria (cited on pages 35, 63).

Rao, R. (1982). "Diversity and dissimilarity coefficients: a unified approach". In: *Theoritical population biology* 21, pages 24–43 (cited on page 62).

Rascher, U., L. Alonso, A. Burkart, C. Cilia, S. Cogliati, R. Colombo, A. Damm, M. Drusch, L. Guanter, J. Hanuš, T. Hyvarinen, T. Julitta, J. Jussila, K. Kataja, P. Kokkalis, S. Kraft, T. Kraska, M. Matveeva, J. Moreno, O. Muller, C. Panigada, M. Pikl, F. Pinto, L. Prey, R. Pude, M. Rossini, A. Schickling, U. Schurr, D. Schüttemeyer, J. Verrelst, and F. Zemek (2015). "Sun-induced fluorescence - a new probe of photosynthesis: First maps from the imaging spectrometer HyPlant". In: *Global Change Biology* 21.12, pages 4673–4684. DOI: 10.1111/gcb.13017 (cited on pages 2, 24, 28, 59).

Reichstein, M., M. Bahn, M. D. Mahecha, J. Kattge, and D. D. Baldocchi (2014). "Linking plant and ecosystem functional biogeography". In: *Proceedings of the National Academy of Sciences* 111.38, pages 13697–13702. DOI: 10.1073/pnas.1216065111 (cited on pages 3, 59).

Richter, K., C. Atzberger, F. Vuolo, P. Weihs, and G. D'Urso (2009). "Experimental assessment of the Sentinel-2 band setting for RTM-based LAI retrieval of sugar beet and maize". In: *Can. J. Remote Sensing* 35.3, pages 230–247 (cited on page 24).

Rivera, J. P., J. Verrelst, G. Leonenko, and J. Moreno (2013). "Multiple cost functions and regularization options for improved retrieval of leaf chlorophyll content and LAI through inversion of the PROSAIL model". In: *Remote Sensing* 5.7, pages 3280–3304. DOI: 10.3390/rs5073280 (cited on pages 24, 31, 33).

Rocchini, D., G. Bacaro, G. Chirici, D. Da Re, H. Feilhauer, G. M. Foody, M. Galluzzi, C. X. Garzon-Lopez, T. W. Gillespie, K. S. He, J. Lenoir, M. Marcantonio, H. Nagendra, C. Ricotta, E. Rommel, S. Schmidtlein, A. K. Skidmore, R. Van De Kerchove, M. Wegmann, and B. Rugani (2018). "Remotely sensed spatial heterogeneity as an exploratory tool for taxonomic and functional diversity study". In: *Ecological Indicators* 85.September, pages 983–990. DOI: 10.1016/j.ecolind.2017.09.055 (cited on pages 74, 75).

Rocchini, D., M. Marcantonio, and C. Ricotta (2017). "Measuring Rao's Q diversity index from remote sensing: An open source solution". In: *Ecological Indicators* 72, pages 234–238. DOI: 10.1016/j.ecolind.2016.07.039 (cited on pages 63, 74, 75).

Rogers, A., B. E. Medlyn, J. S. Dukes, G. B. Bonan, S. von Caemmerer, M. C. Dietze, J. Kattge, A. D. Leakey, L. M. Mercado, Ü. Niinemets, I. Colin Prentice, S. P. Serbin, S. Sitch, D. A. Way, and S. Zaehle (2017). "A roadmap for improving the representation of photosynthesis in Earth system models". In: *New Phytologist* 213.22-42 (cited on page 23).

Rosema, A., W. Verhoef, H. Noorbergen, and J. Borgesius (1992). "A new forest light interaction model in support of forest monitoring". In: *Remote Sensing of Environment* 42.1, pages 23–41. DOI: 10.1016/0034-4257(92)90065-R (cited on page 30).

Rossini, M., M. Meroni, M. Celesti, S. Cogliati, T. Julitta, C. Panigada, U. Rascher, C. van der Tol, and R. Colombo (2016). "Analysis of red and far-red sun-induced chlorophyll fluorescence and their ratio in different canopies based on observed and modeled data". In: *Remote Sensing* 8.5. DOI: 10.3390/rs8050412 (cited on page 2).

Rossini, M., M. Meroni, M. Migliavacca, G. Manca, S. Cogliati, L. Busetto, V. Picchi, A. Cescatti, G. Seufert, and R. Colombo (2010). "High resolution field spectroscopy measurements for estimating gross ecosystem production in a rice field". In: *Agricultural and Forest Meteorology* 150.9, pages 1283–1296. DOI: 10.1016/j.agrformet.2010.05.011 (cited on pages 2, 53).

Rossini, M., L. Nedbal, L. Guanter, A. Ac, L. Alonso, A. Burkart, S. Cogliati, R. Colombo, A. Damm, M. Drusch, J. Hanuš, R. Janoutova, T. Julitta, P. Kokkalis, J. Moreno, J. Novotny, C. Panigada, F. Pinto, A. Schickling, D. Schuettemeyer, F. Zemek, and U. Rascher (2015). "Red and far red Sun-induced chlorophyll fluorescence as a measure of plant photosynthesis". In: *Geophysical Research Letters*, pages 2079–2087. DOI: 10.1002/2014GL062943 (cited on page 2).

Rouse, J., J. Haas, and D. Deering (1974). "Monitoring vegetation systems in the Great Plains with ERTS". In: *Third Earth Resources Technology Satellite-1 Symposium - Volume I: Technical Presentations. Washington D.C. NASA*, pages 309–317 (cited on pages 51, 60, 63).

Ruiz-Benito, P., L. Gómez-Aparicio, A. Paquette, C. Messier, J. Kattge, and M. A. Zavala (2014). "Diversity increases carbon storage and tree productivity in Spanish forests". In: *Global Ecology and Biogeography* 23.3, pages 311–322. DOI: 10.1111/geb.12126. arXiv: arXiv:1011.1669v3 (cited on page 59).

Ryu, Y., D. D. Baldocchi, H. Kobayashi, C. Van Ingen, J. Li, T. A. Black, J. Beringer, E. Van Gorsel, A. Knohl, B. E. Law, and O. Roupsard (2011). "Integration of MODIS land and atmosphere products with a coupled-process model to estimate gross primary productivity and evapotranspiration from 1 km to global scales". In: *Global Biogeochemical Cycles* 25.4, pages 1–24. DOI: 10.1029/2011GB004053 (cited on pages 23, 25, 33, 50, 51).

Ryu, Y., C. Jiang, H. Kobayashi, and M. Detto (2018). "MODIS-derived global land products of shortwave radiation and diffuse and total photosynthetically active radiation at 5 km resolution from 2000". In: *Remote Sensing of Environment* 204.September 2017, pages 812–825. DOI: 10.1016/j.rse.2017.09.021 (cited on page 33).

Saltelli, A., P. Annoni, I. Azzini, F. Campolongo, M. Ratto, and S. Tarantola (2010). "Variance based sensitivity analysis of model output. Design and estimator for the total sensitivity index". In: *Computer Physics Communications* 181.2, pages 259–270. DOI: 10.1016/j.cpc.2009.09.018 (cited on page 31).

Schimel, D. S. (1995). "Terrestrial ecosystems and the carbon cycle". In: *Global Change Biology* October 1994, pages 77–91 (cited on page 22).

Schimel, D. S., R. Pavlick, J. B. Fisher, G. P. Asner, S. Saatchi, P. Townsend, and C. Miller (2015). "Observing terrestrial ecosystems and the carbon cycle from space". In: *Global Change Biology* 21, pages 1762–1776. DOI: 10.1111/gcb.12822 (cited on pages 22, 23).

Schlerf, M. and C. Atzberger (2006). "Inversion of a forest reflectance model to estimate structural canopy variables from hyperspectral remote sensing data". In: *Remote Sensing of Environment* 100.3, pages 281–294. DOI: 10.1016/j.rse.2005.10.006 (cited on pages 30, 48).

Schlerf, M. and C. Atzberger (2012). "Vegetation structure retrieval in beech and spruce forests using spectrodirectional satellite data". In: *IEEE Journal of Selected Topics in Applied Earth Observations and Remote Sensing* 5.1, pages 8–17. DOI: 10.1109/JSTARS.2012.2184268 (cited on page 48).

Schneider, F. D., F. Morsdorf, B. Schmid, O. L. Petchey, A. Hueni, and D. S. Schimel (2017). "Mapping functional diversity from remotely sensed morphological and physiological forest traits". In: *Nature Communications*. DOI: 10.1038/s41467-017-01530-3 (cited on pages 4, 58, 59, 74, 75).

Schulze, E.-D. and H. A. Mooney (1993). *Biodiversity and Ecosystem Function*. Springer-Verlag Berlin Heidelberg New York, page 525 (cited on page 58).

Schwalm, C. R., W. R. Anderegg, A. M. Michalak, J. B. Fisher, F. Biondi, G. Koch, M. Litvak, K. Ogle, J. D. Shaw, A. Wolf, D. N. Huntzinger, K. Schaefer, R. Cook, Y. Wei, Y. Fang, D. Hayes, M. Huang, A. Jain, and H. Tian (2017). "Global patterns of drought recovery". In: *Nature* 548.7666, pages 202–205. DOI: 10.1038/nature23021 (cited on page 58).

Schweiger, A. K., J. Cavender-Bares, P. A. Townsend, S. E. Hobbie, M. D. Madritch, R. Wang, D. Tilman, and J. A. Gamon (2018). "Plant spectral diversity integrates functional and phylogenetic components of biodiversity and predicts ecosystem function". In: *Nature Ecology and Evolution* 2.6, pages 976–982. DOI: 10.1038/s41559-018-0551-1 (cited on page 58).

Shannon, C. E. (1948). "A mathematical theory of communication". In: *The Bell System Technical Journal* 27.April 1924, pages 379–423. DOI: 10.1007/978-3-642-18421-5_11. arXiv: 9411012 [chao-dyn] (cited on page 62).

Sioris, C. E., G. Bazalgette Courrèges-Lacoste, and M.-P. Stoll (2003). "Filling in of Fraunhofer lines by plant fluorescence: Simulations for a nadir-viewing satellite-borne instrument". In: *Journal of Geophysical Research* 108.D4, page 4133. DOI: 10.1029/2001JD001321 (cited on page 2).

Sun, Y., C. Frankenberg, M. Jung, J. Joiner, L. Guanter, P. Köhler, and T. Magney (2018). "Overview of Solar-Induced chlorophyll Fluorescence (SIF) from the Orbiting Carbon Observatory-2: Retrieval, cross-mission comparison, and global

monitoring for GPP". In: *Remote Sensing of Environment* 209.February, pages 808–823. DOI: 10.1016/j.rse.2018.02.016 (cited on page 2).

Sun, Y., C. Frankenberg, J. D. Wood, D. S. Schimel, M. Jung, L. Guanter, D. T. Drewry, M. Verma, A. Porcar-Castell, T. J. Griffis, L. Gu, T. Magney, P. Köhler, B. Evans, and K. Yuen (2017). "OCO-2 advances photosynthesis observation from space via solar-induced chlorophyll fluorescence". In: *Science* 358.6360, eaam5747. DOI: 10.1126/science.aam5747 (cited on pages 2, 23).

Tagliabue, G., C. Panigada, R. Colombo, F. Fava, C. Cilia, F. Baret, K. Vreys, K. Meuleman, and M. Rossini (2016). "Forest species mapping using airborne hyperspectral APEX data". In: *Miscellanea Geographica, Regional Studies on Development* 20.1, pages 1–6. DOI: 10.1515/mgrsd-2016-0002 (cited on page 39).

Thenkabail, P. S., J. G. Lyon, and A. Huete (2011). *Hyperspectral remote sensing of vegetation*. CRC Press. DOI: 10.1201/b11222 (cited on page 1).

Tilman, D., F. Isbell, and J. M. Cowles (2014). "Biodiversity and Ecosystem Functioning". In: *Annual Review of Ecology, Evolution, and Systematics* 335.6065, pages 174–175. DOI: 10.1146/annurev-ecolsys-120213-091917 (cited on page 58).

Tilman, D., J. Knops, D. Wedin, P. Reich, M. Ritchie, and E. Siemann (1997). "The Influence of Functional Diversity and Composition on Ecosystem Processes". In: *Science* 277.5330, pages 1300–1302. DOI: 10.1126/science.277.5330.1300 (cited on page 59).

Tol, C. van der, J. A. Berry, P. K. Campbell, and U. Rascher (2014). "Models of fluorescence and photosynthesis for interpreting measurements of solar-induced chlorophyll fluorescence". In: *Journal of Geophysical Research: Biogeosciences* 119.12, pages 2312–2327. DOI: 10.1002/2014JG002713 (cited on page 52).

Tol, C. van der, W. Verhoef, J. Timmermans, A. Verhoef, and Z. Su (2009). "An integrated model of soil-canopy spectral radiances, photosynthesis, fluorescence, temperature and energy balance". In: *Biogeosciences* 6.12, pages 3109–3129. DOI: 10.5194/bg-6-3109-2009 (cited on pages 23, 53).

Tramontana, G., M. Jung, C. R. Schwalm, K. Ichii, G. Camps-Valls, B. Ráduly, M. Reichstein, M. A. Arain, A. Cescatti, G. Kiely, L. Merbold, P. Serrano-Ortiz, S. Sickert, S. Wolf, and D. Papale (2016). "Predicting carbon dioxide and energy fluxes across global FLUXNET sites with regression algorithms". In: *Biogeosciences* 13.14, pages 4291–4313. DOI: 10.5194/bg-13-4291-2016 (cited on page 23).

Vapnik, V. N. (1995). *The Nature of Statistical Learning Theory*. Springer-Verlag New York, pages 1–314. DOI: 10.1007/978-1-4757-3264-1 (cited on page 61).

Vapnik, V. N. and A. Y. Chervonenkis (1971). "On the Uniform Convergence of Relative Frequencies of Events to their Probabilities". In: *Theory of Probability and its Applications* 16.2, pages 264–280 (cited on page 61).

Verhoef, W. (1984). "Light scattering by leaf layers with application to canopy reflectance modeling: The SAIL model". In: *Remote Sensing of Environment* 16.2, pages 125–141. DOI: 10.1016/0034-4257(84)90057-9 (cited on page 30).

Verhoef, W., C. van der Tol, and E. M. Middleton (2018). "Hyperspectral radiative transfer modeling to explore the combined retrieval of biophysical parameters and canopy fluorescence from FLEX - Sentinel-3 tandem mission multi-sensor data". In: *Remote Sensing of Environment* 204.October 2017, pages 942–963. DOI: 10.1016/j.rse.2017.08.006 (cited on page 29).

Verma, M., D. S. Schimel, B. Evans, C. Frankenberg, J. Beringer, D. T. Drewry, T. Magney, I. Marang, L. Hutley, C. E. Moore, and A. Eldering (2017). "Effect of environmental conditions on the relationship between solar-induced fluorescence and gross primary productivity at an OzFlux grassland site". In: *Journal of Geophysical Research: Biogeosciences* 122.3, pages 716–733. DOI: 10.1002/2016JG003580 (cited on page 53).

Verrelst, J., G. Camps-Valls, J. Muñoz-Marí, J. P. Rivera, F. Veroustraete, J. G. Clevers, and J. Moreno (2015a). "Optical remote sensing and the retrieval of terrestrial vegetation bio-geophysical properties - A review". In: *ISPRS Journal of Photogrammetry and Remote Sensing* 108, pages 273–290. DOI: 10.1016/j.isprsjprs.2015.05.005 (cited on pages 1, 3, 23, 46).

Verrelst, J., Z. Malenovský, C. van der Tol, G. Camps-Valls, J. P. Gastellu-Etchegorry, P. Lewis, P. North, and J. Moreno (2018). "Quantifying Vegetation Biophysical Variables from Imaging Spectroscopy Data: A Review on Retrieval Methods". In: *Surveys in Geophysics*, pages 1–41. DOI: 10.1007/s10712-018-9478-y (cited on pages 1, 3, 23).

Verrelst, J., J. P. Rivera, L. Alonso, and J. Moreno (2011). "ARTMO: an automated radiative transfer models operator toolbox for automated retrieval of biophysical parameters through model inversion". In: *Proceedings of 7th EARSeL Workshop on Imaging Spectrometry, Edinburgh, UK, 11-13 April 2011* (cited on page 33).

Verrelst, J., J. P. Rivera, G. Leonenko, L. Alonso, and J. Moreno (2014). "Optimizing LUT-based RTM inversion for semiautomatic mapping of crop biophysical parameters from Sentinel-2 and -3 data: Role of cost functions". In: *IEEE Transactions on Geoscience and Remote Sensing* 52.1, pages 257–269. DOI: 10.1109/TGRS.2013.2238242 (cited on pages 3, 24, 48, 49).

Verrelst, J., J. P. Rivera, and J. Moreno (2015). "ARTMO's Global Sensitivity Analysis (GSA) Toolbox to Quantify Driving Variables of Leaf and Canopy Radiative Transfer Models". In: *EARSeL eProceedings* 9th EARSeL Imaging Spectroscopy Workshop, pages 1–11. DOI: 10.12760/02-2015-2-01 (cited on page 31).

Verrelst, J., J. P. Rivera, C. van der Tol, F. Magnani, G. H. Mohammed, and J. Moreno (2015b). "Global sensitivity analysis of the SCOPE model: What drives simulated canopy-leaving sun-induced fluorescence?" In: *Remote Sensing of En-*

vironment 166, pages 8–21. DOI: 10.1016/j.rse.2015.06.002 (cited on pages 3, 53).

Verrelst, J., J. P. Rivera, F. Veroustraete, J. Muñoz-Marí, J. G. Clevers, G. Camps-Valls, and J. Moreno (2015c). "Experimental Sentinel-2 LAI estimation using parametric, non-parametric and physical retrieval methods - A comparison". In: *ISPRS Journal of Photogrammetry and Remote Sensing* 108, pages 260–272. DOI: 10.1016/j.isprsjprs.2015.04.013 (cited on pages 3, 24, 49).

Verrelst, J., C. van der Tol, F. Magnani, N. Sabater, J. P. Rivera, G. H. Mohammed, and J. Moreno (2016). "Evaluating the predictive power of sun-induced chlorophyll fluorescence to estimate net photosynthesis of vegetation canopies: A SCOPE modeling study". In: *Remote Sensing of Environment* 176, pages 139–151. DOI: 10.1016/j.rse.2016.01.018 (cited on page 53).

Violle, C., M.-l. Navas, D. Vile, E. Kazakou, and C. Fortunel (2007). "Let the concept of trait be functional!" In: *Oikos* 116.January, pages 882–892. DOI: 10.1111/j.2007.0030-1299.15559.x (cited on page 3).

Wang, Z., A. K. Skidmore, R. Darvishzadeh, and T. Wang (2018). "Mapping forest canopy nitrogen content by inversion of coupled leaf-canopy radiative transfer models from airborne hyperspectral imagery". In: *Agricultural and Forest Meteorology* 253-254.January, pages 247–260. DOI: 10.1016/j.agrformet.2018.02.010 (cited on pages 3, 24, 48, 49).

Waske, B. and J. A. Benediktsson (2010). "Sensitivity of Support Vector Machines to Random Feature Selection in Classification of Hyperspectral Data". In: *IEEE Transactions on Geoscience and Remote Sensing* 48.7, pages 2880–2889 (cited on page 62).

White, H. P., J. R. Miller, and J. M. Chen (2001). "Four-Scale Linear Model for Anisotropic Reflectance (FLAIR) for Plant Canopies - Part I : Model Description and Partial Validation". In: *IEEE Transactions on Geoscience and Remote Sensing* 39.5, pages 1072–1083. DOI: 10.1109/36.921425 (cited on page 48).

Whitley, R., J. Beringer, L. B. Hutley, G. Abramowitz, M. G. D. Kauwe, R. Duursma, B. Evans, V. Haverd, L. Li, Y. Ryu, B. Smith, Y.-P. Wang, M. Williams, and Q. Yu (2016). "A model inter-comparison study to examine limiting factors in modelling Australian tropical savannas". In: *Biogeosciences* 13, pages 3245–3265. DOI: 10.5194/bg-13-3245-2016 (cited on pages 50, 51).

Wieneke, S., H. E. Ahrends, A. Damm, F. Pinto, A. Stadler, M. Rossini, and U. Rascher (2016). "Airborne based spectroscopy of red and far-red sun-induced chlorophyll fluorescence: Implications for improved estimates of gross primary productivity". In: *Remote Sensing of Environment* 184, pages 654–667. DOI: 10.1016/j.rse.2016.07.025 (cited on pages 2, 50).

Yang, G., C. Zhao, Q. Liu, W. Huang, and J. Wang (2011). "Inversion of a radiative transfer model for estimating forest LAI from multisource and multiangular

optical remote sensing data". In: *Geoscience and Remote Sensing, IEEE Transactions on* 49.3, pages 988–1000. DOI: 10.1109/tgrs.2010.2071416 (cited on page 48).

Yang, K., Y. Ryu, B. Dechant, J. A. Berry, Y. Hwang, C. Jiang, M. Kang, J. Kim, H. Kimm, A. Kornfeld, and X. Yang (2018). "Sun-induced chlorophyll fluorescence is more strongly related to absorbed light than to photosynthesis at half-hourly resolution in a rice paddy". In: *Remote Sensing of Environment* 216.June, pages 658–673. DOI: 10.1016/j.rse.2018.07.008 (cited on page 53).

Yang, X., J. Tang, J. F. Mustard, J. E. Lee, M. Rossini, J. Joiner, W. J. Munger, A. Kornfeld, and A. D. Richardson (2015). "Solar-induced chlorophyll fluorescence correlates with canopy photosynthesis on diurnal and seasonal scales in a temperate deciduous forest". In: *Geophysical Research Letters*, pages 2977–2987. DOI: 10.1002/2015GL063201 (cited on pages 2, 23, 53).

Zarco-Tejada, P. J., A. Catalina, M. González, and M. P. Martín (2013). "Relationships between net photosynthesis and steady-state chlorophyll fluorescence retrieved from airborne hyperspectral imagery". In: *Remote Sensing of Environment* 136, pages 247–258. DOI: 10.1016/j.rse.2013.05.011 (cited on page 2).

Zarco-Tejada, P. J. and J. R. Miller (1999). "Land cover mapping at BOREAS using red edge spectral parameters from CASI imagery". In: *Journal of Geophysical Research Atmospheres* 104.D22, pages 27921–27933. DOI: 10.1029/1999JD900161 (cited on page 11).

Zarco-Tejada, P. J., J. R. Miller, A. Morales, A. Berjón, and J. Agüera (2004). "Hyperspectral indices and model simulation for chlorophyll estimation in open-canopy tree crops". In: *Remote Sensing of Environment* 90.4, pages 463–476. DOI: 10.1016/j.rse.2004.01.017 (cited on pages 3, 24).

Zhang, Y., L. Guanter, J. A. Berry, C. van der Tol, X. Yang, J. Tang, and F. Zhang (2016). "Model-based analysis of the relationship between sun-induced chlorophyll fluorescence and gross primary production for remote sensing applications". In: *Remote Sensing of Environment* 187, pages 145–155. DOI: 10.1016/j.rse.2016.10.016 (cited on pages 52, 53).

Zhu, Z., S. Piao, R. B. Myneni, M. Huang, Z. Zeng, J. G. Canadell, P. Ciais, S. Sitch, P. Friedlingstein, A. Arneth, R. Liu, J. Mao, Y. Pan, S. Peng, J. Peñuelas, and B. Poulter (2016). "Greening of the Earth and its drivers". In: *Nature Climate Change* 6, pages 791–796. DOI: 10.1038/NCLIMATE3004 (cited on pages 1, 22).